Dissolution of Valuable Metals from Nickel Smelter Slags by Means of High Pressure Oxidative Acid Leaching

by

Ilya Perederiy

A thesis submitted in conformity with the requirements
for the degree of Doctor of Philosophy

Graduate Department of Chemical Engineering and Applied Chemistry
University of Toronto

Dissolution of Valuable Metals from Nickel Smelter Slags by Means of High Pressure Oxidative Acid Leaching

Ilya Perederiy

Degree of Doctor of Philosophy

Graduate Department of Chemical Engineering and Applied Chemistry
University of Toronto

2011

ABSTRACT

In the production of base metals by smelting of sulphide ore concentrates, large amounts of iron are rejected with iron silicate slags. These slags contain Ni, Cu and Co in concentrations up to several percent units. Extraction of the entrapped base metals using high pressure oxidative acid leaching (HPOXAL) was investigated in this work.

Crystalline slags containing fayalite (Fe_2SiO_4), magnetite (Fe_3O_4), silica (SiO_2) and matte ($MeS_{n<1}$) were found to be highly amenable to leaching at 250°C, 90 psi (6.2 bar) O_2 partial pressure and 70 g/L initial H_2SO_4. Extractions of Ni, Co and Cu exceeded 90% within 15-20 min and arrived at 95-97% after 45 min. The residues of leaching were identified as aggregates of crystalline hematite (Fe_2O_3) and amorphous silica.

Dissolution of fayalite and magnetite was shown to be acid driven. Since HPOXAL operates with substoichiometric additions of sulphuric acid (10-20% of the stoichiometric requirement), acid regeneration facilitated by iron oxidation and hydrolysis is crucial to

high rates of leaching. Low acidities (<10 g/L) were shown to cause precipitation of ferrous sulphate, slowing acid regeneration and slag dissolution. Elevated acidities (>70 g/L) result in excessive concentrations of Fe(III) in the leach solution, complicating downstream processing.

The use of pyrrhotite tailings, an environmentally hazardous waste, as a substitute of sulphuric acid in slag leaching was investigated. Oxidative co-leaching of pyrrhotite tailings with naturally cooled converter slag at 250°C, 90 psi (6.2 bar) O_2, 68 g/L equivalent H_2SO_4 was shown to have kinetics comparable to adding sulphuric acid with final extractions reaching 95-97% in 45 min.

Granulation of slag melt can produce an amorphous solid solution of SiO_2 and metal oxides. Amorphous slag is not amenable to HPOXAL due to the formation of a passive layer of silica. Leaching of amorphous slag at low temperatures was shown to proceed nearly to completion. The difference in the leachability of amorphous slag at high and low temperatures is explained in terms of the rate of silicic acid re-polymerization leading to closure of pores in the leached layer.

ACKNOWLEDGEMENTS

I am most grateful to my supervisor, Professor Vladimiros G. Papangelakis for his guidance and continuous encouragement to excel in critical thinking. I am deeply indebted for his support that enabled me to accomplish my work and led me to the realization that any goal, no matter how difficult, can be achieved with due effort and planning. I am also grateful to Dr. Yunjiao Li who spent several years at the University of Toronto, and guided me through the initial stages of this research project.

This work was greatly enriched by the suggestions of the reading committee members: Professor Charles Jia and Professor Donald Kirk. Professors Honghi Tran, Mansoor Barati, and John Peacey are acknowledged for their willingness to act as examiners and providing me with valuable feedback.

It would have been a very challenging task to learn the "tricks" of scanning electron microscopy if it had not been for the help and advice of George Kretschmann. Installing and operating the conductivity sensor also would have been a very difficult task without the help and supervision of Ramanpal Saini. I am very thankful to both of them for giving me two tools that enabled me to make significant progress in my research.

I am thankful to all former and current members of the Aqueous Process Engineering and Chemistry Group for their friendship, which made it easy to work around them.

I feel immense gratitude to my best friend Ghazal (Dr. Ghazal Azimi) who was a fellow graduate student in the Aqueous Process Engineering and Chemistry Group for several years. Ghazal has been and continues to be my source of inspiration and encouragement. Her friendship positively affected me and my work in a countless number of ways.

It is my pleasant obligation to thank my former supervisor, Professor Stanislav Stepanovich Naboichenko of Ural State Technical University. His guidance and help opened new opportunities in my professional development.

This work would have been impossible without the financial support of the following organizations: NSERC, Ontario Centres of Excellence, Mitacs. Vale Canada Ltd. is acknowledged for both the financial contribution and in-kind support of the project. The personnel of Vale Base Metals Technology Development are thanked for their valuable advice. I would also like to thank Foxboro Co. and Kevin Quackenbush personally for donating parts for the conductivity sensor.

Ilya Perederiy

September 2011

TABLE OF CONTENTS

LIST OF TABLES

LIST OF FIGURES

NOMENCLATURE

Subscripts

aq	Aqueous phase
s	Solid phase

Abbreviations

AARD	Absolute Average Relative Deviations
A/S	Acid to solids ratio (mass-based)
ICP–OES	Inductively coupled plasma–optical emission spectrometer
HPOXAL	High pressure oxidative acid leaching
HPAL	High pressure acid leaching
PAL	Pressure acid leaching
XRD	X-ray diffraction
SEM-BSE	Scanning electron microscopy, back-scattered electron mode

CHAPTER 1 INTRODUCTION

Until recent decades, smelting of ores had been the technology of choice for the production of Ni, Co and Cu in the world. It remains at the core of nickel production in Canada due to the prevalence of sulphide ores. Efforts have been put into making smelting more efficient and environmentally friendly; but despite the progress achieved, new ideas will continue to be in demand in order to keep the technology in line with the modern environmental standards as well as the increasing complexity of ores.

Recovery of Ni, Co and Cu from slags (intermediate products and wastes of smelting) poses a problem that has not been resolved satisfactorily. A number of technical and environmental considerations discussed in detail further emphasize the importance of finding a technology capable of processing slags in an environmentally friendly and economical way.

1.1 Losses of Valuable Metals with Smelter Slags

1.1.1 Pyrometallurgical production of Ni, Co and Cu in Canada

The major minerals present in the Canadian nickel sulphide ores are pentlandite ([Fe, Ni]$_9$S$_8$), pyrrhotite (Fe$_7$S$_8$), pyrite (FeS$_2$) and chalcopyrite (CuFeS$_2$). In addition to nickel and copper, sulphide ores usually contain a smaller quantity of cobalt. The content of nickel in the ore is normally between 1-2%. (Liu, 2004)

In order to increase the content of the base metals (nickel, copper, cobalt), and reject the excess of iron sulphides, milled ores are subjected to froth flotation. *Ore concentrate*, the product of mineral processing, contains up to 20% of Ni+Cu+Co (Liu, 2004). In Ontario's nickel operations *pyrrhotite tailings* constitute the main waste of flotation (Peek et al., 2011). These tailings are discarded despite a small content of the entrained nickel (~0.8%wt) rejected with them.

The conventional technologies used for the recovery of nickel, copper and cobalt from sulphide ore concentrates are based on the oxidation and removal of the iron sulphide

component while preserving the valuable metals (Ni, Cu and Co) in the form of a metal-enriched sulphide.

Vale's Copper Cliff smelter (located in Sudbury, Ontario) utilizes flash smelting to treat a bulk concentrate with ~21%wt of Ni, Cu and Co (Marcuson and Diaz, 2007). A portion of the iron sulphide is oxidized and reacted with silica to produce fayalite (Fe_2SiO_4) forming the base of a lightweight molten phase called *slag*:

$$2FeS + 3O_2 + SiO_2 \rightarrow Fe_2SiO_4 + 2SO_2\uparrow \quad (1.1)$$

Some quantity of iron sulphide is further oxidized into magnetite (Fe_3O_4) which dissolves in slag:

$$3FeS + 5O_2 \rightarrow Fe_3O_4 + 3SO_2\uparrow \quad (1.2)$$

Sulphides of copper and nickel remain largely intact forming a heavy molten phase called *matte* that contains ~45% of Ni, Cu and Co (Marcuson and Diaz, 2007). The furnace slag and matte, separated due to the difference in their densities, are tapped from the flash furnace. The matte proceeds to further processing by converting, and the slag is discarded at a slag dump.

Another approach to the processing of nickel ore concentrates involves roasting followed by calcine smelting in an electric furnace to produce matte and discard slag. This technology is used at Vale's Thompson (Manitoba) smelter as well as Xstrata's Sudbury smelter (Ontario). Mattes produced by electric smelting can contain significant quantities of metallic iron (Diaz et al., 1994; Marcuson and Diaz, 2007).

Molten furnace mattes proceed to converting (in Pierce-Smith converters), during which the iron suphide (or metallic iron) is almost completely removed as per Eq. 1.1, 1.2 and 1.3.

$$2Fe + O_2 + SiO_2 \rightarrow Fe_2SiO_4 \quad (1.3)$$

Bessemer matte, the product of converting containing mostly metal-enriched Ni-Cu-Co sulfides with less than 3% of Fe (Marcuson and Diaz, 2007), is removed from the converter and solidified (either by casting or granulation). A variety of operations are

employed in the subsequent treatment of Bessemer mattes to separate the base metals and refine them. The most typical operations include froth flotation, oxidizing roasting, carbonyl refining or leaching.

Converter slags normally contain several percent of nickel, cobalt and copper. These metals are recovered by re-smelting the converter slag in a furnace. For example, at the Copper Cliff smelter, converter slags are reverted back into the flash furnace (Marcuson and Diaz, 2007), and at Xstrata's Sudbury smelter, converter slags are processed in a separate batch slag cleaning vessel to produce discard slag (Stubina et al., 1994).

1.1.2 Entrapment of Ni, Co and Cu in smelter slags

Most furnace slags from copper/nickel/cobalt smelters contain 0.04–1.2% of Ni, 0.21–0.7% of Co and 0.6–3.7% of Cu (Shen and Forssberg, 2003). The aggressive conditions employed during converting, and the batch character of the process result in high variation in slag quality (some typical converter slag compositions are given in Appendix A). Baghalha et al. (2007) presented chemical analysis of converter slags containing as high as 4.8% of Ni, 1.6% of Co and 1.4% of Cu

Base metals are present in slag partly due to mechanical entrapment of matte in the form of fine dispersions of sulphides (Herreros et al., 1998; Sun, 2006). The extent of matte entrainment is affected by slag viscosity and settling duration.

A portion of base metals are dissolved in slag as oxides chemically bound with silica in fayalite (Curlook et al., 2004). Toscano (2001, 2003) reviewed studies of base metal oxide dissolution in slag, and showed that the dissolution equilibrium is governed by the following reaction:

$$MS_{matte} + FeO_{slag} = MO_{slag} + FeS_{matte} \quad (1.4)$$

The equilibrium constants of cobalt oxide dissolution in slag at 1200 and 1300°C were shown to be an order of magnitude higher than those for nickel oxide (Toscano, 2001). The tendency of cobalt to exist in the oxide form makes cobalt losses with slags of greatest concern. For example, in copper smelting, Sinha and Nagamori (1982) estimated the overall cobalt recoveries as 3% at best.

Typically, nickel and copper furnace slags contain more than 98% of Fe and Co, and 54–95% of Ni and Cu as oxides, depending on the processing method and the furnace type (Gbor et al., 2000a). Low matte grade and low oxygen potential cause matte to be the major form of base metal losses with slag (Sun, 2006).

1.1.3 Environmental impact of slag

The amount of discard slag produced during smelting is comparable to the tonnage of the concentrate processed (Baghalha et al., 2007). Vale, a leading world producer of nickel, disposes 1.2 million t of slag annually, whereas the total inventory of Inco's slag in the Sudbury area after ~90 years of company operation is 115 million t (Li et al., 2008).

The huge quantities of discarded slag result not only in wasting valuable metals, but also cause environmental pollution due to the oxidation of entrained sulphur to sulphuric acid promoting slow leaching of heavy metals (Li et al., 2008).

Manz and Castro (1997) investigated the pollution potential of iron silicate copper smelter slags in the mining district of Sta. Maria de La Paz of the Central Mexican Uplands, and concluded that copper can be dissolved by waters rich in humic substances. An investigation of soil contamination around copper and nickel smelters in Russian Federation suggests that slags contribute to accumulation of base metals (Vodyanitskii et al., 2011). The diagram below illustrates a route for pollution caused by slags (Fig. 1.1).

Processing of converter slags by re-smelting also has a detrimental impact on the environment. First of all, the processed (discard) slag still contains nickel, cobalt and copper. Second, recycling of converter slag into the furnace causes extra fugitive emissions of sulphur dioxide to the atmosphere.

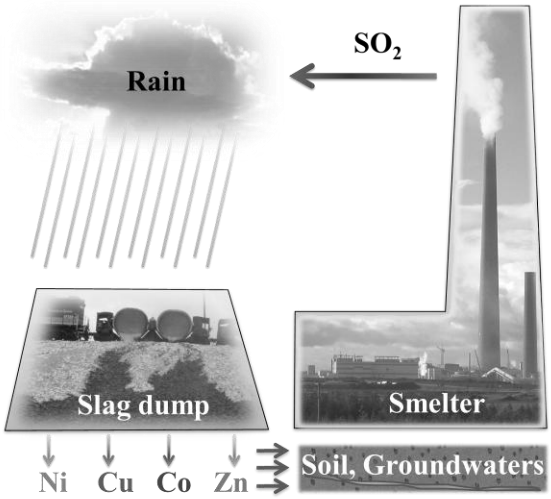

Fig. 1.1 Pollution from discard slags

1.2 Previous Studies of Metal Extraction from Smelter Slags

In terms of nickel content, discarded slags are comparable to laterite ores, a resource of nickel accounting for ~40% of world nickel production (Gleeson et al., 2003). These ores typically contain 1.05–2.3% Ni and 0.05–0.3% Co (Whittington et al., 2003; Agatzini-Leonardou and Zafiratos, 2004; Chen, 2004). The accumulated quantity of nickel slags makes them a prospective resource of Ni, Co and Cu.

1.2.1 Pyrometallurgical treatment

Base metals are routinely recovered from converter slag by re-smelting. At the Copper Cliff smelter, converter slags are reverted back into the flash furnace (Marcuson and Diaz, 2007). Recycling decreases the throughput of the smelting furnace and affects process stability. Also, the addition of slag into the furnace results in the accumulation of undesirable impurities (which end up in the converter matte).

A stand-alone slag cleaning vessel is used at Xstrata's Sudbury smelter to process converter slags (Stubina et al., 1994; Liu, 2004). All nickel sulphide smelters using Outokumpu flash furnace either operate in conjunction with stand-alone electric furnaces for slag cleaning, or have an extension of the furnace equipped with electrodes (Liu, 2004). It must be noted that operation of separate slag cleaning furnaces is possible only

when the value of the recovered metals justifies the capital and operating costs. Hence, the application of pyrometallurgical slag processing is limited to slags rich in base metals (such as converter slags).

Wolf (2008) investigated the effect of various reductants and fluxes on the pyrometallurgical recovery of Ni, Cu and Co from converter slags of the Copper Cliff smelter. Recoveries of nickel and copper approached 80%; however, the maximum cobalt recovery was only 40%.

1.2.2 Flotation

Several Chilean smelters have used flotation to produce copper sulphide concentrates from smelter slags (Demetrio et al., 2000). Das et al. (2010) attempted flotation of a discarded slag with 1.53% of copper (mostly associated with sulphur), and were able to recover over 90% of copper (collector: sodium isopropyl xanthate, pH 9). Shen and Forssberg (2003) refer to an investigation by Rao and Nayak (1992) who conducted flotation experiments (collector: potassium amyl xanthate, frother: pine oil, pH 8–9) with a converter slag containing 3.7% Cu. A concentrate with 42–44% Cu was obtained. 82–96% of copper was recovered; however, cobalt and nickel, being in the oxide form, reported into the tailings.

Heinrich (1989) characterized a discarded nickel smelter slag (from the Sudbury area) with 0.5%wt of Ni, Co and Cu in total, and determined that only ~5% of Co and 40% of Ni were associated with sulphide aggregates (matte), making this slag unsuitable for flotation. Mineral characterization work by Gbor et al. (2000a) confirmed that >98% of cobalt was associated with oxides in flash and electric furnace slags originating from the Sudbury smelters. About 20% of nickel was estimated to exist in the sulphide form

1.2.3 Low temperature leaching of slags

Liberation of base metals from slags by leaching in aqueous solutions presents an alternative to pyrometallurgical treatment and flotation. A number of researchers have investigated the feasibility of low temperature (i.e. below the normal boiling point) leaching.

Lindblad and Dufresne (1974) reported the results of atmospheric sulphuric acid leaching of copper and zinc from an aged reverberatory discarded slag. Recoveries of 85% for Cu and 93% for Zn were obtained. However, a substantial amount of iron was leached along with the copper and zinc

Heinrich (1989) leached a discarded nickel slag in 20% sulphuric acid with addition of 0.8 g/L NaCl at 100°C for 4 hours. 97% of Co and 92% of Fe reported into the leach solution, yet only 12% Cu and no Ni dissolved.

Jia et al. (1999) investigated the leaching behaviour of furnace slag in dilute sulphuric acid at room temperature. Over 65% of nickel and 75% of cobalt along with a comparable amount of iron were dissolved from the slags in sulfuric acid in 20 hours. Gbor et al. (2000b) from the same group attempted sulphur dioxide leaching of nickel furnace slags. Both sulphuric acid and sulphur dioxide are readily available at smelting operations. Co and Ni extractions reached 77% and 35%, respectively, after 3 hours of leaching in a 1 M solution of dissolved SO_2 at 35°C. The behaviour of iron was found to be similar to cobalt in terms of the extent and the rate of dissolution.

Taking into account the fact that the iron content in slags typically exceeds 30%, it is clear that iron dissolution would determine the consumption of acid during leaching. Low temperature leaching with sulphuric acid has been found demanding in terms of acid consumption as per the stoichiometry of the fayalite dissolution reaction:

$$Fe_2SiO_4 + 2H_2SO_4 \rightarrow 2FeSO_{4(aq)} + Si(OH)_{4(aq)} \qquad (1.5)$$

To control the iron content in the leach solution and reduce the consumption of acid, leaching in the presence of oxidants has been attempted. Banza et al (2002) employed hydrogen peroxide during sulfuric acid leaching of a copper furnace slag. Over 75% of copper and 90% of cobalt and zinc with less than 5% iron were dissolved at 70°C and pH 2.5 in 2 hours with an addition of ~ 60 L H_2O_2/t slag. Altundogan et al. (2004) studied leaching of a cobalt-bearing copper converter slag by sulphuric acid (up to 1 M) in the presence of potassium dichromate (up to 0.3 M). Addition of dichromate improved copper extraction and suppressed iron dissolution – however, cobalt dissolution was also suppressed by potassium dichromate.

Other reagents used in studies of low temperature slag leaching include ferric chloride (Anand et al., 1980) and chlorine (Herreros, 1998) The presence of chlorides complicates further extraction of metals from the solutions, since open-cell electrowinning, the most widely used operation for base metal recovery from leach solutions, is performed in sulphate media.

Besides slow kinetics, incomplete metal recovery and extensive acid consumption, low temperature acid leaching of silicates in known to cause formation of metastable colloidal silica by means of gradual polymerization of silicic acid (Matthew and Elsner, 1977). The presence of colloidal silica complicates slurry filtration and subsequent electrowinning.

1.2.4 Pressure leaching of slags

Pressure oxidative leaching (at temperatures above the normal boiling point) can be used to resolve the issue of low metal extractions, slow kinetics and excessive consumption of acid without using prohibitively expensive reagents such as hydrogen peroxide. Elevated temperatures and the presence of oxygen promote oxidation of ferrous iron and subsequent hydrolysis of ferric iron (Reid, 2006) resulting in zero net consumption of sulphuric acid (for fayalite dissolution):

$$Fe_2SiO_4 + 1/2O_2 + 2H_2O \rightarrow Fe_2O_{3(s)} + Si(OH)_{4(aq)} \quad (1.6)$$

Another benefit of leaching at elevated temperatures is precipitation of solid aggregates of amorphous silica per Eq. 1.7 (Whittington, 2003) thus avoiding the formation of metastable colloidal silica.

$$nSi(OH)_{4(aq)} \rightarrow SiO_{2(s)} \cdot mH_2O + (n-m)H_2O \quad (1.7)$$

Klein and Stevens (1972) patented a process involving pressure oxidative acid leaching of slag at temperatures between 120-230°C. In their experiments copper was completely dissolved within two hours at 50 psi (3.5 bar) O_2 and ~50 g/L of H_2SO_4.

Anand et al. (1983) investigated medium temperature leaching of a copper converter slag (130°C, up to 5.9 bar O_2, 0.35 N H_2SO_4). Over 92% of Cu and more than 95% of Ni and Co could be extracted with less than 0.8% dissolution of iron; however, the required retention time of 4 hours made the process uneconomic.

Sobol (1993) was able to achieve extractions in excess of 90% for Ni, Cu and Co from a converter slag in less than an hour at temperatures of 150-190°C. Leaching of various nickel furnace and converter slags at even higher temperatures (200-250°C) was investigated at the University of Toronto (Curlook et al., 2004; Baghalha et al., 2007). The process combines the traits of laterite high pressure acid leaching – HPAL (Krause, 1997; Georgiou, 1998; Whittington, 2000) and high-temperature pressure oxidation of sulphides (King et al., 1993). It was found that crystalline (obtained by slow/natural cooling) slags respond well to leaching (Fig. 1.2). However, the performance of the high pressure oxidative acid leaching (HPOXAL) process with amorphous (water-granulated) slags was found to be inadequate (Fig. 1.3).

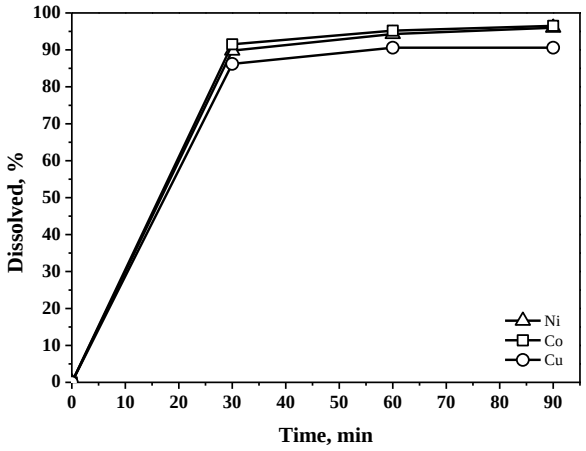

Fig. 1.2 Leaching experiment carried out by Baghalha (from an internal report). Discarded furnace slag (naturally cooled) from the Copper Cliff smelter, 250°C, 130 g/L initial H_2SO_4, 75 psi (5.2 bar) O_2, 30%wt solids, 600 rpm

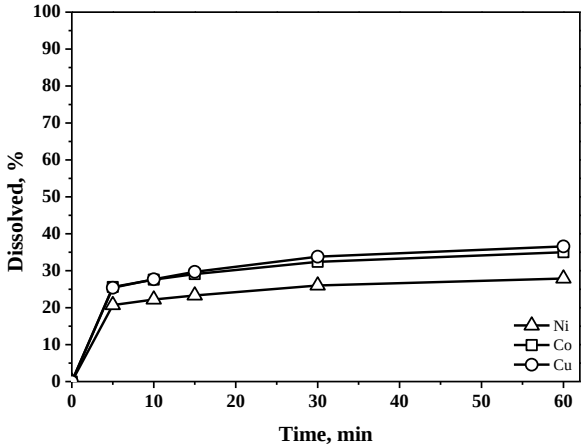

Fig. 1.3 Leaching experiment carried out by Baghalha (from an internal report). Discarded furnace slag (granulated) from Xstrata's Sudbury smelter, 250°C, 130 g/L initial H_2SO_4, 75 psi (5.2 bar) O_2, 30%wt solids, 750 rpm

1.3 Objectives

Taking into account the process kinetics, quality of products, cost of reagents and the environmental impact, high pressure oxidative acid leaching was deemed to be the most promising process for the recovery of base metals from nickel smelter slags. This study takes off based on the preliminary findings obtained at the University of Toronto (Curlook et al., 2004; Baghalha et al., 2007).

The following objectives were set for this study:

- Investigate the effect of slag mineralogy on the performance of leaching
- Evaluate and explain the effect of the main process parameters (temperature, acidity, partial pressure of O_2)
- Identify process chemistry
- Determine the mechanism of slag dissolution
- Investigate the use of pyrrhotite tailings as a substitute for sulphuric acid
- Explain the poor performance of HPOXAL with amorphous slags
- Evaluate the quality of leach solutions and residues

1.4 Thesis Overview

Chapter 1 introduces the problem of base metal recovery from slags produced at nickel smelters, and states the objectives of the work undertaken.

Chapter 2 provides information about the experimental procedures, autoclave setup, analytical and materials characterization techniques. Excerpts from the following journal manuscript were used in this chapter:

- Perederiy, I., Papangelakis, V.G., Buarzaiga, M., Mihaylov, I., 2011. Co-treatment of converter slag and pyrrhotite tailings via high pressure oxidative leaching, J. Haz. Mat.

Chapter 3 presents the slag materials used in this work. The description of a flash furnace slag in section 3.1 is credited to Dr. Yunjiao Li (Li et al., 2009), a postdoctoral fellow who was assigned to the project during 2006-2008. This chapter is a compilation of the following publications:

- Perederiy, I., Papangelakis, V.G., Buarzaiga, M., Mihaylov, I., 2011. Co-treatment of converter slag and pyrrhotite tailings via high pressure oxidative leaching, J. Haz. Mat

- Perederiy, I., Papangelakis, V.G. High pressure oxidative leaching of crystalline converter slags: leaching mechanism (in preparation)

- Perederiy, I., Papangelakis, V.G. High pressure oxidative leaching of amorphous FeO-SiO_2 slag: leaching mechanism (in preparation)

Chapter 4 focuses on the leaching of various crystalline slags. It discusses the effect of process parameters and slag mineralogy on the performance of leaching, talks about the chemistry of leaching as well as the mechanism of dissolution. Overall, chapter 4 combines the following papers:

- Li, Y., Perederiy, I., Papangelakis, V.G., 2008. Cleaning of waste smelter slags and recovery of valuable metals by pressure oxidative leaching. J. Haz. Mat.

- Perederiy, I., Papangelakis, V.G., Jia, C.Q., 2009. Pressure oxidative leaching of slags from nickel smelters: an update. Proceedings of 39th annual Hydrometallurgy Meeting

- Perederiy, I., Papangelakis, V.G., Buarzaiga, M., Mihaylov, I. ,2011. Co-treatment of converter slag and pyrrhotite tailings via high pressure oxidative leaching, J. Haz. Mat.

- Perederiy, I., Papangelakis, V.G. High pressure oxidative leaching of crystalline converter slags: leaching mechanism (in preparation)

Chapter 5 describes a modified leaching process in which slags are co-leached with pyrrhotite tailings for additional economic and environmental benefit. The following publication was incorporated into this chapter:

- Perederiy, I., Papangelakis, V.G., Buarzaiga, M., Mihaylov, I., 2011. Co-treatment of converter slag and pyrrhotite tailings via high pressure oxidative leaching, J. Haz. Mat.

Chapter 6 describes leaching of amorphous slags. The reason for poor metal extractions at high temperatures is identified via characterization of the residues. Results of low temperature leaching are presented for comparison, and the mechanism of dissolution is deduced. This chapter is based on a manuscript in preparation:

- Perederiy, I., Papangelakis, V.G. High pressure oxidative leaching of amorphous $FeO\text{-}SiO_2$ slag: leaching mechanism (in preparation)

Chapter 7 summarizes the results presented in the previous chapters and talks about the industrial implications. Chapter 8 provides recommendations for future work on high pressure oxidative acid leaching of slags.

Referencing in this document is done on a chapter-by-chapter basis.

References

Agatzini-Leonardou, S., Zafiratos, I.G., 2004. Beneficiation of a Greek serpentinic nickeliferous ore. Part II. Sulphuric acid heap and agitation leaching, Hydrometallurgy 74, 267–275.

Altundogan, H.S., Boyrazli, M., Tumen, F., 2004. A study on the sulphuric acid leaching of copper converter slag in the presence of dichromate. Minerals Engineering 17, 465–467.

Anand, S., Rao, P. Kanta, X, Jena, P.K., 1980. Recovery of metal values from copper converter and smelter slags by ferric chloride leaching. Hydrometallurgy 5 (4), 355–365.

Anand, S., Sarveswara Rao, K., Jena, P.K., 1983. Pressure leaching of copper converter slag using dilute sulphuric acid for the extraction of cobalt, nickel and copper values. Hydrometallurgy 10 (3), 305–312.

Baghalha, M., Papangelakis, V.G., Curlook, W., 2007. Factors affecting the leachability of Ni/Co/Cu slags at high temperature. Hydrometallurgy 85, 42-52.

Banza, A.N., Gock, E., Kongolo, K., 2002. Base metals recovery from copper smelter slag by oxidizing leaching and solvent extraction. Hydrometallurgy 67, 63–69.

Chen, T.T., Dutrizac, J.E., Krause, E., Osborne, R., 2004. Mineralogical characterization of nickel laterites from new Caledonia and Indonesia, in: W.P. Imrie, D.M. Lane, S.C.C. Barnett, et al. (Eds.), Proceedings of the International Laterite Nickel Symposium—2004 Mineralogy and Geometallurgy, TMS, Charlotte, North Carolina, pp. 79–99.

Collins, R.J., Ciesielski, S.K., 1994. Recycling and use of waste materials and by-products in highway construction. Synthesis of Highway Practice No. 199. Transportation Research Board, Washington, DC.

Curlook, W., Papangelakis, V.G., 2004. Pressure acid leaching of non-ferrous smelter slags for the recovery of their base metal values, in: M.J. Collins, V.G. Papangelakis (Eds.), Pressure Hydrometallurgy 2004 (conference proceedings), Canadian Institute of Mining, Metallurgy and Petroleum, Montreal, pp. 823-837.

Das, B., Mishra, B.K., Angadi, S., Pradhan, S.K., Prakash, S., Mohanty, J., 2010. Characteerization and recovery of copper values from discarded slag. Waste Management & Research 28, 561-567.

Davenport,W.G., Jones, D.M.M., King, J., Partelpoeg, E.H., 2001. Flash smelting: analysis, control and optimization. The Minerals, Metals & Materials Society,Warrendale, Pa, p. 219.

Demetrio, S., Ahumada, S.A.J., Durán, M.A., Mast, E., Rojas, U., Sanhueza, J., Reyes, P., Morales, E., 2000. Slag cleaning: the Chilean copper smelter experience. JOM Journal of the Minerals, Metals and Materials Society 52, 20-25

Diaz, C., Conard, B.R., O'Neill, C.E., Dalvi, A.D., 1994. Inco roast-reduction smelting of nickel concentrate. CIM Bulletin, 87, 62-71.

Ettler, V., Nihaljevic, M., Touray, J.-C., Piantone, P., 2002. Leaching of polished sections: an intergrated approach for studying the liberation of heavy metals from lead–zinc metallurgical slags. Bulletin of Society of Geologists, France 173 (2), 161–169.

Georgiou, D., Papangelakis, V.G., 1998. Sulphuric acid leaching of a limonitic laterite: chemistry and kinetics, Hydrometallurgy 49, 23–46.

Gbor, P.K., Mokri, V., Jia, C.Q., 2000a. Characterization of smelter slags. Journal of Environmental Science and Health A35 (2), 147–167.

Gbor, P.K., Ahmed, I.B., Jia, C.Q., 2000b. Behavior of Co and Ni during aqueous sulphur dioxide leaching of nickel smelter slag. Hydrometallurgy 57, 13–22.

Gleeson, S.A., Butt, C.R.M., Elias, M., 2003. Nickel laterites: a review. SEG Newsletter 54, pp. 1 and 12-18.

Gonzalez, C., Parra, R., Klenovcanova, A., Imris, I., Sanchez, M., 2005. Reduction of Chilean copper slags: a case of waste management project. Scandinavian Journal of Metallurgy 34, 143–149.

Heinrich, G., 1989. On the utilization of nickel smelter slags. CIM Bulletin 82, 87-91.

Herreros, O., Quiroz, R., Manzano, E., Bou, C., Vinals, J., 1998. Copper extraction from reverberatory and flash furnace slags by chlorine leaching. Hydrometallurgy 49 (1–2), 87–101.

Jia, C.Q., Xiao, J.Z., Orr, R.G., 1999. Behaviour of metals in discard nickel smelter slag upon reacting with sulphuric acid, J. Environ. Sci. Health A34(5), 1013-1034.

Klein, L.C., Stevens, L.G. 1972. Recovery of copper values from slags. U.S. Patent, No. 3,632,308.

King, J.A., Dreisinger, D.B., Knight, D.A.,1993. The total oxidation of copper concentrates, in: R.G. Reddy, R.N. Weizenbach (Eds.), Extractive metallurgy of copper, nickel and cobalt (Proceedings of the Paul E. Queneau international symposium), The Minerals, Metals and Materials Society, pp. 735-756.

Krause, E., Singhal, A., Blakey, B.C., Papangelakis, V.G., Georgiou, D., 1997. Sulfuric acid leaching of nickeliferous laterites. In: W.C. Cooper, I. Mihaylov (Eds.), Proceedings of Nickel–Cobalt 97 Int. Symp., Hydrometallurgy and Refining of Nickel and Cobalt. Canadian Institute of Mining, Metallurgy and Petroleum, Montreal, pp. 441–458.

Li, Y., Perederiy, I., Papangelakis, V.G., 2008. Cleaning of waste smelter slags and recovery of valuable metals by pressure oxidative leaching. J. Haz. Mat. 152, 607-615.

Li, Y., Papangelakis, V.G., Perederiy, I., 2009. High pressure oxidative acid leaching of nickel smelter slag: Characterization of feed and residue. Hydrometallurgy 97,185-193.

Linblad, K.D., Dufresne, R.E., 1974. Acid leach of copper reverberatory slag—a new approach, J. Met. 26, 29–31.

Liu, H., Papangelakis, V.G., Alam, M.S., Singh, G., 2003. Solubility of hematite in H2SO4 solutions a7 230–270 °C. Canadian Metallurgical Quarterly 42 (2), 199–207.

Liu, J., 2004. Study of the kinetics of carbon reduction of matte/oxysulfide/slag in nickel/copper flash smelting. Ph.D. thesis, University of Toronto.

Manz, M., Castro, L.J., 1997. The environmental hazard caused by smelter slags from the Sta. Maria de la Paz mining district in Mexico, Environ. Pollution 98, 7–13.

Marcuson, S.W., Diaz, C.M., 2007. The changing Canadian nickel smelting landscape – late 19th century to early 21st century. Canadian Metallurgical Quarterly, 46, 33-46.

Matthew, I.G., Elsner, D., 1977. The hydrometallurgical treatment of zinc silicate ores. Metallurgical Transactions B 8B, 73-83.

Parsons, M.B., Bird, D.K., Einaudi, M.T., Alpers, C.N., 2001. Geochemistry and mineralogical controls on trace element release from the Penn Mine base-metal slag dump, California. Applied Geochemistry 16, 1567–1593.

Peek, E., Barnes, A., Tuzun, A., 2011. Nickeliferous pyrrhotite – ‘‘Waste or resource?’’ Minerals Engineering, 24, 625–637

Perederiy, I., Papangelakis, V.G., Jia, C.Q., 2009. Pressure oxidative leaching of slags from nickel smelters: an update. In: J.J. Budac, R. Fraser, I. Mihaylov, V.G. Papangelakis, D.J. Robinson (Eds.), Hydrometallurgy of nickel and cobalt (Proceedings of 39th annual Hydrometallurgy Meeting), Canadian Institute of Mining, Metallurgy and Petroleum, Montreal, 2009, pp. 87-96.

Perederiy, I., Papangelakis, V.G., Buarzaiga, M., Mihaylov, I. 2011. Co-treatment of converter slag and pyrrhotite tailings via high pressure oxidative leaching, J. Haz. Mat. (doi:10.1016/j.jhazmat.2011.08.012)

Rao, G.V., Nayak, B.D., 1992. Flotation of copper from converter slags. Journal of Mines, Metals & Fuels 40, 131.

Reid, M., Papangelakis, V.G., 2006. New data on hematite solubility in sulphuric acid solutions from 130 to 270 °C. In: Dutrizac, J.E., Riveros, P.A. (Eds.), Iron Control Technologies. CIM, Montreal, pp. 673–688.

H. Shen, E. Forssberg, An overviewof recovery of metals from slags, Waste Management 23 (2003) 933–949.

Sinha, S.N., Nagamori, M., 1982. Activities of CoS and FeS in copper mattes and the behavior of cobalt in copper smelting, Metallurgical Transactions 13B, 461-470.

Sobol, S.I., 1993. Chemistry and kinetics of oxidative sulphuric acid leaching of cobalt-bearing converter slags, in: Extractive Metallurgy of Copper, Nickel and Cobalt, vol.

1, Fundamental Aspects (Proceedings of the Paul E. Queneau International Symposium), TMS, Denver, pp. 803-811.

Stubina, N., Chao, J., Tan, C., 1994. Recent electric furnace developments at Falconbridge (Sudbury Operations). CIM Bulletin, 87, 57-61.

Sun, H., 2006. Inverstigation of physically entrained matte in the flash furnace slag. Ph.D. thesis, University of Toronto.

Toscano, P.A., 2001. Minimization of dissolved nickel and cobalt slag losses at high matte grades. M.A.Sc. thesis, University of Toronto.

Toscano, P., Utigard, T.A., 2003. Nickel, cobalt, and copper slag losses during converting. Metallurgical and Materials Transactions B, 34B, 121-125.

Vodyanitskii, Y.N., Plekhanova, I.O., Prokopovich, E.V., Savichev, A.T., 2011. Soil contamination with emissions of non-ferrous metallurgical plants. Eurasian Soil Science, 44, 217–226.

Whittington, B.I., Muir, D., 2000. Pressure acid leaching of nickel laterites: a review. Mineral Processing and Extractive Metallurgy Review 21, 6,527–599.

Whittington, B.I., Johnson, J.A., Quan, L.P., McDonald, R.G., Muir, D.M., 2003. Pressure acid leaching of arid-region nickel laterite ore. Part II. Effect of ore type, Hydrometallurgy 70, 47–62.

Wolf, A., 2008. Ni, Cu and Co recovery from Copper Cliff converter slag. M.A.Sc. Thesis, University of Toronto.

CHAPTER 2 EXPERIMENTAL EQUIPMENT AND PROCEDURES

2.1 Leaching Experiments

Leaching experiments were conducted in a 2 L titanium autoclave (manufactured by Parr Instrument Company) equipped with a custom-made acid injector consisting of a stainless steel cylinder connected to an oxygen supply via a PID pressure controller. Injection of acid and subsequent feeding of oxygen was performed through a tantalum dip tube.

Solution samples were collected by filtering out solids with an *in situ* filter (graphite 45 µm or titanium 5-40 µm) and withdrawing the liquid via a water-cooled heat exchanger. The removal of the filter in one experiment made it possible to withdraw solid samples at various times by flashing.

The autoclave was stirred at 700-800 rpm by two 4-blade impellers on a shaft connected to a magnetic drive. A schematic of the experimental setup is shown in Fig. 2.1.

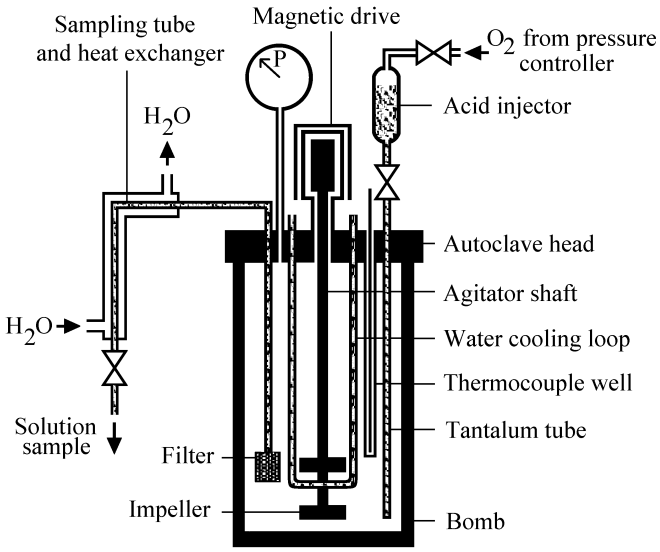

Fig. 2.1 Experimental setup

Due to the sensitivity of water vapour pressure to temperature at 250°C (±10 psi or 0.7 bar for ±1°C), the pressure setpoint on the controller was continuously adjusted with the help of computer software based on autoclave temperature readings such that oxygen partial pressure remained with minimal oscillations.

Temperature setpoint was maintained by a PID controller through both electric heating and water cooling of the autoclave. The retention time was counted from the moment of oxygen introduction into the system, which typically occurred at 20°C below the setpoint. Samples were withdrawn at time intervals of 5 min and greater.

Flashed slurry samples were diluted with water upon collection and filtered in 10-15 min after collection. Following the initial filtration, the residues were washed with a 5 g/L solution of sulphuric acid and then with deionized water. The residues were then vacuum-dried ~70-80°C in an oven within a few hours.

Upon test completion, the autoclave was cooled to 70°C and depressurized. Cooling typically took ~15 min. The slurry was filtered, and the cake of the primary filtration was washed (on the filter) with 0.5 L of 5 g/L H_2SO_4 followed by 0.5-1 L of water. The residue was then dried at ~70-80°C in an oven for 1-3 days.

2.2 Measurement of Conductivity and Acidity Estimation

The experimental setup was retrofitted in some experiments with a modified electrodeless conductivity sensor (Fig. 2.2) from Foxboro Inc. The sensor contained two toroidal coils placed inside a glass enclosure with empty spaces filled with alumina powder (Saini and Papangelakis, 2009).

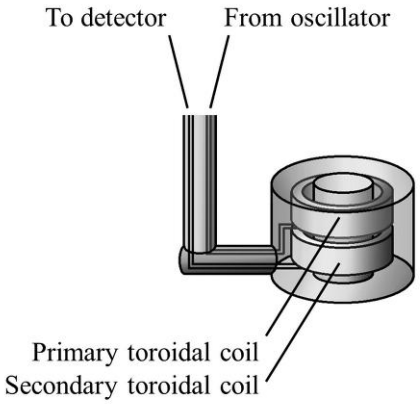

Fig. 2.2 Electrodeless conductivity sensor

The conductivity measurements were used to estimate acidity online following a procedure previously established by Huang and Papangelakis (2008). The estimated and

measured (by titration) acidities were compared using the average relative deviation (ARD).

$$ARD = \frac{\Sigma\left|\frac{c_{\exp} - c_{calc}}{c_{\exp}}\right|}{N} \times 100\% \tag{2.1}$$

2.3 Chemical Analysis

Intermediate solution samples, filtrates as well as solutions after and residue digestion were analyzed for metals, silicon and sulphur using Inductively Coupled Plasma – Optical Emission Spectroscopy (ICP-OES). All concentrations reported are based on solution volume at 25°C.

The extractions *at temperature* (*solution-based*) reported in sections 4.2 and 4.3 (except 4.3.3) were calculated according to the following equation:

$$\alpha_i = \frac{\sum_{j=1}^{i} c_j V_j + c_i(\hat{V} - \sum_{j=1}^{i} V_j)}{X_s \cdot m_s} \cdot 100 \tag{2.2}$$

c_i, c_j – concentrations in the i-th and j-th (of N) samples [g/L],
V_j – volume of the j-th sample [L],
$\hat{V}$ – initial volume of solution inside the autoclave (based on room temperature) [L],
X_s, m_s – metal mass fraction in the slag and the mass of the slag [g/g, g].

The denominator of the fraction represents the total amount of metal loaded into the autoclave with the feed material (slag).

Final *residue-based* extractions were calculated as follows:

$$\alpha = 100 - \frac{X_r \cdot m_r}{X_s \cdot m_s} \cdot 100 \tag{2.3}$$

X_r, m_r – metal mass fraction in the residue and the mass of the residue [g/g, g].

Residue-based extractions in excess of 50% being less sensitive to analytical errors were used to verify solution-based extractions. The difference did not exceed 5% units.

Eq. 2.2. was deemed unsuitable for experiments involving pyrrhotite tailings due to feed inhomogeneity causing variation in the amount of metal loaded into the autoclave with the feed. The following equation was used instead to calculate the extractions reported in section 4.3.3 and further:

$$\alpha_i = \frac{\sum_{j=1}^{i} c_j V_j + c_i(\hat{V} - \sum_{j=1}^{i} V_j)}{\sum_{j=1}^{N} c_j V_j + c_F V_F + c_W V_W + X_r \cdot m_r} \cdot 100 \qquad (2.4)$$

c_i, c_j – concentrations in the i-th and j-th (of N) samples [g/L],
V_j – volume of the j-th sample [L],
$\hat{V}$ – initial volume of solution inside the autoclave (based on room temperature) [L],
c_F, c_W – concentrations in the primary and wash filtrates [g/L],
V_F, V_W – volumes of the primary and wash filtrates [L],
X_r, m_r – metal mass fraction in the residue and the mass of the residue [g/g, g].

The denominator of the fraction (Eq. 2.4) estimates the total amount of metal loaded into the autoclave by taking into account the amount of metal leaving the autoclave with the solution samples, filtrates and the residue. When applied to experiments using a slag feed (section 4.3.3), this equation improves the extraction calculations by 3% in comparison with Eq. 2.2.

Free sulphuric acid in solutions was determined by titration with NaOH in the presence of CaCDTA as a masking agent. Fe(II) was determined by express-titration with $KMnO_4$ and verified with $K_2Cr_2O_7$ for select samples (Kolthoff et al., 1969; Vogel, 1989; Mermet et al., 2004).

2.4 Solids Characterization

The particle size distributions of the powder materials were determined using a light scattering technique with a Malvern Mastersizer S instrument.

Powder X-ray diffraction (XRD) patterns were obtained on a Philips instrument using Cu Kα x-rays.

Cross-section images of slag were obtained on a JEOL JSM-840 scanning electron microscope utilizing back-scattered electrons (BSE) at 15-20 keV accelerating potential difference. Energy-dispersive X-ray (EDX) spectra were obtained with the same instrument. The intensities of Kα lines were used to construct elemental maps of slag particles with a resolution of 200 by 100 points.

Elemental spot analysis of slag particles was performed by measuring the intensities of Kα X-rays using Wavelength Dispersive X-ray Spectroscopy (WDS) on a Cameca SX50 electron microprobe instrument.

References

Mermet, J.M., Otto, M., Valcarcel, M. 2004. Analytical Chemistry, second ed., Wiley–VCH Verlag Gmbh & Co. KGaA, Weinheim, 2004, p. 344.

Huang, M., Papangelakis, V.G., 2008. Online free acidity measurement of solutions containing base metals, Can. Metall. Quart. 47, 269-276.

Kolthoff, I.M. et al., 1969. Quantitative chemical analysis, 4th edition. Macmillan, New York.

Saini, R.S., Papangelakis, V.G., 2009. On-line acid measurements via electrodeless conductivity in HPAL processes for Ni/Co extraction, in: J.J. Budac, R. Fraser, I. Mihaylov, V.G. Papangelakis, D.J. Robinson (Eds.), Hydrometallurgy of nickel and cobalt (Proceedings of 39th annual Hydrometallurgy Meeting), Canadian Institute of Mining Metallurgy and Petroleum, Montreal, pp. 87-96.

Vogel, A.I., 1989. Vogel's textbook of quantitative chemical analysis, 5th edition. Wiley, New York.

CHAPTER 3 CHARACTERIZATION OF SMELTER SLAGS

This chapter describes the slag materials used as feed in the leaching experiments in this study. The following materials have been tested: crystalline (naturally cooled) flash furnace slag, crystalline converter slags (one naturally cooled and one granulated), amorphous (granulated) electric furnace slag. Characterization of the flash furnace slag (section 3.1) is credited to Y. Li and was published in co-authorship with V.G. Papangelakis and I. Perederiy (Li et al., 2009). The other sections in this chapter contain excerpts from the following manuscripts

- Perederiy, I., Papangelakis, V.G., Buarzaiga, M., Mihaylov, I, 2011. Co-treatment of converter slag and pyrrhotite tailings via high pressure oxidative leaching, J. Haz. Mat.
- Perederiy, I., Papangelakis, V.G. High pressure oxidative leaching of crystalline converter slags: leaching mechanism (in preparation)
- Perederiy, I., Papangelakis, V.G. High pressure oxidative leaching of amorphous FeO-SiO_2 slag: leaching mechanism (in preparation)

3.1 Crystalline Flash Furnace Slag

The flash smelter slag originated from the Copper Cliff smelter (Sudbury, Ontario). The slag sample was crushed, ground and sieved into samples with various particle size distributions (Appendix B). The leaching experiments described in section 4.2 were conducted with two samples, the particle size distributions of which are shown in Fig. 3.11, and the chemical compositions are given in Table 3.1. Iron and silicon are the main elements accounting for 57.5%wt of the slag mass. Nickel and copper each constitute around 1% of slag mass together with some cobalt (0.24%wt). Sulphur accounts for 1.54% as sulphide phases.

Table 3.1 Assay of flash furnace slag, %wt

Sample	Ni	Co	Cu	Zn	Al	Si	S	Mg	Ca	Fe(II)	Fe(tot)
#0	1.02	0.24	1.07	0.14	1.65	17.7	1.54	0.80	0.79	34.7	39.8
#2	1.04	0.24	1.06	0.14	1.64	17.9	1.56	0.80	0.70	36.0	41.0

The diffractogram shown in Fig. 3.1 indicates that the slag consists of fayalite (Fe_2SiO_4) and magnetite (Fe_3O_4). The distinctly strong and narrow fayalite peaks demonstrate a high degree of crystallinity obtained during natural cooling (Baghalha et al., 2007; Curlook et al., 2004). The weak peaks detected at 2θ values of 30.22°, 35.58°, 43.30°, 57.08° and 62.70° are consistent with the existence of spinel magnetite which is formed under high oxygen overpressure at a high temperature during smelting (Gilchrist, 1989) as per Eq. 1.2.

Fayalite, the main component of slag, is the iron-rich end member of olivine solid-solution. It crystallizes in the orthorhombic system with cell parameters a 4.82 Å, b 10.48 Å and c 6.09 Å. Fayalite can be dissolved in acid even at pH 2 in fully oxygenated and anoxic solutions to release iron and silica (Santell et al., 2001). This property makes it possible to liberate the entrapped Ni, Co and Cu by acid leaching.

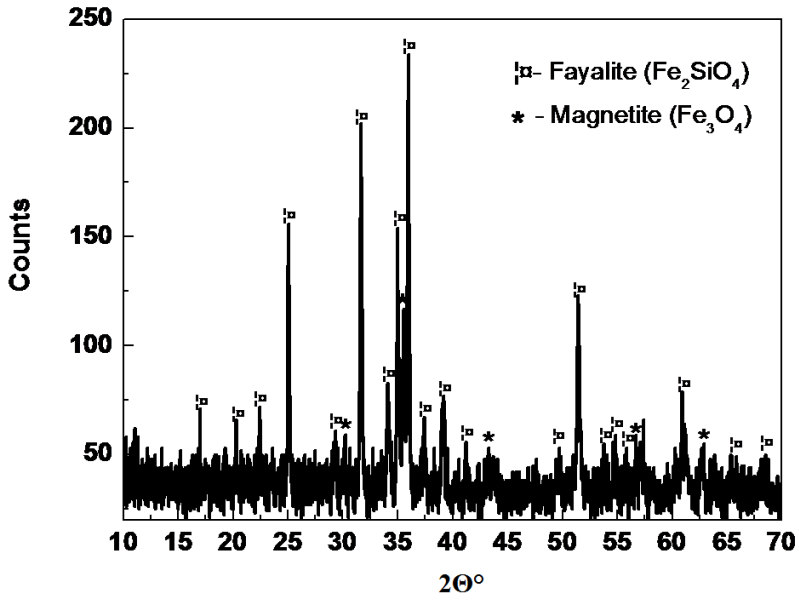

Fig. 3.1 Powder X-ray diffractogram of flash furnace slag (sample #0)

Assuming magnetite is the only significant phase containing Fe(III), the slag is estimated to contain 11%wt of magnetite and 59% of fayalite by weight (1:5.4 ratio) based on the chemical analysis shown in Table 1. Based on the silicon content, 20% of SiO_2 present is free amorphous silica or metal silicates, except for fayalite. The rest of the slag (10%) includes metal oxides such as MgO, CaO, Al_2O_3.

Fig. 3.2 shows SEM images and EDX spectra of a sectioned block sample. A backscattered electron (BSE) image shown in Fig. 3.2(a) is accompanied by a higher-resolution, enlarged view – Fig. 3.2(b). EDX measurements were carried out on different areas and the typical EDX spectra are shown in Fig. 3.2(c) to (f). Four distinct phases, fayalite (Fe_2SiO_4), silica (SiO_2), matte (MeS_x) and magnetite (Fe_3O_4) were identified. The bright-white small dots (e.g., *Area 1*), 2-20 μm in diameter, are entrapped matte droplets as confirmed by the EDX spectrum shown in Fig. 3.2(c). The large dark grey region (*Area 2*) is fayalite. As expected, large amounts of silicon and iron, as well as a trace portion of magnesium appeared in this area, as shown in Fig. 3.2(d). The EDX spectrum in Fig. 3.2(e) came from the small dark-colored region (*Area 3*).The predominant counts of silicon and small counts of potassium, calcium and aluminum in Fig. 3.2(e) indicate that silica is in a mixture with some (K, Ca, Al)-containing silicates such as feldspar. The light-grey regions (e.g., *Area 4*) were identified with the help of the EDX spectrum in Fig. 3.2(f) as spinel magnetite (Fe_3O_4 or $FeFe_2O_4$) crystals with a small portion of Cr being a substitution in a possible form of $FeCr_2O_4$

Fig. 3.3(a) shows a BSE image of a matte inclusion from another area. The point microanalysis results at *positions 1, 2 and 3* are shown in Fig. 3.3(b), (c) and (d), respectively. An uneven distribution of base metals was found in this particle. At *position 1*, strong copper peaks and distinct iron and zinc peaks are present, but no significant amount of sulphur was detected. However, this particle contains a large amount of sulphur as well as a moderate amount of iron and a small amount of copper at *position 2* (Fig. 3.3(c)). At *position 3* (Fig. 3 (d)), besides sulphur, iron and copper, a small amount of nickel was detected.

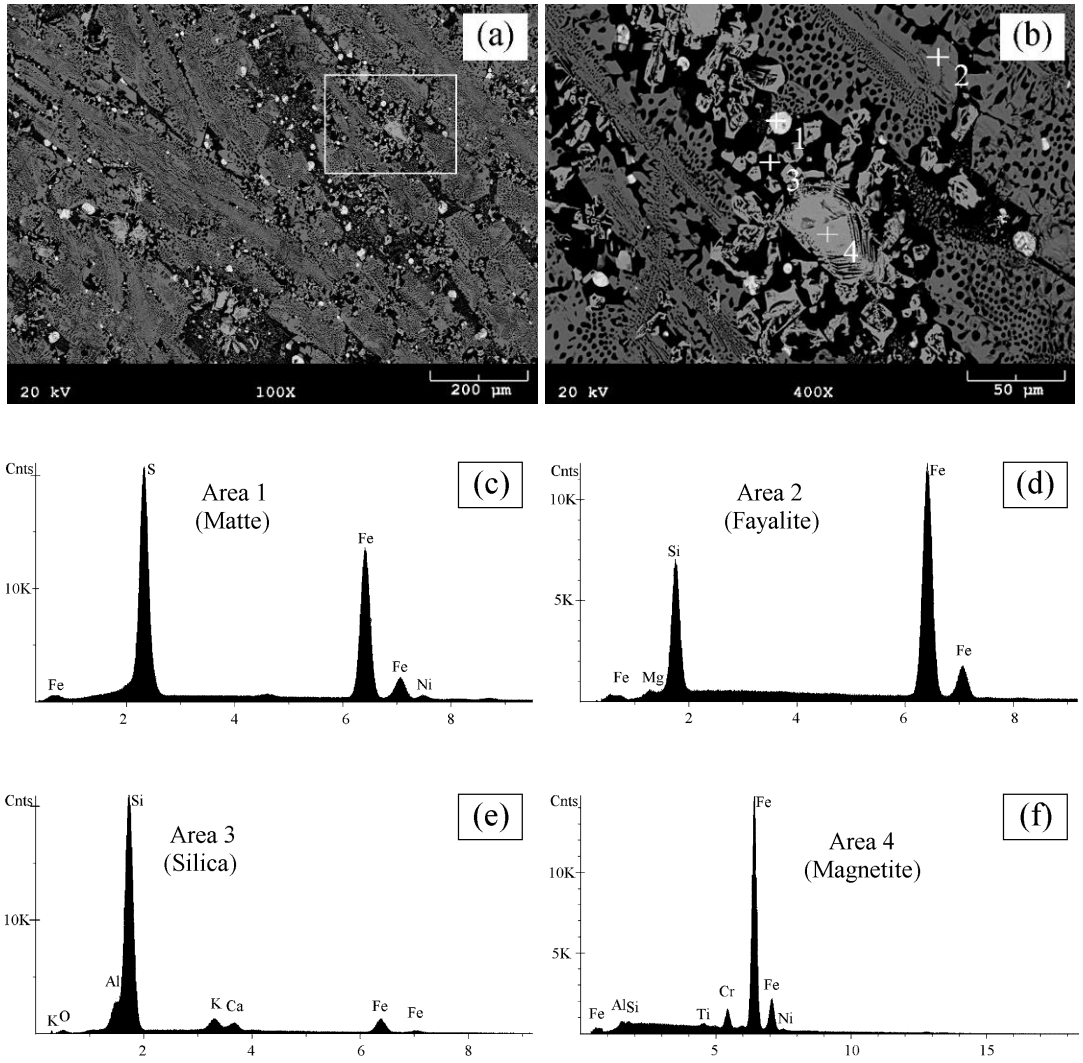

Fig. 3.2 BSE images and EDX spectra of a slag sample.EDX x-axis: energy, keV

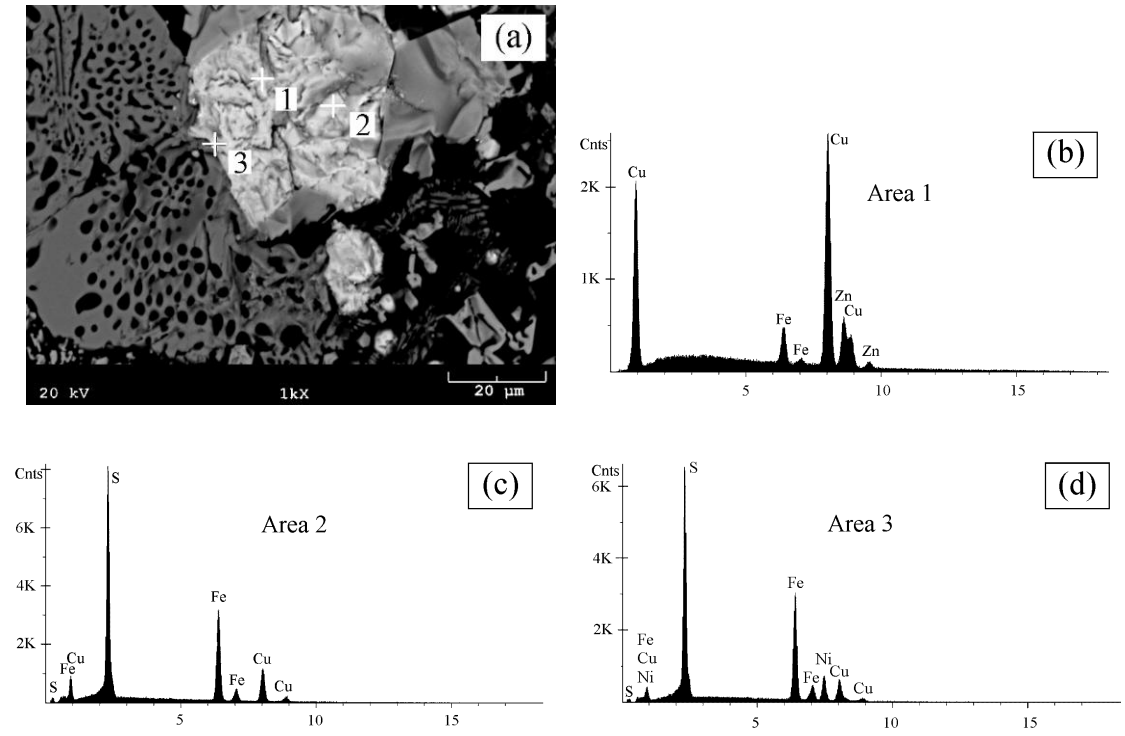

Fig. 3.3 BSE images and EDX spectra of a matte particle. EDX x-axis: energy, keV

An additional image of the slag as well as X-ray elemental maps are shown in Appendix C.

3.2 Crystalline Converter Slags

3.2.1 Naturally cooled converter slag

Two Copper Cliff converter slag samples used in this work were obtained from the core portion of a ladle after natural cooling. The samples were crushed and ground, and the final particle size distribution (shown in Fig. 3.11) was chosen such as to ensure that all particles could be suspended by stirring, keeping the grinding to the minimum. Both slags were found to be similar in terms of their chemical compositions (Table 3.2), and indistinguishable in terms of microstructure, as revealed by SEM-BSE (Fig. 3.4).

Table 3.2 Assay of converter slag samples, %wt.

Sample	Ni	Cu	Co	Zn	Fe	S	Si	Al	Ca	Mg	K	Pb	Mn	Cr
#1	1.05	0.69	0.63	0.16	52.8	0.77	12.1	0.17	0.08	0.06	0.04	0.04	0.02	0.02
#2	1.07	0.68	0.67	0.15	52.5	0.76	12.7	0.20	0.09	0.07	0.08	0.07	0.02	0.01

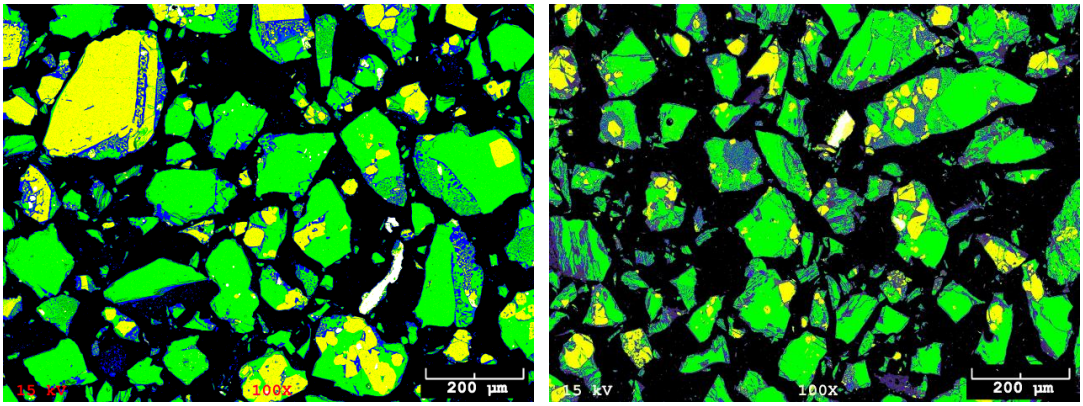

Fig. 3.4 Colour-coded SEM-BSE images of sample #1 (left) and #2 (right): green – fayalite, yellow – magnetite, blue – silica, white – matte

Natural cooling led to the formation of well-developed crystalline fayalite (Fe_2SiO_4) and magnetite (Fe_3O_4) as shown by XRD (Fig. 3.5). The ratio of magnetite to fayalite determined with Rietveld refinement of powder X-ray diffractograms is ~ 1:4 (by weight). Such elevated ratios are typical in slags produced in the beginning of a converting process (Appendix A).

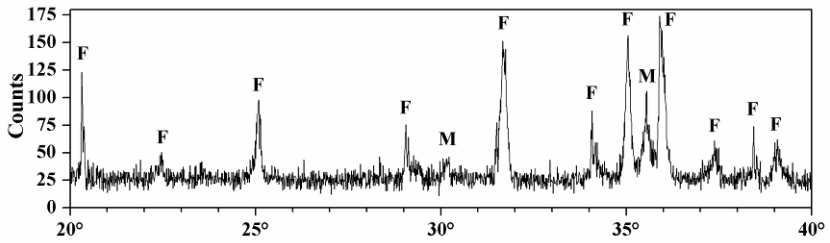

Fig. 3.5 Powder X-ray diffractogram of converter slag (Symbols: F - fayalite, M - magnetite)

SEM-BSE cross-section images of typical multi-phase slag particles (Slag #2) are shown in Fig. 3.6. Four mineral phases were identified with the help of EDX spectra: fayalite, magnetite, silica and mixed matte. *Areas A and 1* on Fig. 3.6 represent fayalite, the mesh-like structure of which suggests that it contained dissolved silica, which segregated during solidification. Matte appeared in the form of entrapped droplets in *areas B and 4* and in several other bright spots. Ni:Cu:Fe ratios in matte particles were found to be highly variable from particle to particle, with Cu-Fe matte being more abundant than Ni-Fe matte. Magnetite usually appeared as large chunks (*areas C and 2*) as well as small

inclusions in silica (around *area C*). Silica usually surrounded fayalite and magnetite such as in *areas D and 3*. Copper and nickel were encountered within matte inclusions, although in rare cases very small peaks for nickel were also seen on EDX spectra for fayalite and magnetite. Cobalt was never observed due to its high dispersion in the silicate-oxide phases as well as overlapping of its Kα spectral lines with those of iron.

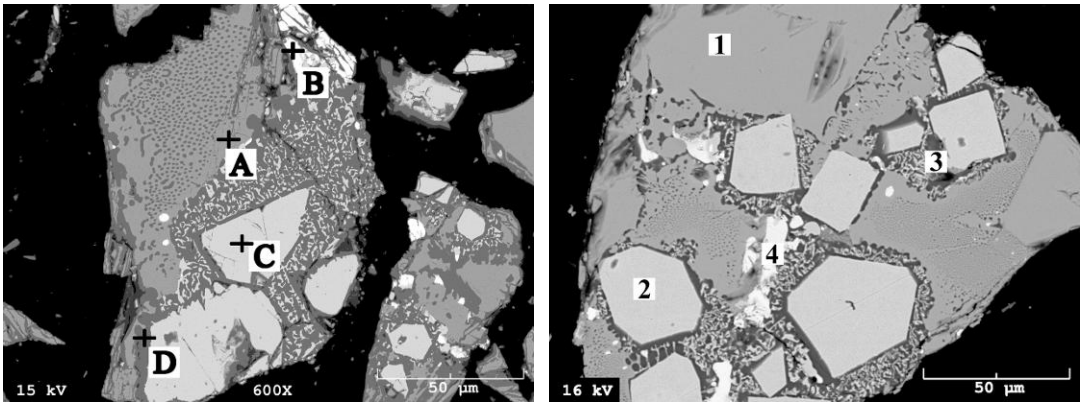

Fig. 3.6 SEM-BSE images of typical multi-phase converter slag particles

Elemental maps (Fig. 3.7) of the particle shown in Fig. 3.6 (right) were obtained with the help of Energy Dispersive Spectrometry (EDX). It can be seen that sulphur (sulphide) and oxygen (oxide) zones are mutually exclusive. The bulk of Cu as well as minute amounts of Fe are associated with sulphur, while Ni, Al, Ca, Mg, Si and the bulk of Fe are associated with oxygen. Si is seen present in fayalite as well as around magnetite in higher concentrations. Significant concentrations of Al are encountered in association with the silica component of the slag which indicates that Al may exist as aluminium silicate rather than dissolved oxide. Ca and Mg are present in noticeable quantities only in a few small spots which are, like Al, associated with silica. Ni is found only in a very dilute form which makes it difficult to distinguish its counts from the background noise. Slightly higher counts associated with magnetite can be explained by the presence of trevorite ($NiFe_2O_4$) dissolved in magnetite, as was the case with two different furnace slags characterized by Gbor et al. (2000).

Fayalite zones in a few random slag particles were probed using an electron microprobe equipped with detectors for Wavelength Dispersive X-ray Spectroscopy (WDS). The

elemental compositions obtained with WDS are presented in Table 3.3. The reduced ratio of Fe:Si in some points is due to silica inclusions in fayalite – such as those seen in Fig. 3.6 (around area A).

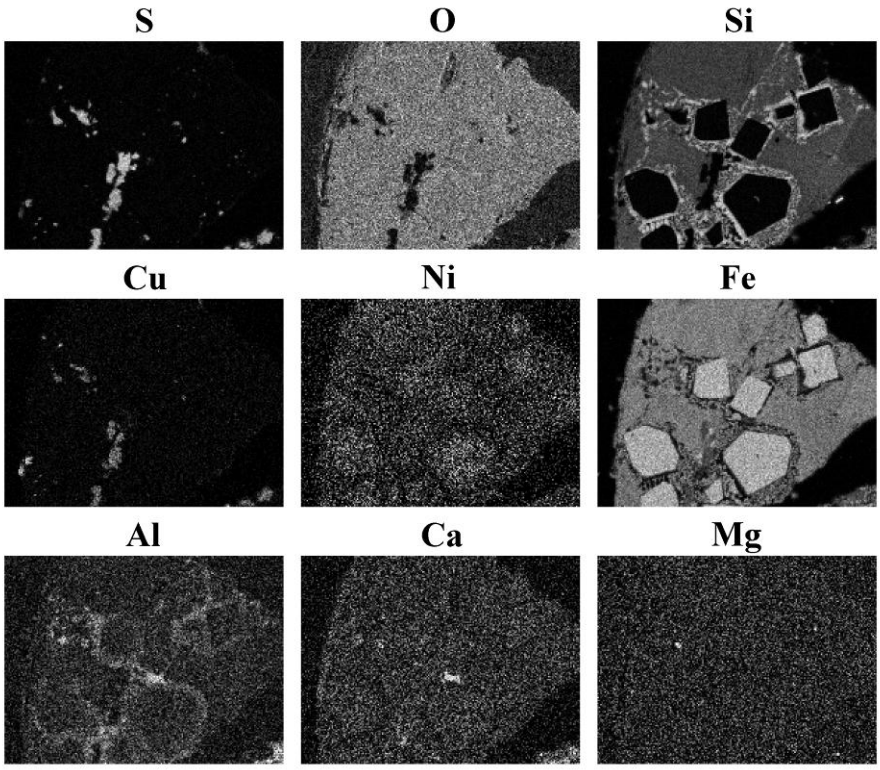

Fig. 3.7 Elemental maps of a converter slag particle

Table 3.3 Elemental contents (in wt%) in a fayalite standard and converter slag determined with the help of WDS

Material	Fe	Si	Al	Mg
Fayalite standard	54.9	13.8	0.0	0.0
Fayalite in slag	48.9-53.3	13.7-15.9	0-0.1	0-0.1

Additional SEM images and elemental maps can be found in Appendix D.

Overall, the mineralogy of the converter slags used in this work is similar to the flash furnace slag described in section 3.1 (Li et al., 2009), although the ratio of the constituting minerals is different.

3.2.2 Granulated converter slag

A portion of the naturally-cooled converter slag sample #1 was re-melted at 1270°C in an Al_2O_3 crucible for 3 hours. The melt was then quenched with the help of a shower-type granulator (Fig. 3.8).

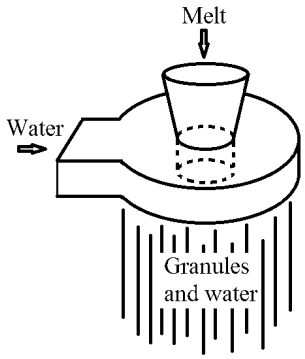

Fig. 3.8 Shower-type granulator

The composition of the granulated slag is compared to the original naturally-cooled samples in Table 3.4. Re-melting resulted in a small increase in the content of Al due to partial dissolution of the crucible. Ni content dropped during re-melting – probably due to metal concentration in the crust on the walls of the crucible.

Table 3.4 Assay of the natural-cooled and granulated slag samples

Feed	Ni	Co	Cu	Zn	Fe	Al	Mg	Ca	Si	S
Naturally cooled	1.05	0.63	0.69	0.16	52.8	0.17	0.06	0.08	12.1	0.77
Granulated	0.67	0.56	0.62	0.13	51.3	0.41	0.24	0.16	12.7	0.93

The granulated material retained its crystalline structure as can be seen from the X-ray diffractogram (Fig. 3.9). However, rapid solidification suppressed the development of large areas of magnetite and silica observed in the naturally-cooled samples. An SEM-BSE image of a typical particle is shown in Fig. 3.10. Magnetite crystallized in the form of needles surrounded not by pure silica but a solution of silica in fayalite. Matte is present as fine inclusions dispersed in the fayalite matrix.

The granulated material was ground to a particle size shown in Fig 3.11.

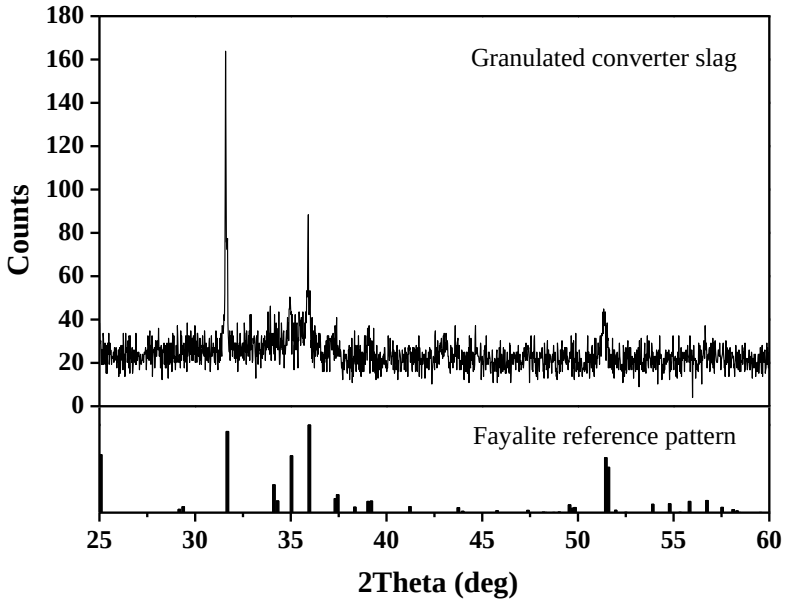

Fig. 3.9 Powder X-ray diffractogram of granulated converter slag

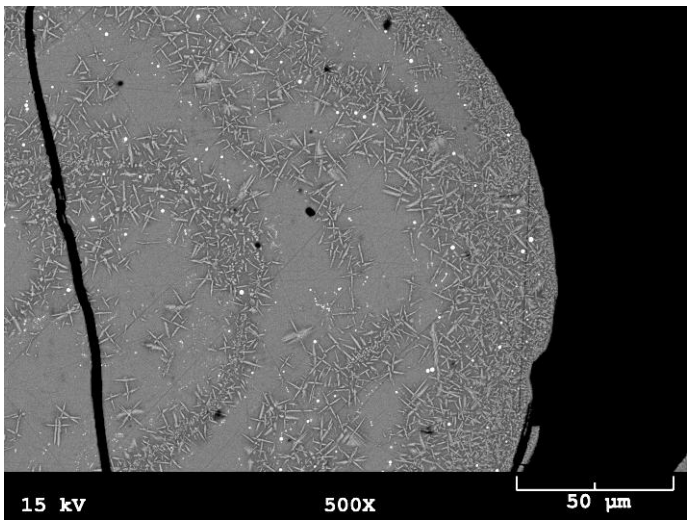

Fig. 3.10 SEM-BSE cross-section image of a typical granulated slag particle.
(White dots - matte, brighter needles - magnetite, light grey background – fayalite)

3.3 Amorphous Electric Furnace Slag

An electric furnace slag with a composition shown in Table 1 was obtained by granulation at the smelter. The material was ground to the same size (Fig. 3.11) as the naturally-cooled converter slag. A powder X-ray diffractogram (Fig. 3.12) confirms that the slag is mainly amorphous with occasional fine inclusions of magnetite (Fe_3O_4) and matte (MeS_x). SEM imaging (Fig. 3.13, Appendix E) reveals that the slag is largely

homogeneous. The composition of the slag material can be approximated by the following formula: $1.04FeO \cdot 0.3MgO \cdot 0.12Al_2O_3 \cdot SiO_2$ (in comparison, fayalite is represented as $2FeO \cdot SiO_2$). Some particles (Fig. E2) contain zones with tightly intergrown fine crystalline phases (iron silicates enriched in Al or Mg). The non-random arrangement of magnetite inclusions in some particles (Fig. E4) suggests that the structure of amorphous silicate may be anisotropic.

Table 3.5 Amorphous slag assay, %wt.

Ni	Cu	Co	Zn	Fe	S	Si	Al	Ca	Mg	Na	K
0.23	0.27	0.12	0.10	32.7	0.56	15.9	3.6	1.37	3.13	1.22	0.62

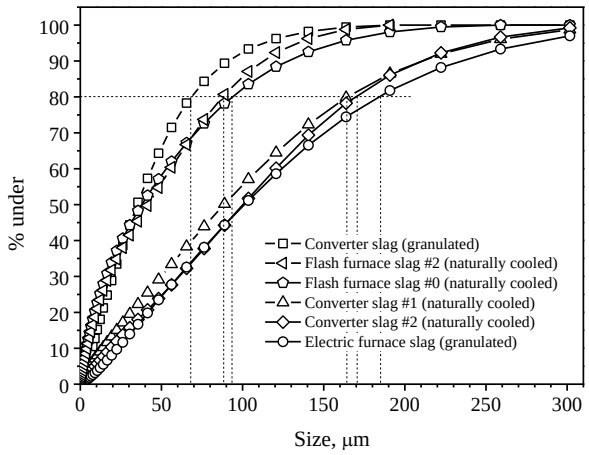

Fig. 3.11 Particle size distribution of the ground slag materials

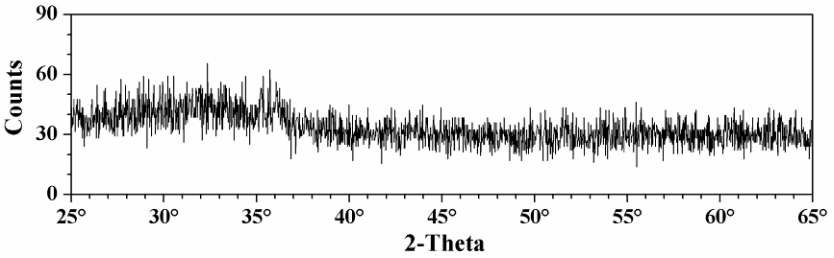

Fig. 3.12 Powder XRD of amorphous electric furnace slag

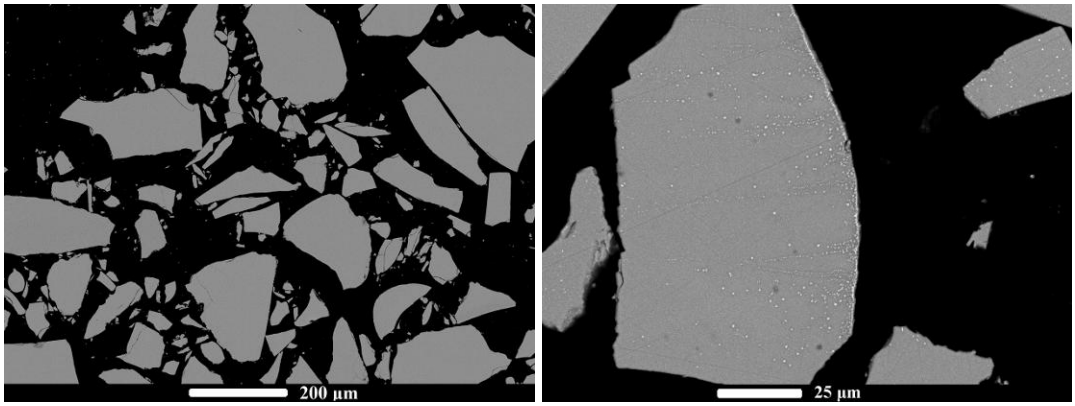

Fig. 3.13 SEM-BSE images of slag particle cross sections

A slag particle milled with a focused ion beam to a thickness of a few tens of nanometers was examined with the help of scanning transmission electron microscopy for signs of nano-scale structure. Excluding entrapped matte droplets, the slag was found to be homogeneous on the scale in excess of 4 nm.

3.4 Summary

Crystalline slag samples contain fayalite (Fe_2SiO_4) as the dominant mineral phase. Natural cooling promotes the segregation and growth of magnetite (Fe_3O_4) zones, which are often surrounded by silica (SiO_2). Granulation can lead to poorly segregated crystalline structures or homogeneous amorphous solid solutions of FeO, SiO_2 and other metal oxides with minor inclusions of fine matte and magnetite.

Considering the fact that large portions of nickel and cobalt are dissolved in the oxide and silicate mineral phases, and that matte inclusions are often only a couple of micrometers in diameter, flotation is not effective for the removal of base metals from slags. As a result, the base metals need to be chemically liberated.

References

Baghalha, M., Papangelakis, V.G., Curlook, W., 2007. Factors affecting the leachability of Ni/Co/Cu slags at high temperature. Hydrometallurgy 85, 42-52.

Curlook, W., Papangelakis, V.G., 2004. Pressure acid leaching of non-ferrous smelter slags for the recovery of their base metal values, in: M.J. Collins, V.G. Papangelakis (Eds.), Pressure Hydrometallurgy 2004 (conference proceedings), Canadian Institute of Mining, Metallurgy and Petroleum, Montreal, pp. 823-837.

Gbor, P.K., Mokri, V., Jia, C.Q., 2000a. Characterization of smelter slags. Journal of Environmental Science and Health A35 (2), 147–167.

Gilchrist, J.D., 1989. Extractive Metallurgy, 3rd ed. Pergamon Press, Toronto, Canada, p. 205.

Li, Y., Papangelakis, V.G., Perederiy, I., 2009. High pressure oxidative acid leaching of nickel smelter slag: Characterization of feed and residue. Hydrometallurgy 97,185-193.

Perederiy, I., Papangelakis, V.G., Buarzaiga, M., Mihaylov, I., 2011. Co-treatment of converter slag and pyrrhotite tailings via high pressure oxidative leaching, J. Haz. Mat. (doi:10.1016/j.jhazmat.2011.08.012).

Perederiy, I., Papangelakis, V.G. High pressure oxidative leaching of crystalline converter slags: leaching mechanism (in preparation)

Perederiy, I., Papangelakis, V.G. High pressure oxidative leaching of amorphous FeO-SiO2 slag: leaching mechanism (in preparation)

Santell, C.M., Welch, S.A., Westrich, H.R., Banfield, J.F., 2001. The effect of Fe-oxidizing bacteria on Fe-silicate mineral dissolution. Chemical Geology 180, 99–115.

CHAPTER 4 LEACHING OF CRYSTALLINE SLAGS

This chapter focuses on the leaching of various crystalline slags. The effect of temperature, acidity, oxygen partial pressure and slag mineralogy are discussed. The chemistry of leaching is identified, and the mechanism of leaching is deduced based on solution analysis and characterization of residues.

Characterization of the residues of flash furnace slag leaching (section 4.1.4) is credited to Y. Li and was published in co-authorship with V.G. Papangelakis and I. Perederiy (Li et al., 2009). The other sections in this chapter contain excerpts from the following manuscripts

- Perederiy, I., Papangelakis, V.G., Buarzaiga, M., Mihaylov, I., 2011. Co-treatment of converter slag and pyrrhotite tailings via high pressure oxidative leaching, J. Haz. Mat.
- Perederiy, I., Papangelakis, V.G. High pressure oxidative leaching of crystalline converter slags: leaching mechanism (in preparation)

4.1 Leaching of Flash Furnace Slag

4.1.1 Effect of temperature

Fig. 4.1 shows extractions of base metals in 2 hours as a function of temperature at 20%wt solids loading, 83.3 g/L initial H_2SO_4 (acid to slag ratio 0.33), 0-73 psi (0-5 bar) O_2, flow rate restricted at 2 sccm/g of slag (the conditions were selected based on preliminary work). Extractions increase with temperature from 175 to 250°C. Cobalt is leached preferentially from the slag at lower temperatures. Nickel is similar to copper in terms of leachability. From a mineralogical study (Gbor et al., 2000), it is known that cobalt mainly exists in the slag in the oxide form which can be easily dissolved by acid. However, nickel and copper exist in the slag as sulphides, which are finely dispersed matte inclusions. It appears that high temperatures are required to dissolve them.

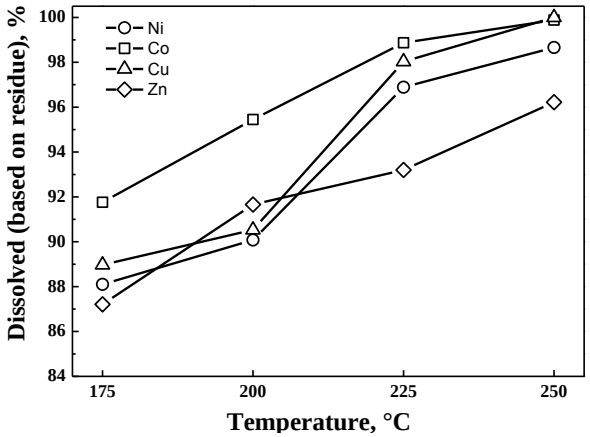

Fig. 4.1 Base metal extractions versus temperature within 2h. Sample #2, 20% solids, initial acidity 83.3 g/L (A/S 0.33), 0-73 psi (0-5 bar) O_2 (flow rate: 2 sccm/g of slag), 700 rpm

Fig 4.2 shows that the degree of iron solubilization decreases with an increase in temperature. Thus, a temperature of 250°C or higher is preferable in terms of leaching selectivity of base metals versus iron.

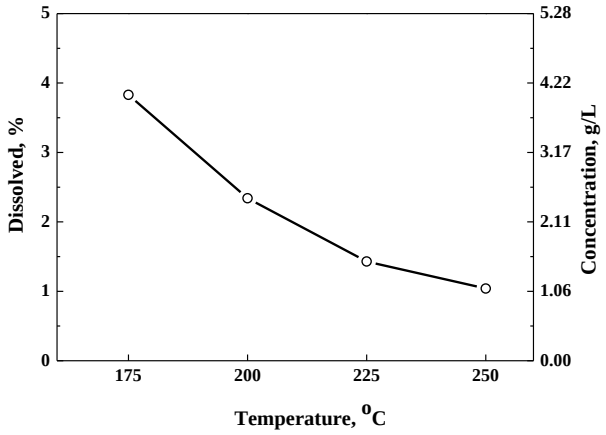

Fig. 4.2 Effect of temperature on iron dissolution (at temperature). Sample #2, 20% solids, initial acidity 83.3 g/L (A/S 0.33), 0-73 psi (0-5 bar) O_2 (flow rate: 2 sccm/g of slag), 700 rpm, 2 hours

4.1.2 Effect of acid addition

A series of tests were performed at 250°C with acid addition levels ranging from 15 to 30% of the slag mass, which corresponds to the initial acid concentrations of 50 to 100

g/L at 25% solids loading. The extractions of metal values after two hours of leaching are shown in Fig. 4.3. It can be seen that 67 g/L of initial H_2SO_4 is sufficient to extract 97% of Ni, Co and Cu. Further increase in acidity does not improve the extractions of base metals, but increases the extent of iron dissolution (Fig. 4.4) both at 250°C and after cooling and filtration.

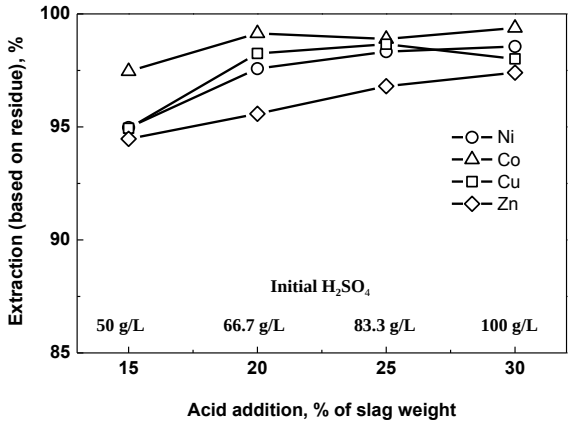

Figure 4.3 Effect of acid addition on metal extraction. Sample #0, 250°C, 25% solids, 0-73 psi (0-5 bar) O_2 (flow rate: 2 sccm/g of slag), 700 rpm, 2 hours

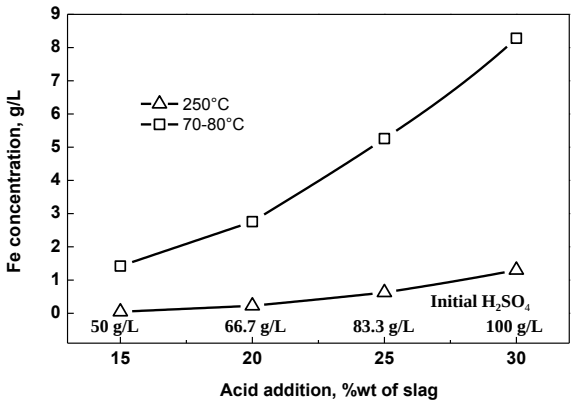

Fig. 4.4 Effect of acid addition on iron dissolution. Sample #0, 250°C, 25% solids, 0-73 psi (0-5 bar) O_2 (flow rate: 2 sccm/g of slag), 700 rpm, 2 hours

4.1.3 Kinetics and chemistry of leaching

The kinetics of base metal dissolution as well as iron and acid profiles are shown in Fig. 4.5 (250°C, 25%wt solids, initial H_2SO_4 83 g/L). Extraction of Ni, Co an Cu exceeded 90% in 20 min, and the final extractions after 2 hours were ~97%. The experiment was run at very low oxygen partial pressures (5-10 psi or 0.3-0.7 bar) for the initial 15 min

due a restriction in the flow rate of oxygen (2 sccm / g of slag). This resulted in the build-up of Fe(II) and a sharp drop in H_2SO_4 at 10 min (Eq. 4.1 and 4.2).

$$Fe_2SiO_4 + 4H^+ = 2Fe^{2+} + Si(OH)_{4(aq)} \quad (4.1)$$

The silicic acid produced is removed from the solution as silica (Eq. 1.7).

$$Fe_3O_4 + 8H^+ = Fe^{2+} + 2Fe^{3+} + 4H_2O \quad (4.2)$$

Oxygen at this point is rapidly consumed to oxidize Fe(II) and matte (Eq. 4.3 and 4.4).

$$Fe^{2+} + {}^1/_4O_2 + H^+ = Fe^{3+} + {}^1/_2H_2O \quad (4.3)$$

$$MeS_{n<1} + (0.5+1.5n)O_2 + (2-n)H^+ = Me^{2+} + nHSO_4^- + (1-n)H_2O \quad (4.4)$$

Ferric iron does not accumulate significantly due to hydrolysis:

$$2Fe^{3+} + 3H_2O = Fe_2O_3 + 6H^+ \quad (4.5)$$

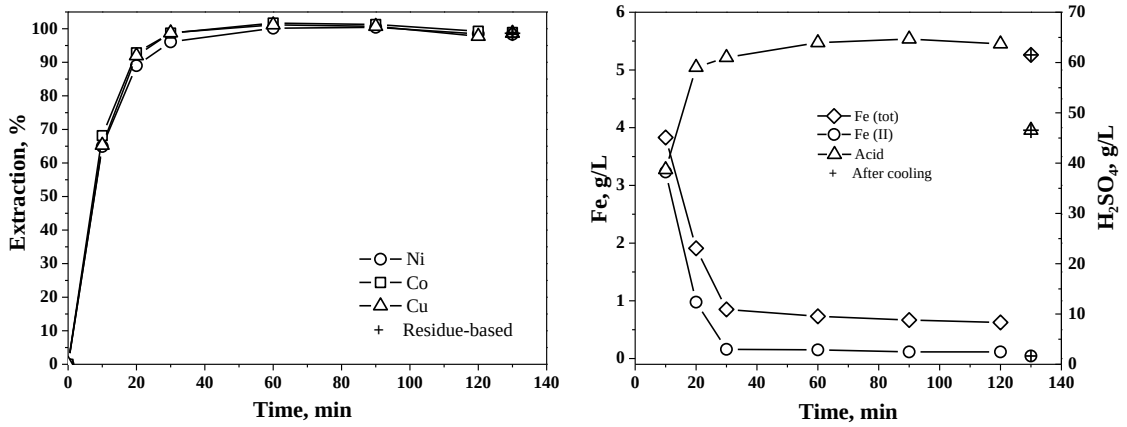

Fig. 4.5 Kinetics of leaching. Sample #0, 250°C, 25%wt solids, initial H_2SO_4 83 g/L (A/S 0.25), 0-73 psi (0-5 bar) O_2 (flow rate: 2 sccm/g of slag), 700 rpm. Note: data after cooling is reported without reference to the actual time

The solubility of precipitated hematite (Eq. 4.5) strongly depends on the temperature (Reid et al., 2006). Increased solubility at low temperatures results in partial re-dissolution during autoclave cooling and subsequent filtrations.

4.1.4 Residues of leaching

The composition of typical residues is shown in Table 4.1. The residues contain less than 1% of the Ni, Co and Cu content in the original slag material. Hematite was determined with the help of XRD to be the only crystalline compound in the residue (Fig. 4.6). Si in the residue exists in the form of amorphous silica, precipitated according to Eq. 1.7.

Table 4.1 Typical residue composition (%wt.)

Ni	Co	Cu	Zn	Al	Si
0.009-0.011	0.001-0.002	0.013-0.019	0.008-0.011	1.4-1.5	17.2-17.4
S(VI)	Mg	Ca	Fe(II)	Fe(T)	
0.32-0.35	0.01-0.02	0.48-0.52	0.89-0.95	36.9-37.9	

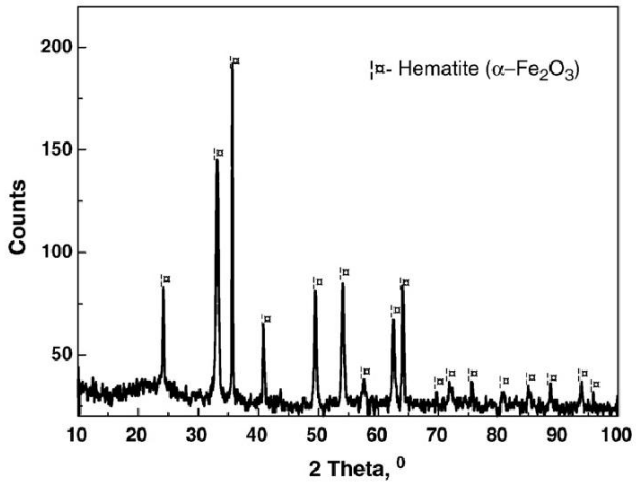

Fig. 4.6 X-ray diffractogram of a typical residue.

Fig. 4.7 shows SEM images of a typical residue. Particles appear to be in the range from a few micrometers to ~40 μm, with the larger particles being complex aggregates of silica and hematite.

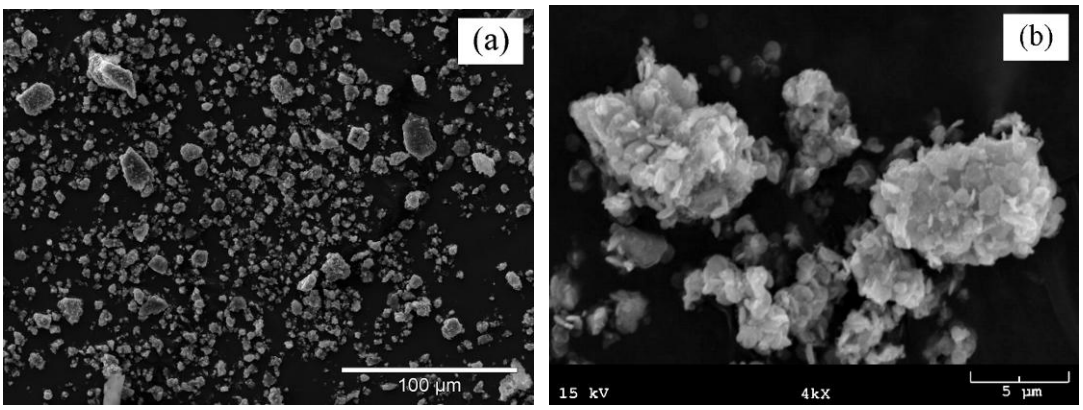

Fig. 4.7 SEM-SE images of residue. Leaching conditions: flash furnace slag (sample #0), 250°C, 25%wt solids, initial H_2SO_4 83 g/L (A/S 0.25), 0-73 psi (0-5 bar) O_2 (flow rate: 2 sccm/g of slag), 700 rpm, 2 hours.

4.2 Leaching of Converter Slags

4.2.1 Effect of oxygen partial pressure

A number of experiments were run with the converter slag to determine the effect of oxygen overpressure on the kinetics of leaching. A reduced initial acidity level of 34 g/L (A/S 0.1) was selected to minimize heat generation leading to temperature and pressure oscillations. The dissolution curves for Ni, Co and Cu along with the actual pressure profiles are shown in Fig. 4.8.

Copper dissolution (Fig. 4.8) is most sensitive to the partial pressure of oxygen. It suggests that copper is present as matte. The effect of oxygen pressure or the kinetic of nickel and cobalt dissolution can be explained in terms of the rate of acid regeneration (Eq. 4.3, 4.5) by following the iron and acid profiles (Fig. 4.9).

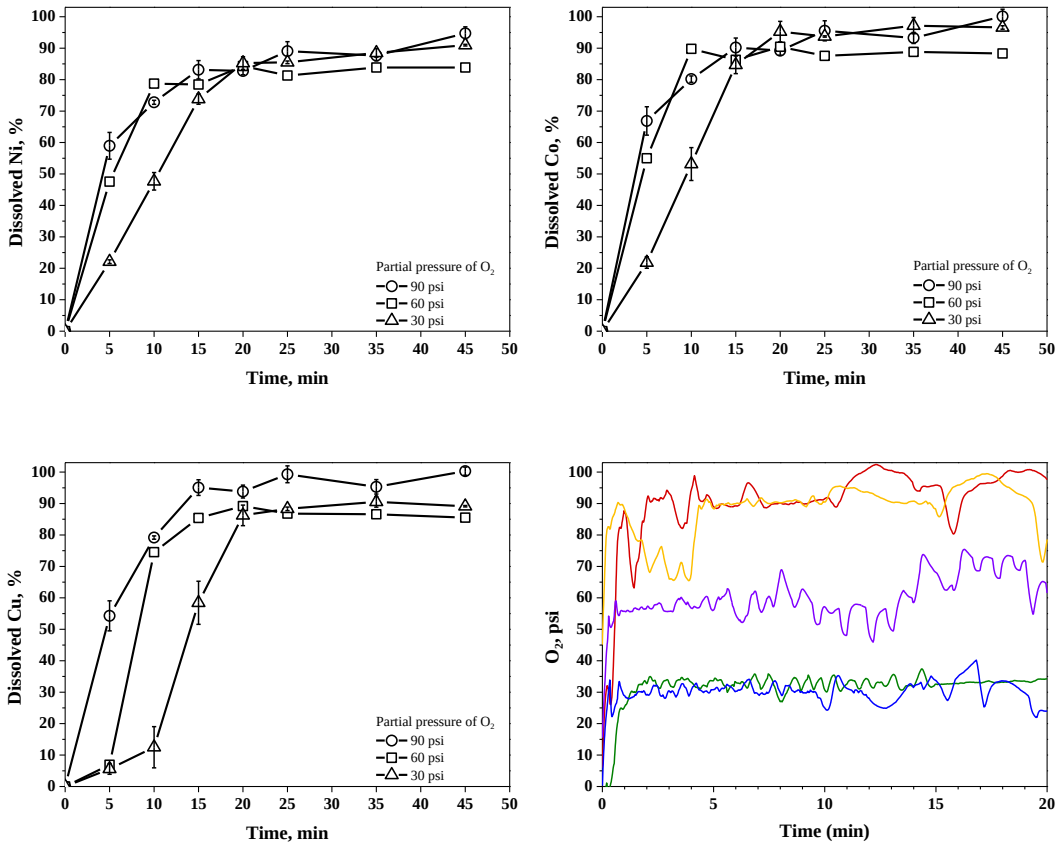

Fig. 4.8 Dissolution of Ni, Co, Cu and pressure profiles. Conv. slag sample #2, 250°C, 25%wt solids, initial H_2SO_4 34 g/L (A/S 0.1), 700 rpm. Note: data after cooling is reported without reference to the actual time

The initial drop in acidity (at 5 min) indicates that fayalite dissolution (Eq. 4.1) is a fast acid-driven reaction. The levels of dissolved Si (Fig. 4.9) at 5 min depend on the extent of initial dissolution which increases from 30 to 90 psi (from 2.1 to 6.2 bar); however, the build-up of acid causes precipitation of silica and reduces the concentration of Si to the level determined by solution acidity.

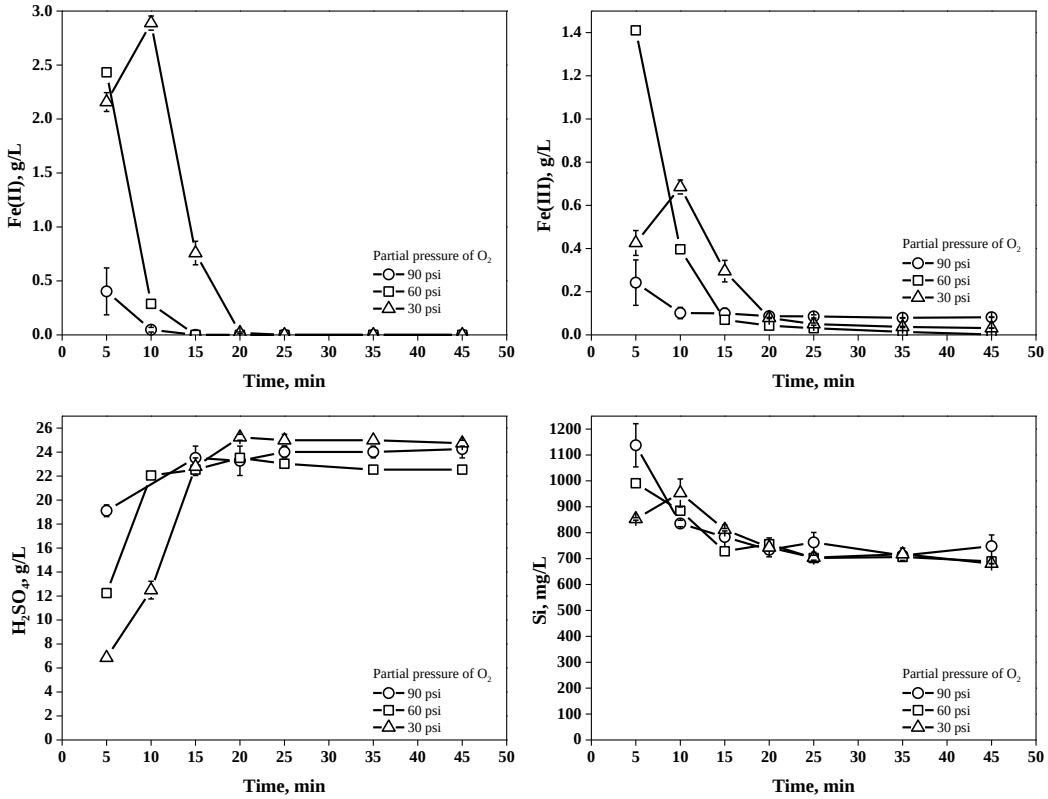

Fig. 4.9 Fe, H_2SO_4 and Si profiles. Conv. slag sample #2, 250°C, 25%wt solids, initial H_2SO_4 34 g/L (A/S 0.1), 700 rpm. Note: data after cooling is reported without reference to the actual time

4.2.2 Refined conditions

Since it was determined that acidity plays an important role in slag dissolution, and oxygen partial pressure affects the rate of acid regeneration, it was decided to revise the conditions of experiments with converter slag. Three experiments were conducted to obtain kinetic curves at 250°C, 70 g/L initial H_2SO_4 (A/S 0.2), 25% solids, 90 psi or 6.2 bar O_2, 800 rpm). These results, presented in Fig. 4.10, can be used to compare the behaviour of the two converter slag samples. Extractions of Ni, Co and Cu achieved 90% within 15-20 min after acid injection and oxygen introduction.

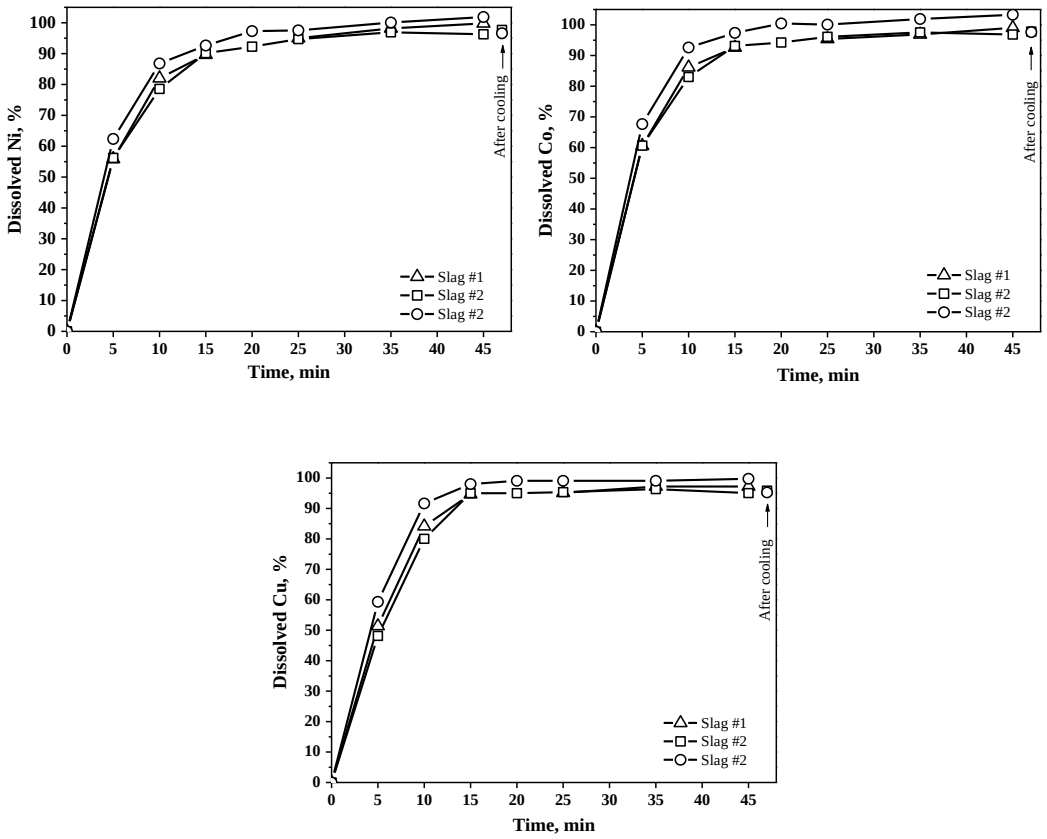

Fig 4.10 Dissolution of Ni, Co, Cu. Conv. slag, 250°C, 70 g/L H_2SO_4 (A/S 0.2), 25% solids in slurry, 90 psi (6.2 bar) O_2, 800 rpm. Note: data after cooling is reported without reference to the actual time

The bulk of the sulphuric acid injected enters the autoclave instantaneously; therefore the decreased acidity (29-37 g/L) in 5 min (Fig. 4.11) proves that dissolution of fayalite is a very fast reaction, while acid regeneration due to Fe(II) oxidation and Fe(III) hydrolysis is a slower process. Acid is regenerated to ~75% of its initial level (70 g/L) at temperature, but cooling results in lower acidities due to the re-dissolution of the precipitated iron (III) compounds (predominantly, hematite): ~36 g/L or 52% of the initial acidity. This corresponds to the following net acid consumptions: 0.05 kg H_2SO_4 / kg slag at 250°C, and 0.1 kg H_2SO_4 / kg slag after cooling and filtration.

The concentration of dissolved Si in these experiments was lower than in experiments with 35 g/L initial H_2SO_4. Cooling the autoclave reduces the concentration of Si from

~0.6 to 0.2 g/L due to a drop in the solubility of SiO_2. Silica scaling may be of concern when pressure let-down is carried out in several stages (Queneau, 1983).

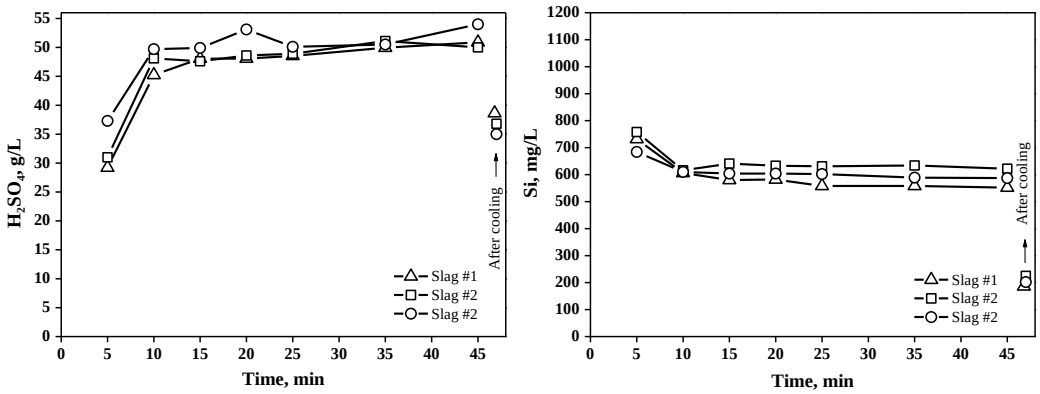

Fig 4.11 H_2SO_4 and Si profiles. Conv. slag, 250°C, 70 g/L H_2SO_4 (A/S 0.2), 25% solids in slurry, 90 psi (6.2 bar) O_2, 800 rpm. Note: data after cooling is reported without reference to the actual time

4.2.3 Characterization of solids withdrawn during leaching

In order to investigate the behaviour of individual minerals in converter slag during leaching, slurry samples were obtained at various stages of dissolution. The oxygen flow rate was restricted at 12 sccm per 1 g of slag feed (versus initial flow rates exceeding 36 sccm per 1 g of slag in the unrestricted mode at 90 psi or 6.2 bar) such that the target partial pressure of oxygen (30 psi or 2.1 bar) was attained in 17 min. Three slurry samples were taken at times 5, 10 and 15 min. The dissolution profiles of Ni, Co and Cu (shown in Fig. 4.12) were obtained in a replicate experiment, in which only liquid samples were withdrawn.

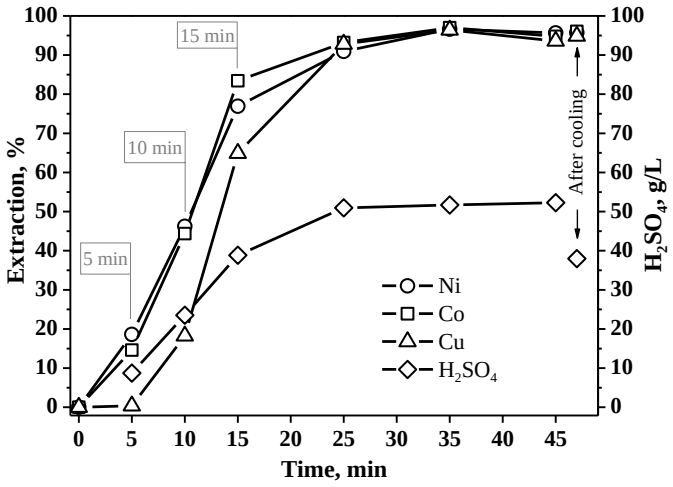

Fig. 4.12 Extractions of Ni, Co, Cu and acid profile

X-ray diffractograms of the three samples (after filtration and drying) are compared to diffractograms of the original slag and the final residue in Fig. 4.13. Magnetite appears to be practically intact in the sample withdrawn at 5 min, while the content of fayalite is greatly reduced. Both fayalite and magnetite become undetectable in the second sample taken at 10 min, whereas the presence of hematite becomes pronounced. The drop in the magnetite content agrees well with the results of Liu et al. (2010) who carried out acid leaching experiments with a laterite ore containing magnetite at 270°C, 10-30 g/L H_2SO_4, and concluded based on Fe (II) profiles that the majority of magnetite dissolved after 15 min of leaching.

The progress of leaching can also be tracked with the help of residue particle size measurements (Fig. 4.14). The sample taken after 5 minutes of leaching exhibits an overall reduction in particle size attributable to particle disintegration due to the reaction of fayalite and magnetite with sulphuric acid (Eq. 4.1 and 4.2). Further overall reduction in the particle size and build-up of submicron particles is seen at 10 min. However, leaching for extra five minutes does not affect the particle size distribution.

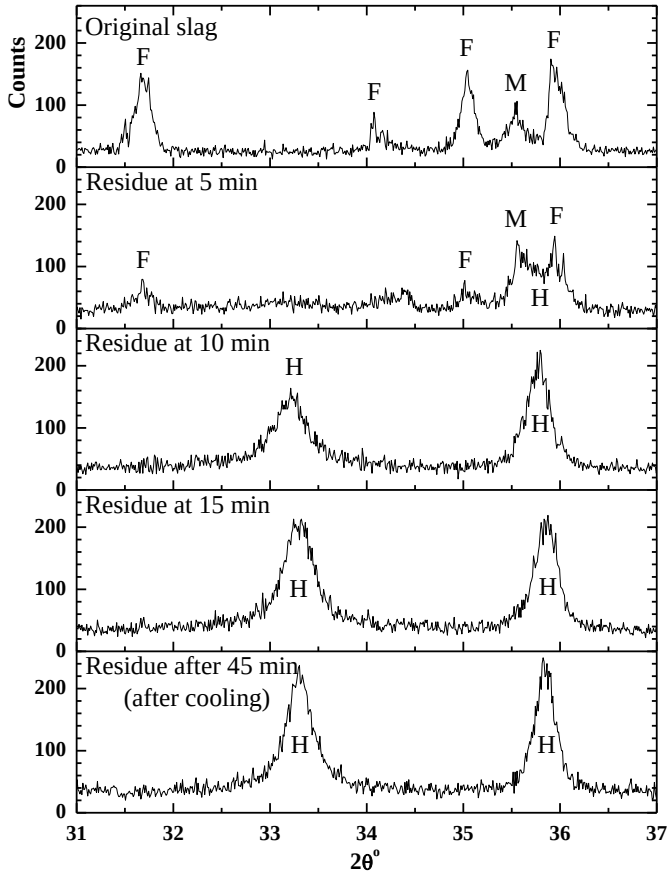

Fig. 4.13 Powder X-ray diffractograms of slag and solids obtained after 5, 10, 15 and 45 min of leaching (peaks: F – fayalite, M – magnetite, H – hematite)

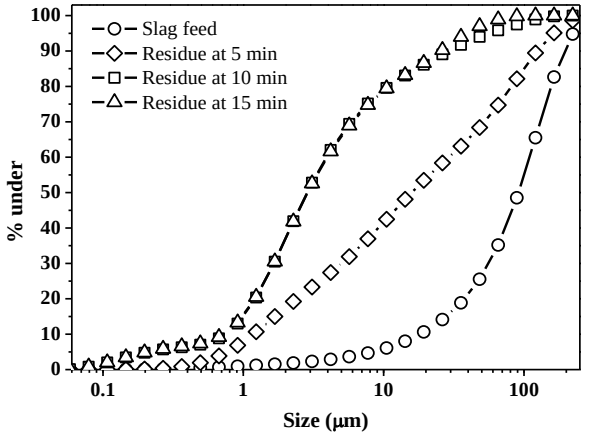

Fig. 4.14 Particle size distributions of the feed and residues (logarithmic scale)

As can be seen from the SEM-BSE image presented in Fig. 4.15, the solids after leaching for 5 minutes contain coarse partially reacted particles with serrated edges. At this point only fayalite was attacked on the surface (e.g., *area 1*). The darker spots (e.g., in *area 2*) are aggregates of fine particles identified as hematite (Fe_2O_3) and silica (SiO_2) with the help of EDX microanalysis. A number of bright exposed matte particles can be seen in the residue (e.g. above area 2).

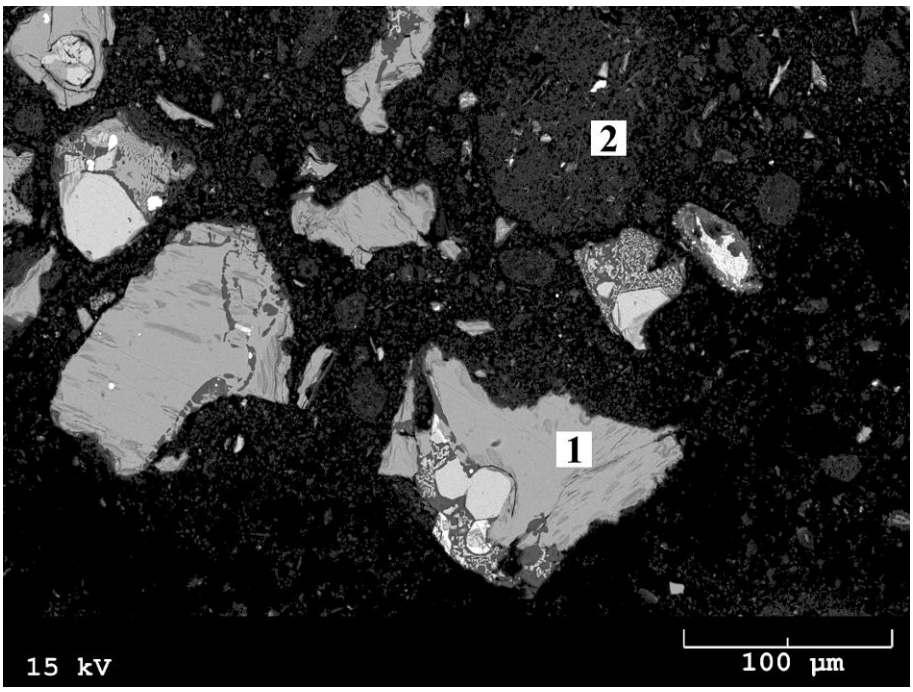

Fig. 4.15 SEM-BSE cross-section image of residue particles after 5 min of leaching

The sample obtained after 10 minutes of leaching (Fig. 4.16) contains a number of dark coarse particles (e.g. the two particles to the right of area 1) identified as silica. These are chunks of silica-rich portions of slag particles (e.g. *area D* in Fig. 3.6) remaining after selective dissolution of magnetite and fayalite. A crystal of magnetite is seen protruding from the edge of a partially reacted particle (to the left of *area 2*) as a result of preferential dissolution of the surrounding fayalite. In addition, magnetite-silica and fine hematite-silica particles are present in the residue (such as around *area 3*).

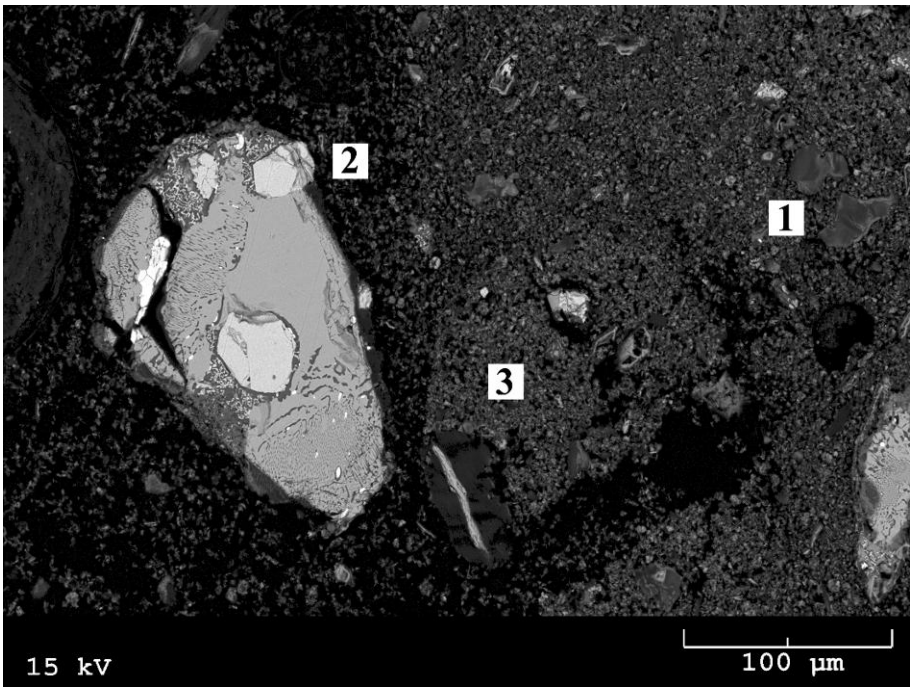

Fig. 4.16 SEM-BSE cross-section image of residue particles after 10 min of leaching

Leaching for additional five minutes greatly reduced the occurrence of fayalite-containing particles in the residue (Fig. 4.17). The partially reacted particles present consist mainly of silica (to the left of *area 1*), silica-fayalite mix (e.g., to the left of *area 2*) as well as magnetite (e.g., to the right of *area 3*). The abundance of silica-fayalite particles after 15 minutes of leaching can be attributed to acid build-up (Fig. 4.12) which caused the formation of deep pores in fayalite and promoted precipitation of silica within the pores. This is opposite of mild fayalite surface etching which was found in the samples after 5 and 10 minutes of leaching.

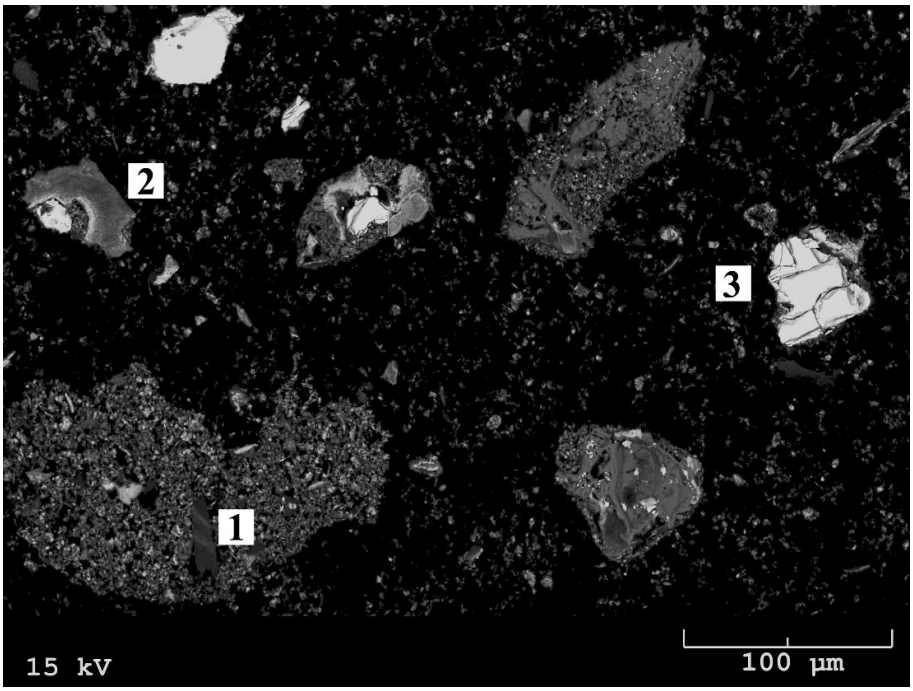

Fig. 4.17 SEM-BSE cross-section image of residue particles after 15 min of leaching

Pore development can be better seen in a residue obtained after leaching a coarser fraction of the converter slag (+150-300 µm) for 20 min under regular conditions (250°C, ~70 g/L H_2SO_4 initial, 25% solids, 90 psi or 6.2 bar O_2, 800 rpm). A cross-section of a typical particle from the final residue at a higher magnification is shown in Fig. 4.18. It is observed that the two magnetite crystals in the centre (around *area 1*) were attacked by acid, but did not dissolve completely, although the smaller chunks of magnetite that were once embedded in a silica matrix (such as in *area 3* in Fig. 3.6) have now dissolved and left empty pores in silica (e.g., in *area 2*, Fig. 4.18). The fayalite portion of the particle was also affected by sulphuric acid which created a network of pores that were partially sealed by precipitated silica (e.g., around *area 3*).

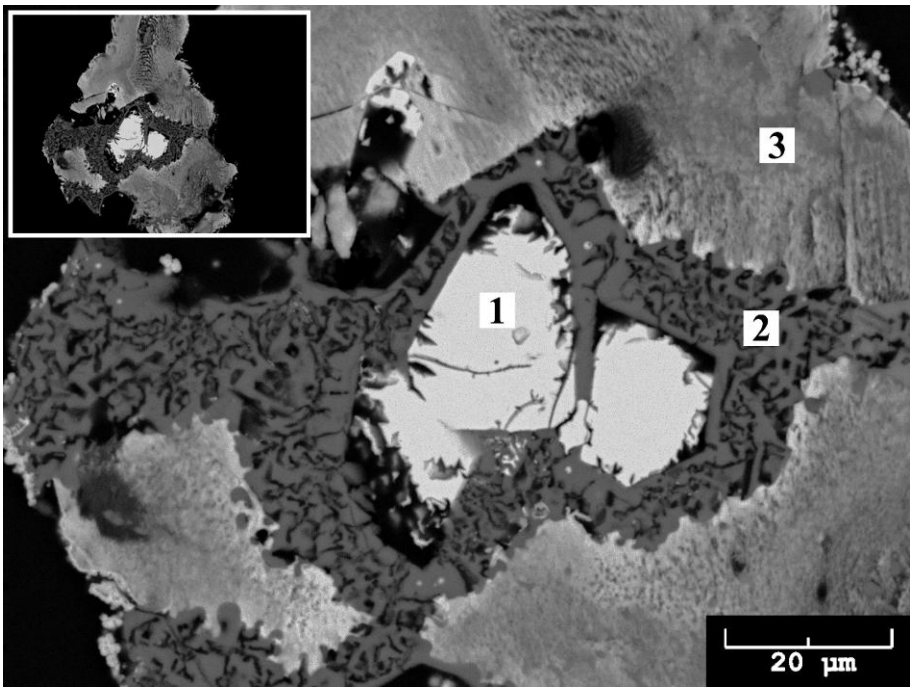

Fig. 4.18 Cross-section image of a typical residue particle after leaching a coarse particle fraction of slag

4.3 Mechanism of Crystalline Slag Leaching

Based on the characterization work described in section 4.2.3, a dissolution mechanism is proposed. It can be best illustrated by the schematic shown in Fig. 4.19. The original particle (Fig. 4.19, a) consists of five zones representing the typical minerals and their combinations in the slag: 1 - magnetite, 2 - silica, 3 - matte; 4 - fayalite; 5 - fayalite with silica inclusions; 6 - silica with magnetite inclusions. This particle undergoes dissolution and disintegration during leaching.

Fayalite (*zones 4 and 5*), being a highly reactive mineral in the slag, is initially subjected to surface etching favoured by low acidities (illustrated by Fig. 4.19, b) as evident from the image of the residue after 5 min of leaching (Fig. 4.15). The appearance of the residue of coarse slag leaching (Fig. 4.18) suggests that excessive pore formation takes place in fayalite when acid builds up (illustrated by Fig 4.19, c). The pores created are partially filled by precipitated silica from dissolved fayalite (Eq. 4.1 and 1.7).

Matte (*zone 3*) is found exposed in the residue until 10 minutes of leaching (Fig. 4.16). This is consistent with the dissolution profile of copper (Fig. 4.12) – an element tightly associated with sulphur (Fig. 3.7). Acid build up between 15 and 25 min of leaching (Fig. 4.12) indicates the completion of iron oxidation and the availability of oxidants (oxygen or ferric iron) for matte oxidation. Hence, it can be concluded that matte is leached only when the bulk of fayalite has dissolved and most ferrous iron has been oxidized. This is comparable to the finding of King and Dreisinger (1993) who reported that over 97% of copper was extracted from various chalcopyrite ($CuFeS_2$) ore concentrates within 15 min in batch leaching experiments at 225°C, 100 psi (6.9 bar) O_2, 5 g/L initial H_2SO_4. Marsden et al (2003) confirmed the importance of oxygen partial pressure based on continuous pilot plant leaching of chalcopyrite concentrates at 225°C.

Magnetite (*zone 1 and 6*) undergoes only minor dissolution on the surface (Fig 4.19, b) during the initial stages of leaching when the acidity is low (e.g. at 5 min, Fig. 4.15). According to XRD, the majority of magnetite had been dissolved before 10 minutes (Fig. 4.16). However, a few magnetite particles were seen remaining almost intact even after 15 min of leaching (Fig. 4.17) when nickel and cobalt extractions were in the 75-85% range. This is attributed to both the chemical properties of the mineral, and its close proximity to silica regions. Eventually, most magnetite undergoes dissolution through surface etching (Fig 4.19, c).

Silica (*zones 2, 5 and 6*) is an inert mineral phase, which remains largely unaffected during leaching. Most silica zones remain intact, although some can be partially disintegrated (most likely, mechanically, when other minerals surrounding weak spots get dissolved). It could not be determined whether silica undergoes direct solid transformations from one amorphous form to another. Any modifications of silica surface that may have taken place were always masked by precipitation of silica from silicic acid.

The particle after leaching is completely disintegrated (the shape was retained in Fig. 4.19, d for illustrative purposes only). Fayalite (*zones 4 and 5*), matte (*zone 3*) and most of magnetite (*zones 1 and 6*) disappear completely. The porous silica regions left after fayalite dissolution (*zones 4 and 5*) are filled with hematite, mechanically disintegrated and mixed with fine precipitates of hematite and silica. Larger silica zones (*2 and 6*) are

only partially disintegrated, and can be easily seen in the residue due to their relatively large size.

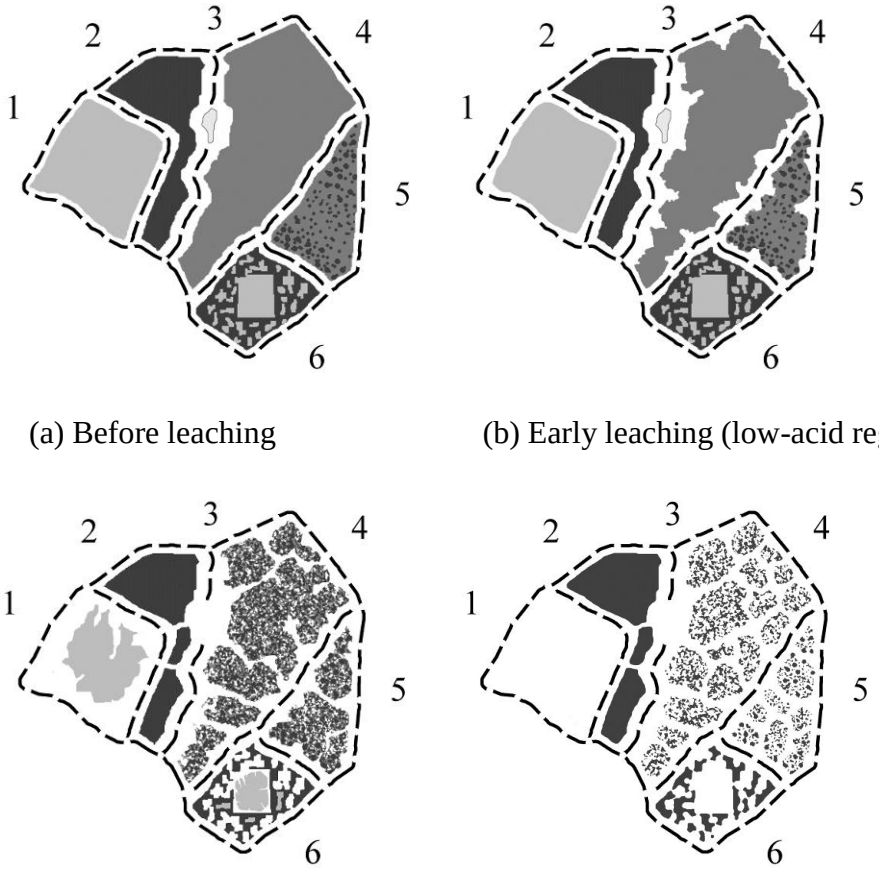

(a) Before leaching (b) Early leaching (low-acid regime)

(c) Advanced leaching (high-acid regime) (d) After leaching

Fig. 4.19 Schematic of particle dissolution mechanism

4.4 Summary

High pressure oxidative acid leaching (HPOXAL) was successfully applied to crystalline flash furnace and converter slags. Extractions of Ni, Co and Cu exceeded 90% within 15-20 min and arrived at 95-97% after 45 min at 250°C, 90 psi (6.2 bar) O_2 overpressure and 70 g/L initial H_2SO_4.

Fayalite dissolves fastest; hence, leaching performance is best when the slag has base metals associated with fayalite. Fayalite dissolution is an acid-driven reaction; therefore,

the fastest dissolution can be seen at higher concentrations of acid (or in slags with a lower CaO and MgO content causing irreversible acid consumption). High acidity favours fayalite disintegration via pore formation deep into the centre of the particle.

Copper is present in tighter association with sulphur in matte. The absence of matte particles in the residue of leaching at later stages, as well as high copper extractions, are indicative of matte's ability to dissolve when oxidants are supplied. A slag with a high content of matte would require higher oxygen partial pressures (e.g., 90 psi or 6.2 bar) and/or retention times in excess of 25 min.

The occurrence of magnetite falls below the detection limit of XRD by the time the acidity reaches 25 g/L; however, some magnetite is found in the residue of leaching even when more than 80% of Ni and Co dissolved and the acid concentration exceeded 40 g/L. The increase in nickel extraction from ~90% to ~97% over the last 25-30 minutes of leaching is likely related to the slow dissolution of the remaining magnetite.

Silica is found to be least affected by leaching. Although it is neither a major mineral phase nor a carrier of base metals, it can act as an efficient barrier for reagent transport to other minerals. Hence leaching rates will be slower with slags that have a high degree of intergrowth of silica with other minerals. However, as can be seen from the photomicrographs reported by Das et al. (1987), promoting crystal growth by reducing the rate of cooling can mitigate intergrowth.

References

Das, R.P., Anand, S., Sarveswara Rao, K., Jena, P.K., 1987. Leaching behaviour of copper converter slag obtained under different cooling conditions. Transaction of the Institute of Mining and Metallurgy C96, 156-162.

Gbor, P.K., Mokri, V., Jia, C.Q., 2000a. Characterization of smelter slags. Journal of Environmental Science and Health A35 (2), 147–167.

King, J.A., Dreisinger, D.B., Knight, D.A., 1993. The total oxidation of copper concentrates, in: R.G. Reddy, R.N. Weizenbach (Eds.), Extractive metallurgy of

copper, nickel and cobalt (Proceedings of the Paul E. Queneau international symposium), The Minerals, Metals and Materials Society, pp. 735-756.

Li, Y., Perederiy, I., Papangelakis, V.G., 2008. Cleaning of waste smelter slags and recovery of valuable metals by pressure oxidative leaching. J. Haz. Mat. 152, 607-615.

Li, Y., Papangelakis, V.G., Perederiy, I., 2009. High pressure oxidative acid leaching of nickel smelter slag: Characterization of feed and residue. Hydrometallurgy 97,185-193.

Liu, K. Chen, Q., Hu, H. Yin Zh., Wu, B., 2010. Pressure acid leaching of a Chinese laterite ore containing mainly maghemite and magnetite. Hydrometallurgy 104, 32-38.

Marsden, J.O., Brewer, R.E., Hazen, N., 2003. Copper concentrate leaching developments by Phelps Dodge corporation, in: C.A. Young, A.M. Alfantazi, C.G. Anderson, D.B. Dreisinger, B. Harris and A. James (Eds.), Hydrometallurgy 2003 (Proceedings of the fifth international conference in honor of professor Ian Ritchie), The Minerals, Metals and Materials Society, pp. 1429-1446.

Queneau, P.B., Berggren, M.H., Cooperrider, M.W., Doane, R.E., 1983. Control of silica deposition during pressure let-down of acidic leach slurries. Hydrometallurgy Research, Development and Plant Practice, Atlanta; GA, pp. 121-137.

Perederiy, I., Papangelakis, V.G., Jia, C.Q., 2009. Pressure oxidative leaching of slags from nickel smelters: an update, in: J.J. Budac, R. Fraser, I. Mihaylov, V.G. Papangelakis, D.J. Robinson (Eds.), Hydrometallurgy of nickel and cobalt (Proceedings of 39th annual hydrometallurgy meeting), Canadian Institute of Mining Metallurgy and Petroleum, Montreal, pp. 87-96.

Perederiy, I., Papangelakis, V.G., Buarzaiga, M., Mihaylov, I. 2011. Co-treatment of converter slag and pyrrhotite tailings via high pressure oxidative leaching, J. Haz. Mat. (doi:10.1016/j.jhazmat.2011.08.012).

Reid, M., Papangelakis, V.G., 2006. New data on hematite solubility in sulphuric acid solutions from 130 to 270 °C. In: Dutrizac, J.E., Riveros, P.A. (Eds.), Iron Control Technologies. CIM, Montreal, pp. 673–688.

CHAPTER 5 CO-TREATMENT OF CONVERTER SLAG AND PYRRHOTITE TAILINGS VIA HIGH PRESSURE OXIDATIVE LEACHING

This chapter focuses on a modified leaching process in which sulphuric acid is generated in situ from the oxidation of pyrrhotite tailings, a waste of sulphide ore flotation. The effect of metal sulphate precipitation at low acidities on base metal extractions is revealed. Further evidence of fast dissolution of fayalite in acid is given based on continuous acidity measurements performed with the help of an electrodeless conductivity sensor. Finally, leachability of granulated converter slag is discussed.

This chapter incorporates a portion of a manuscript published in the Journal of Hazardous Materials:

- Perederiy, I., Papangelakis, V.G., Buarzaiga, M., Mihaylov, I., 2011. Co-treatment of converter slag and pyrrhotite tailings via high pressure oxidative leaching, J. Haz. Mat.

5.1 Introduction

Compared to atmospheric leaching (Jia et al., 1999 and Banza et al., 2002), HPOXAL requires significantly less sulphuric acid due to acid regeneration (Eq. 4.3 and 4.5). It was found that an acid addition of only 20 wt% of slag weight is needed, while a minimum of 175 wt% would be required stoichiometrically according to Eq. 4.1 and 4.2 in atmospheric leaching (without acid regeneration). Yet, even a 20% addition of sulphuric acid may have a detrimental effect on the process economics. The issue of operating costs in HPOXAL is further aggravated if the heat balance is taken into consideration. Operation at 250°C would require multi-stage steam recycling as well as an additional source of heat. These concerns provide an incentive to seek a cheaper substitution for sulphuric acid as well as an alternative source of heat.

It has been reported in the past (Seidel and Fitzhugh Jr., 1968, O'Neill, 1974; Opratko et al., 1974; Ferron and Fleming, 2004) that it is possible to produce sulphuric acid (and heat) from iron sulphide compounds such as pyrite (FeS_2) or pyrrhotite (Fe_7S_8) in situ. The following overall stoichiometric reaction holds for pyrrhotite:

$$Fe_7S_8 + 17.25\ O_2 + 8\ H_2O = 3.5\ Fe_2O_3 + 8\ H_2SO_4 \quad (5.1)$$

Ferron and Fleming (2004) reported on the co-treatment of limonitic laterites with sulphur bearing materials (including pyrrhotite flotation tailings) in a pressure oxidative process under conditions similar to those in HPOXAL. In this work we chose to test pyrrhotite tailings (a reject stream from pentlandite ore separation by flotation) from Vale's Clarabelle Mill in Sudbury as an acid source material in converter slag HPOXAL.

Highly reactive pyrrhotite in the tailings can cause acid mine drainage due to weathering (Moncur et al., 2009), which complicates containment of impounded tailings. In the co-treatement of slags with tailings, pyrrhotite is converted to stable hematite which is safer for disposal. Pyrrhotite tailings also contain a small amount of nickel (0.6-1%) which can be recovered in this process.

5.2 Pressure Oxidation of Pyrrhotite Tailings

Pyrrhotite tailings from Vale's Clarabelle Mill were used in this work as a replacement for sulphuric acid. The assay is shown in Table 5.1.

Table 5.1 Pyrrhotite tailings assay, %wt.

Ni	Cu	Co	Zn	Fe	S	Si	Al	Ca	Mg	K	Ti	Mn	Cr
0.595	0.086	0.021	0.020	39.1	21.4	8.49	2.39	1.45	0.995	0.425	0.253	0.06	0.03

The tailings sample used in this work was dried at 70°C – as a result, the originally fine material got clumped. In order to return the material into its original state, it was passed through a roller crusher such that re-grinding was avoided. The particle size distribution of the obtained material is shown in Fig. 5.1.

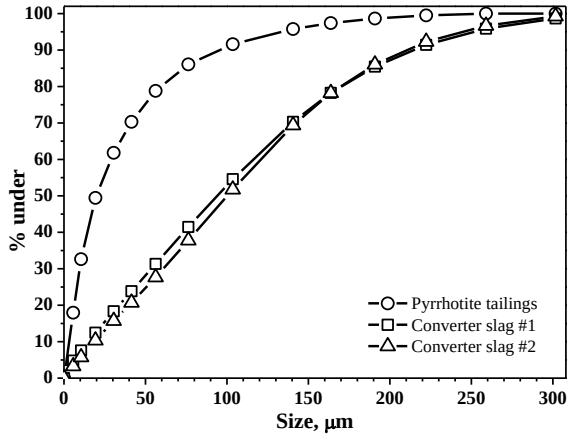

Fig. 5.1 Particle size distributions of pyrrhotite tailings and slags

Powder X-ray diffraction did not detect any products of pyrrhotite oxidation in the dried tailings, and minor surface oxidation is not believed to introduce any significant bias into the assessment of the acid generation capacity of the tailings.

Several pressure oxidation experiments with the tailings alone were conducted at 225° and 250°C. Acid generation is completed in 10 min regardless of temperature (225° and 250°C) with less than 61.5 g of tailings addition per kg of water as indicated by the acid profiles in Fig.5.2. Increasing the addition of the pyrrhotite tailings prolongs acid generation. Based on sulphur dissolution profiles, pyrrhotite oxidation is virtually complete in 20 min with over 96% of sulphur dissolved (as sulphate) – Fig. 5.3.

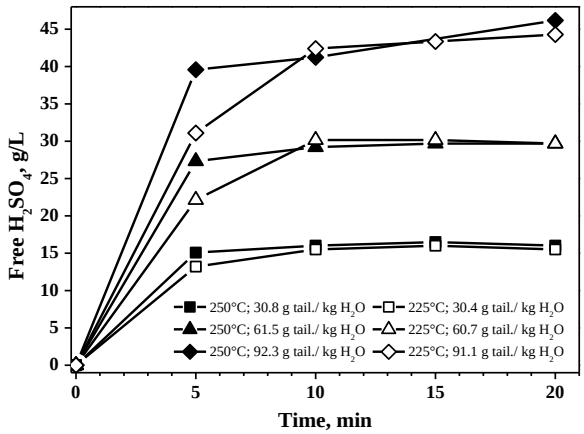

Fig. 5.2 Acid profiles during pressure oxidation of pyrrhotite in tailings at 90 psi (6.2 bar) O_2

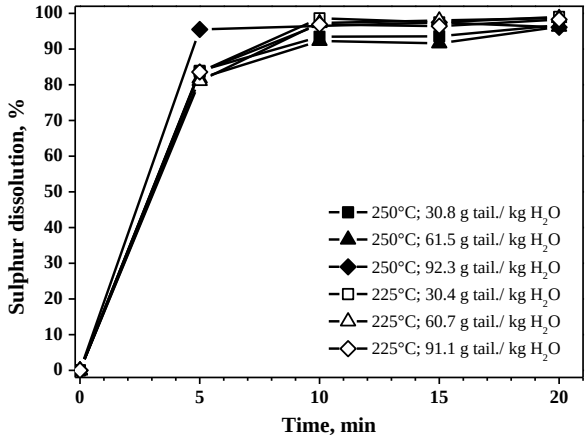

Fig. 5.3 Sulphur dissolution during pressure oxidation of pyrrhotite in tailings at 90 psi (6.2 bar) O_2

Stoichiometrically equivalent acidities (defined as the concentration of free H_2SO_4 plus the concentration of H_2SO_4 that could be obtained by hydrolyzing all the iron present in the solution – as per the reaction in Eq. 5.1) after 20 minutes of pressure oxidation are shown in Fig. 5.4. The plot reveals the same linear relationship between equivalent acidity and pyrrhotite addition for both temperatures.

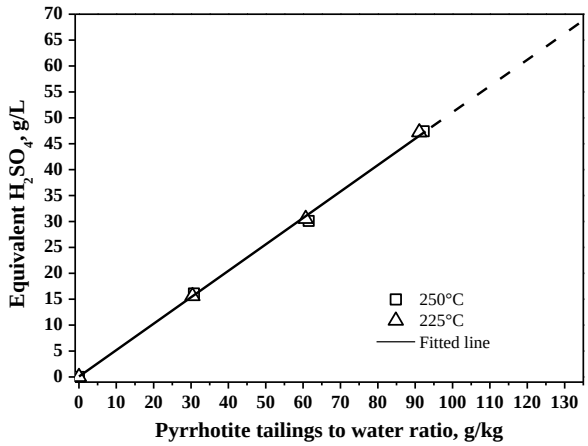

Fig. 5.4 Equivalent acidity from pressure oxidation of pyrrhotite in tailings at 90 psi (6.2 bar) O_2 in 20 min

5.3 Co-treatment of Naturally Cooled Converter Slag and Pyrrhotite Tailings

The equivalent acidities tested in this work are 34 and 68 g/L, and the required pyrrhotite additions are found from Fig. 5.4 to be 67 and 133 g/kg of water. Experiments at these acidities were conducted at 225° and 250°C, and compared to an experiment run at 250°C, in which acid was injected to make the initial concentration 70 g/L. The kinetic curves for Ni, Co, Cu and free acidity are shown in Fig. 5.5.

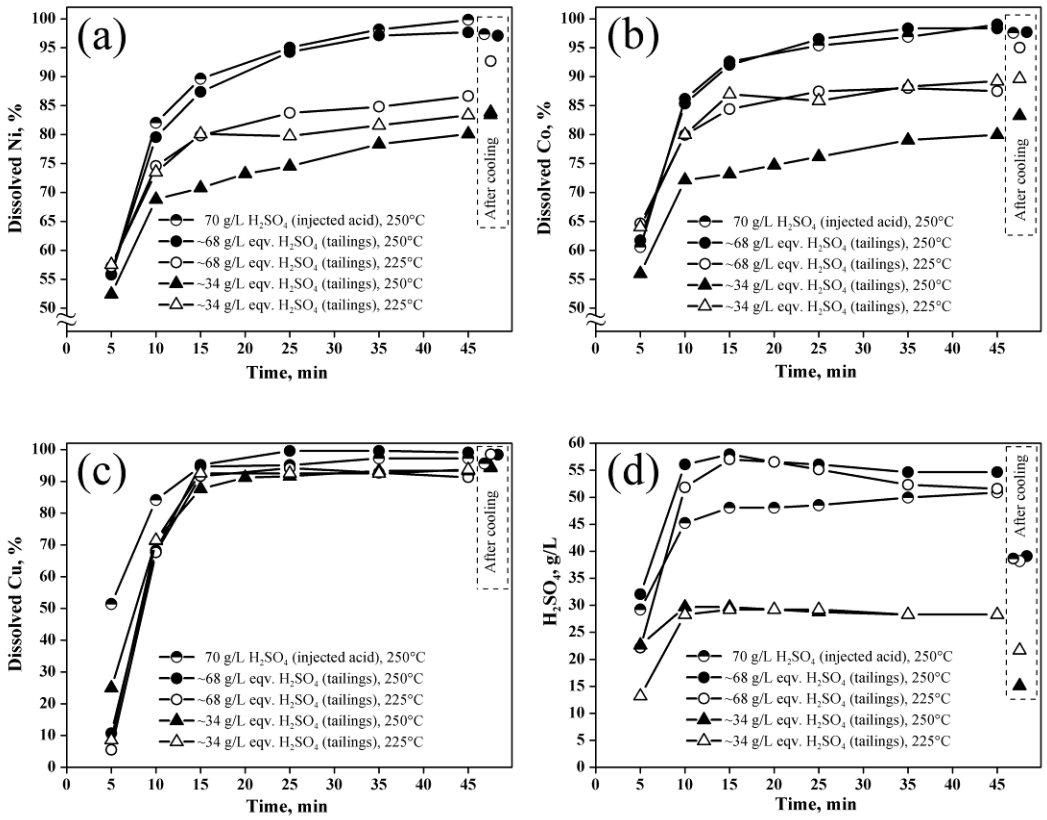

Fig. 5.5 Kinetics of leaching: 90 psi (6.2 bar) O_2, 25 wt% total solids (slag #1 and pyrrhotite tailings), 800 rpm. Note: data after cooling is reported without reference to the actual time

As is clear, only a combination of high temperature and acidity (i.e., 250°C and ~68 g/L) leads to extractions of Ni and Co in excess of 90% after 15-20 min of leaching (Fig. 5.5a, b). It is also only under these conditions that leaching is completed within 45 min (96-97% of Ni and Co extracted). At 68 g/L equivalent acidity, a decrease in temperature to

225°C naturally results in a slower leaching rate – only 86-87% of Ni and Co are extracted in 45 min (at temperature), but extractions after cooling and filtration increase up to 92% for Ni and 95% for Co (Fig. 5.5a, b).

Interestingly, in experiments with 34 g/L equivalent acidity, decreasing the temperature from 250° to 225°C improves Co extraction (from 80% to 89% in 45 min at temperature, and from 83% to 90% after cooling and filtration) as can be seen from Fig. 5.5b. Such behaviour can be explained by precipitation of $CoSO_4$ at 250°C when acidity is low due to fast fayalite dissolution (Fig. 5.5d).

It has been shown that introduction of magnesium sulphate, a typical divalent metal sulphate, into high temperature H_2SO_4-H_2O systems results in the decrease of the concentration of H^+ due to the formation of the bisulphate ion (Baghalha and Papangelakis, 1998). Equilibrium is governed by the following equations:

$$MgSO_4 = Mg^{2+} + SO_4^{2-} \tag{5.2}$$

$$H^+ + SO_4^{2-} = HSO_4^- \tag{5.3}$$

A decrease in the free acidity would increase the concentration of the sulphate ion in the system (Eq. 5.3), which in turn would cause precipitation of magnesium sulphate (Eq. 5.2). Other divalent metal sulphates are known to behave in the same manner. Modelling and experimental data (Jankovic et al., 2009; Bruhn et al., 1965; Hasegawa et al., 1996) confirm that the solubility of metal sulphates such as $MgSO_4$, $NiSO_4$ and $FeSO_4$ decreases with decreasing acidity and increasing temperature in H_2SO_4-H_2O systems at temperatures of 200 to 250°C.

It is likely that in the experiment at 250°C and 34 g/L equivalent acidity, $FeSO_4$, $NiSO_4$ and $CoSO_4$ precipitated during the first few minutes of leaching, when acid was spent to dissolve slag. Precipitation of ferrous sulphate was confirmed by an increase in the concentration of ferrous iron from under 100 ppm at 250°C to more than 1 g/L after cooling and filtration. Similarly, the concentrations of Ni and Co increased after cooling and filtration in the experiment run at 250° (34 g/L equivalent acidity), while it was not

the case in the experiment run at 225°C. Precipitation of metal sulphates is discussed in more detail in Appendix F.

Prolonging leaching to 120 min in the experiment at 250°C and 34 g/L equivalent acidity improves both Ni and Co extractions from 83% to approximately 92% (Fig. 5.6).

Copper extractions (Fig. 5.5c) are practically insensitive to the conditions used. Naturally, copper dissolution proceeds slower in the case of leaching with pyrrhotite tailings compared to tests with injected sulphuric acid (Fig. 5.5c). This is due to the fact that copper sulphide is more stable than pyrrhotite.

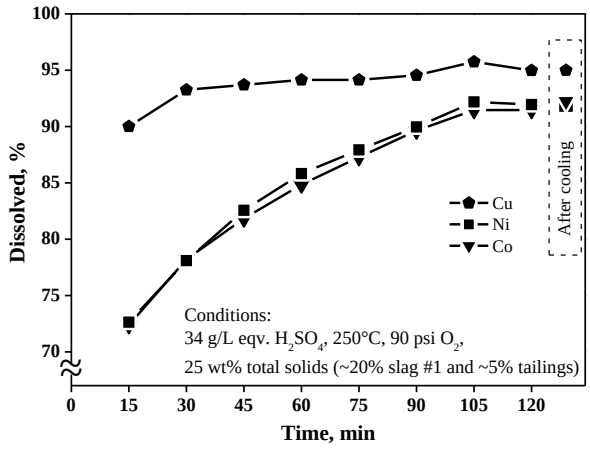

Fig. 5.6 Kinetics of prolonged leaching: 34 g/L eqv. H_2SO_4, 250°C, 90 psi (6.2 bar) O_2. Note: data after cooling is reported without reference to the actual time

Acidity plays a major role in the dissolution of fayalite and magnetite that leads to the release of the entrapped base metals. The effect of oxygen partial pressure on the rate of acid generation and nickel dissolution in the presence of pyrrhotite tailings can be illustrated by two experiments run at 45 and 90 psi (3.1 and 6.2 bar) O_2 (Fig. 5.7). In order to interpret the kinetic results accurately, solution analysis data was complemented with in-situ conductivity measurements using an electrodeless sensor. The conductivity measurements were then used to measure acidity online following a procedure previously established by Huang and Papangelakis (2008). Molality was converted to grams per liter (at room temperature) using an average conversion factor of 96.2 $g \cdot L^{-1} \cdot kg \cdot mol^{-1}$ based on

the solution samples. The average relative deviation (ARD) value between the estimated and measured acidities (calculated according to Eq. 2.1) was found to be below 4.6%.

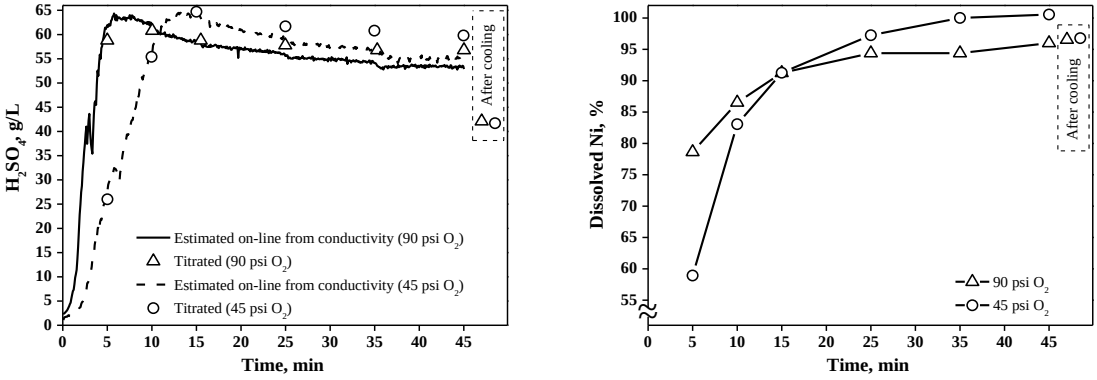

(a) (b)

Fig. 5.7. On-line acid profiles and leaching kinetics: Slag #1 and pyrrhotite tailings, 250°C, 25% total solids in slurry (including 9.75% tailings), ~68 g/L eqv. H_2SO_4

Monitoring the acidity using conductivity makes it possible to obtain information about the processes taking place during the first few minutes of the experiment, which is not possible with a conventional sampling technique. As expected, acidity builds up gradually (Fig. 5.7), with the maximum build-up rate attained after an induction period of 1-2 min during which sufficient amounts of ferric iron are expected to accumulate in order to support fast hydrolysis.

Dips on the acidity curves (Fig. 5.7) at ~3 and 6 min are attributed to disruption in oxygen dispersion due to pressure overshoots, which forced the controller to interrupt the flow of the gas through the dip tube allowing acid consuming reactions (mainly fayalite dissolution according to Eq. 4.1) to briefly take over acid generation (Eq. 4.5). The magnitude of the dips suggests high rates of fayalite dissolution.

The concentration of free acid reaches its maximum at ~7 min (at 90 psi or 6.2 bar O_2) and 13 min (at 45 psi or 3.1 bar O_2), and then decreases slowly with a tendency towards levelling off (Fig. 5.7). Dissolution of fayalite and magnetite at the latter stage of the experiment can be ruled out as a reason for the decrease in acidity because the

concentrations of both Fe(II) and Fe(III) are decreasing. Therefore, this decrease in acidity is attributed to the neutralization by metal oxides (NiO, CoO, CaO, MgO, Al_2O_3).

Although the partial pressure of oxygen (or oxygen dispersion) affects the kinetics of nickel dissolution at the early stages of leaching (Fig. 5.7), extractions after 10 min (>80%) do not differ significantly in experiments with 45 and 90 psi (3.1 and 6.2 bar) O_2. The 5% difference in the extractions at 45 min is attributed to errors in the determination of the liquor volume in the autoclave due to steam leakage. It is possible that higher partial pressures of oxygen (or better means of gas dispersion) could further improve the kinetics of leaching; however, it was not possible to carry out such experiments due to extreme heat generation that makes the experiment go into the "runaway" regime.

5.4 Co-treatment of Granulated Converter Slag and Pyrrhotite Tailings

Experiments with re-melted and granulated converter slag were attempted to assess the leachability of crystalline slags with a high degree of mineral intergrowth. Pyrrhotite tailings were used a substitute for acid in experiments run at 250°C and 90 psi (6.2 bar) O_2 partial pressure. The dissolution profiles of Ni, Co and Cu are shown in Fig. 5.8. Base metal extractions reach 90% within 10 min, owing to the fine grind of the slag feed. This confirms that granulated slag are amenable to leaching if they are crystalline.

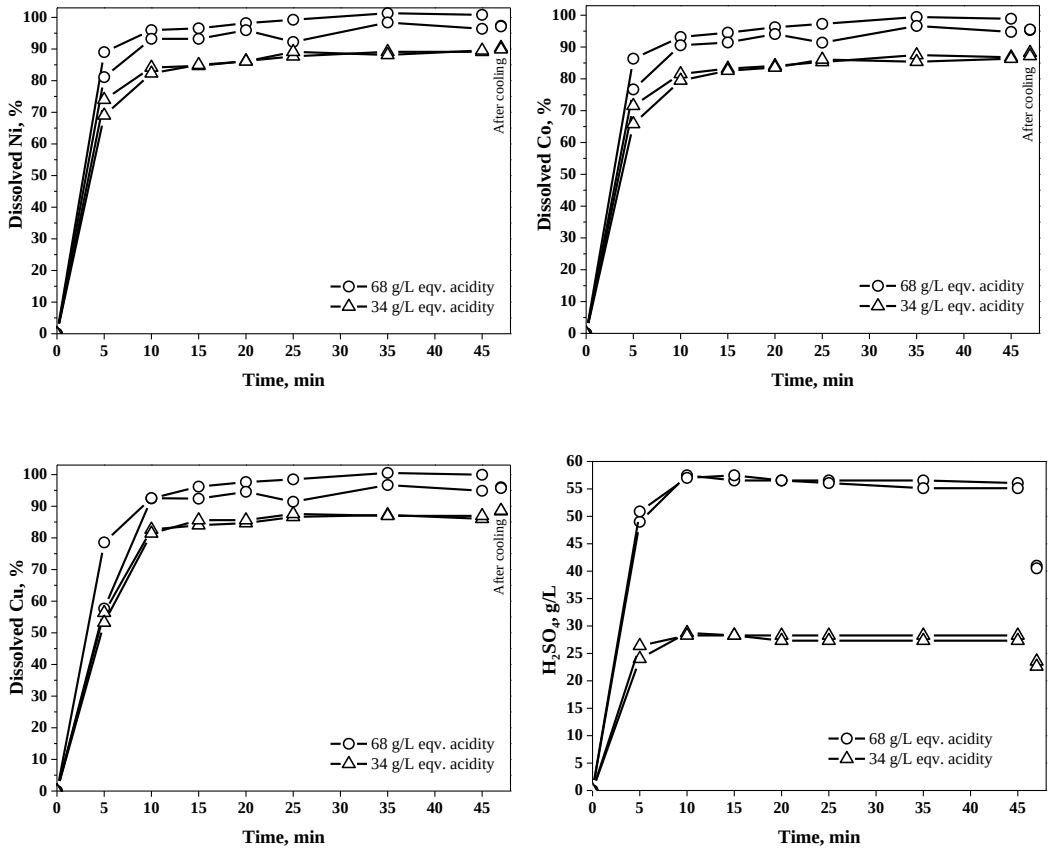

Fig. 5.8 Dissolution of Ni, Co and Cu and acid profiles. 90 psi (6.2 bar) O_2, 20 wt% total solids (gran. conv. slag and pyrrhotite tailings), 800 rpm. Note: data after cooling is reported without reference to the actual time

5.5 Summary

A modified high pressure oxidation process was tested in order to evaluate the performance of an iron sulphide feed as a substitute for sulphuric acid. Pyrrhotite tailings were selected for their content of Ni (~0.6%) and reactivity. The amount of equivalent acid produced was found to be a linear function of tailings addition. Pyrrhotite oxidation and iron hydrolysis were completed within ~20 min for pyrrhotite tailing additions under 92 g/ kg H_2O at 250°C, 90 psi (6.2 bar) O_2 overpressure.

Oxidative co-leaching of pyrrhotite tailings with naturally cooled converter slag at 250°C, 90 psi (6.2 bar) O_2, 68 g/L equivalent H_2SO_4 (corresponding to an acid addition

of ~20% of solid feed weight at 25% solids) was shown to have kinetics comparable to adding sulphuric acid with final extractions reaching 95-97% in 45 min.

An explanation was offered to the detrimental effect of high temperature (250°C) combined with a low equivalent acidity (34 g/L – corresponding to an acid addition of ~10% of solid feed weight at 25% solids) on the kinetics of Ni and Co dissolution. It was shown that divalent metal sulphates ($FeSO_4$, $NiSO_4$, $CoSO_4$) precipitate at low acidities.

On-line acid monitoring using conductivity in co-leaching experiments (at 250°C, 45 and 90 psi O_2, ~68 g/L equivalent H_2SO_4) confirmed that acidity gradually builds up in the system in the first 7-13 min, with oxygen overpressure (and dispersion) determining the rate of acid generation and re-generation. It is likely that achieving oxygen overpressures above 90 psi (or better means of gas dispersion) could improve the rate of acid generation and, ultimately, base metal dissolution on the early stages of leaching.

It was shown that granulated converter with intergrown crystalline mineral phases is also amenable to pressure leaching. Extraction of Ni, Co and Cu exceeded 90% in 10 min at 250°C, 68 g/L equivalent H_2SO_4, 90 psi (6.2 bar) O_2.

References

Baghalha, M, Papangelakis, V.G., 1998. The ion-association-interaction approach as applied to aqueous H_2SO_4-$Al_2(SO_4)_3$-$MgSO_4$ solutions at 250°C, Metall. Mater. Trans. 29B, 1021-1030.

Banza, A.N., Gock, E.G., Kongolo, K., 2002. Base metals recovery from copper smelter slag by oxidising leaching and solvent extraction, Hydrometallurgy 67, 63-69.

Bruhn Von, G., Gerlach, J., Pawlek, F., 1965. Untersuchungen fiber die löslichkeiten von salzen and gasen in wasser and wäβrigen losungen bei temperaturen oberhalb 100°C, Zeitschrift für anorganische and allgemeine Chemie 337, 68–79.

Ferron, C.J., Fleming, C.A., 2004. Co-treatment of limonitic laterites and sulphur-bearing materials as an alternative to the HPAL process, in: W.P. Imrie et al. (Eds.), Pressure

acid leaching (Proceeding of the International Laterite Nickel Symposium – 2004), TMS, 2004, pp. 245-261.

Hasegawa, F., Tozawa, K., Nishimura, T., 1996. Solubility of ferrous sulfate in aqueous solutions at high temperatures, Shigen to Sozai 112, 879-884.

Huang, M., Papangelakis, V.G., 2008. Online free acidity measurement of solutions containing base metals, Can. Metall. Quart. 47, 269-276.

Jankovic, J., Papangelakis, V.G., Lvov, S.N., 2009. Effect of nickel and magnesium sulphate on pH of sulphuric acid solutions at elevated temperatures, J. Appl. Electrochem 39, 751-759.

Jia, C.Q., Xiao, J.Z., Orr, R.G., 1999. Behaviour of metals in discard nickel smelter slag upon reacting with sulphuric acid, J. Environ. Sci. Health A34, 1013-1034.

Moncur, M.C. Jambor, J.L., Ptacek, C.J., Blowes, D.W., 2009. Mine drainage from the weathering of sulphide minerals and magnetite, Applied Geochemistry 24, 2362-2373.

O'Neill, C.E., Acid leaching of lateritic ores, Canadian Patent No. 947,089, May 4, 1974.

Opratko, V. et al., 1974. Acid leaching of lateritic ores, U.S. Patent 3,809,549

Perederiy, I., Papangelakis, V.G., Buarzaiga, M., Mihaylov, I., 2011. Co-treatment of converter slag and pyrrhotite tailings via high pressure oxidative leaching, J. Haz. Mat. (doi:10.1016/j.jhazmat.2011.08.012).

Seidel, D.C., Fitzhugh Jr., E.F., 1968. A hydrothermal process for oxidized nickel ores, Mining Engineering, April, 80-86.

CHAPTER 6 LEACHING OF AMORPHOUS SLAG

This chapter discusses leachability of amorphous slag at high and low temperatures. The mechanism of leaching is proposed based on characterization of slag and residue structure as well as studies of silicate glass dissolution. The chapter is based on a manuscript in preparation:

- Perederiy, I., Papangelakis, V.G. High pressure oxidative leaching of amorphous FeO-SiO_2 slag: leaching mechanism (in preparation)

6.1 Introduction

Amorphous materials, being metastable in nature, normally dissolve faster than their crystalline counterparts – this property is often utilized in pharmaceutics (Pandit, 2007; He, 2009). However, silicate slags were found to exhibit a different behaviour. Baghalha et al. (2007) compared the performance of high pressure oxidative acid leaching with crystalline (slow-cooled) and amorphous (granulated) electric furnace slag, and showed that dissolution of Ni, Co and Cu is slower in the case of amorphous slags. Extractions of Ni, Co and Cu from amorphous slags were only in the 20-30% range after one hour, whereas 75 to 85% of Ni, Co and Cu dissolved from crystalline slags under the conditions employed (250°C, 0.3 kg of acid per kg of slag, 28%$_{wt}$ solids, 0.52 MPa O_2).

It is also known that hazardous elements in industrial wastes can be immobilized by means of vitrification, i.e. converting a material into a glassy amorphous solid (Park and Heo, 2002; Yalmali et al, 2007; Basegio et al, 2009). Kuo et al. (2008) investigated the effect of cooling rate (air cooling versus water-quenching) on the leaching behaviour of slags obtained from vitrification of incinerator fly ash with SiO_2 at 1450°C. It was found that the extent of Cd, Cu and Zn dissolution (toxicity characteristic leaching procedure SW846 Method 1311, US EPA) decreased with an increase in the content of amorphous material. In addition to the environmental stability tests, the slags were also treated with 3% HCl for 7 days, and then the surface was imaged with the help of scanning electron microscopy. The slags with a higher content of the amorphous phase (obtained by quenching in water) retained smoother surfaces in comparison with the more crystalline slags.

The ability of amorphous silicate slags to resist acid attack over a wider range of temperatures and concentrations has not been explained yet. However, studies of glass dissolution hint at the formation of silica-enriched protective surface films due to the preferential removal of the metal oxide components by acid (Hench and Clark, 1978; Cailleteau, 2008). Selective leaching of sodium from glasses can be illustrated by the following equation (Pierce et al., 2008):

$$\equiv Si{-}O{-}Na + H^{+} \rightarrow \equiv Si{-}OH + Na^{+} \quad (6.1)$$

The triple dash in the equation above represents three unbroken network bonds.

Like glass, certain silicate minerals are also known to dissolve incongruently under ambient conditions, leaving silica-enriched material behind (Terry, 1983). Incongruent dissolution of wollastonite ($CaSiO_3$) was reported by Weissbart and Rimstidt (2000) as well by Ptáček et al. (2011). Casey et al. (1989) observed a silica-rich layer on the surface labradorite feldspar (average formula $Ca_{0.605}Na_{0.38}Al_{1.61}Si_{2.4}O_8$) treated with acid.

It can be hypothesized that amorphous $FeO\text{-}SiO_2$ slags are not as amenable to leaching as crystalline slags due to the incongruent regime of dissolution leading to the formation of a protective silica-enriched layer.

6.2 High Temperature Oxidative Acid Leaching

6.2.1 Kinetics of leaching

Several leaching experiments were conducted at temperatures of 60-250°C with 20% solids, 70 g/L initial H_2SO_4, 90 psi (6.2 bar) O_2. The first leaching experiment was run at a fixed temperature of 250°C for 45 min. Extractions of Ni, Co and Cu were in the 27-43% range after 5 minutes of leaching (Fig. 6.1), but after that leaching slowed down, and no further dissolution took place after 35 min. It was noticed, however, that cooling the autoclave and filtering resulted in a noticeable increase in the extraction of Co and Cu (close to +10%). This is attributed to additional dissolution of slag taking place at lower

temperatures as evidenced by an increase in the concentration of ferrous iron (from 0.2 to 11 g/L) and a drop in acidity (from 42 to 3g/L) – Fig. 6.2.

To test whether it is possible to utilize the low-temperature dissolution, two experiments with variable temperatures (the actual temperature profiles are shown in Fig. 6.1) were run. Unfortunately, the dissolution profiles improved insignificantly, and even prolonging leaching to 2 hours made no practical difference.

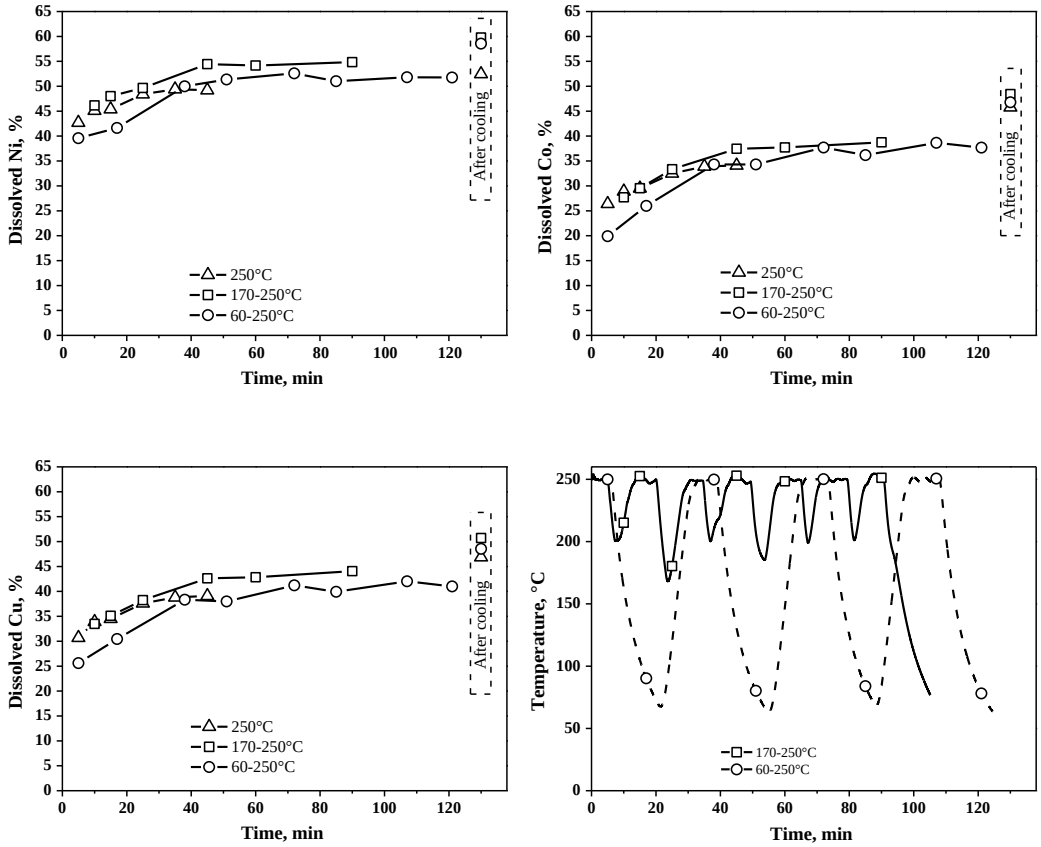

Fig. 6.1 Extractions of Ni, Co and Cu, and temperature profiles. Amorphous electric furnace slag, 20% solids, ~70 g/L initial H_2SO_4, ~90 psi (6.2 bar) O_2 (at temperature)

The extent of post-autoclave dissolution of silicon (Fig. 6.2) was found to depend on the duration of post-leaching contact (during cooling and filtration) of the residue and the leach liquor. The following concentrations of Si were measured in the filtrate: 4.9 g/L (90 min experiment, 30 min cooling, >3 h filtration), 4.3 g/L (45 min experiment, 30 min cooling and 30 min filtration) and 2.1 g/L after (120 min, 30 min cooling, 6 min filtration). The variation in the filtration times was caused by changes in the morphology

of precipitated hematite (Fe_2O_3) and silica (SiO_2) triggered by changes in the acidity (Li et al., 2009) and oxygen pressure during the cooling-heating cycles

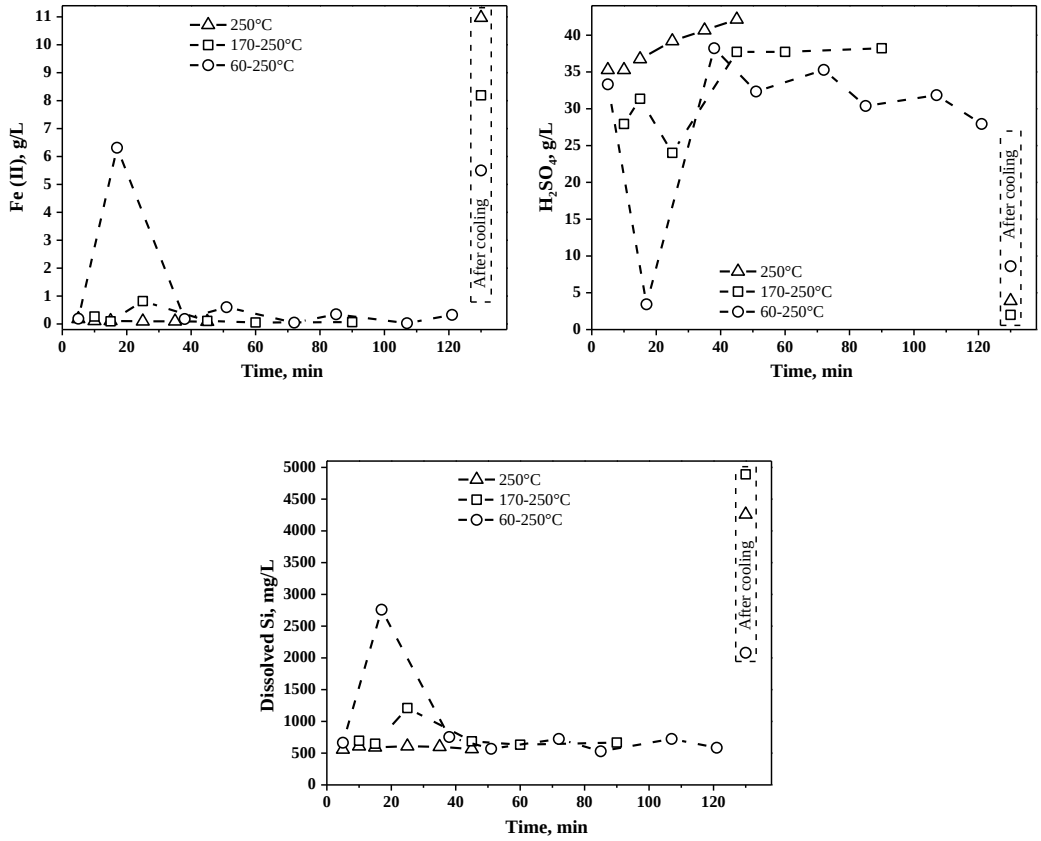

Fig. 6.2 Profiles of Fe(II), Si and H_2SO_4. Amorphous electric furnace slag, 20% solids, ~70 g/L initial H_2SO_4, ~90 psi (6.2 bar) O_2 (at temperature)

6.2.2 Characterization of residues

The residues of leaching were examined under SEM to determine the reason for poor kinetics and low final extractions. All residues appeared to be similar, containing a mix of unreacted and partially reacted particles retaining their original shapes, such as those shown in Fig. 6.3 and 6.4 (additional images are shown in Appendix G). Many particles consist of a bright unreacted core with a darker rim of metal-depleted (silica-rich) material ranging from a tenth to tens of micrometers. Some particles appear dark with a few bright spots of original slag material or hematite precipitated inside. Variation in the

thickness of the reacted metal depleted layer is likely related to structural anisotropy stemming from the presence of small crystalline mineral phases.

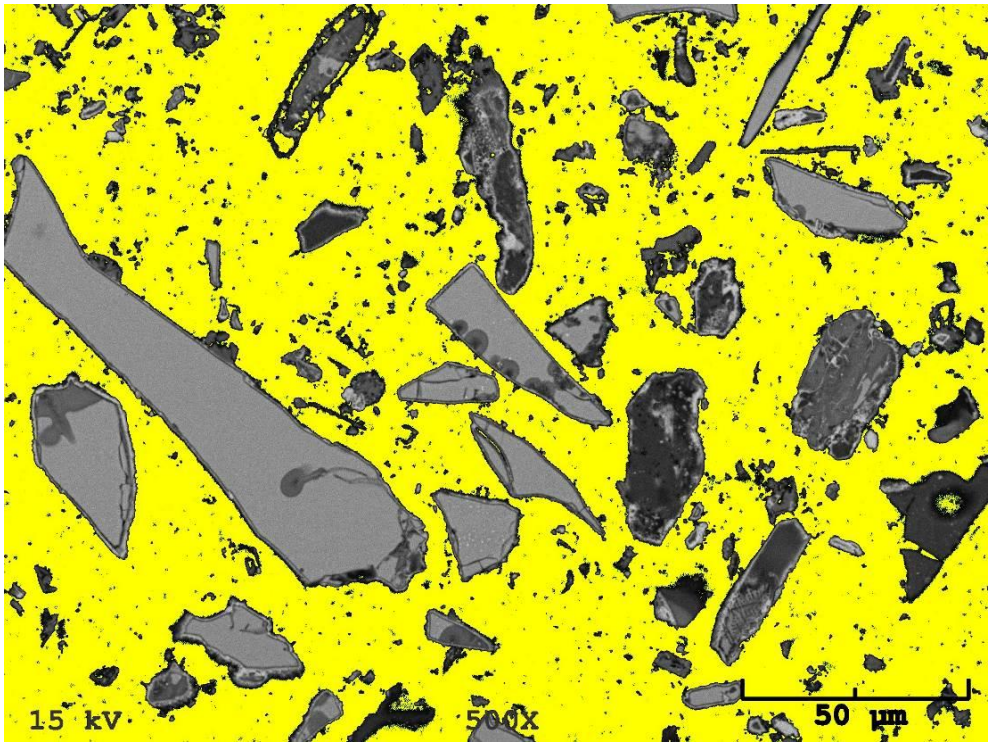

Fig. 6.3 SEM-BSE cross-section image of residue of the 45 min experiment (250°C). The black background was substituted with yellow colour for better contrast near the rims.

Fig 6.4 shows a high-magnification image of a particle which was attacked from two sides, and Fig. 6.5 shows elemental maps for the same particle. The shape of the particle suggests that the silica layer was formed by preferential dissolution of iron from the original slag material. Interestingly, the reacted layer was porous enough at some point to allow Fe(II) to diffuse out of the core, and oxygen diffuse towards the core – as a result, some iron got oxidized, and hematite precipitated inside the siliceous layer close to the edges. Aluminium also precipitated within the siliceous layer (closer to the core) as hydronium alunite, $H_3OAl_3(SO_4)_2(OH)_6$ according to XRD. These precipitates can be easily identified on the sulphur map.

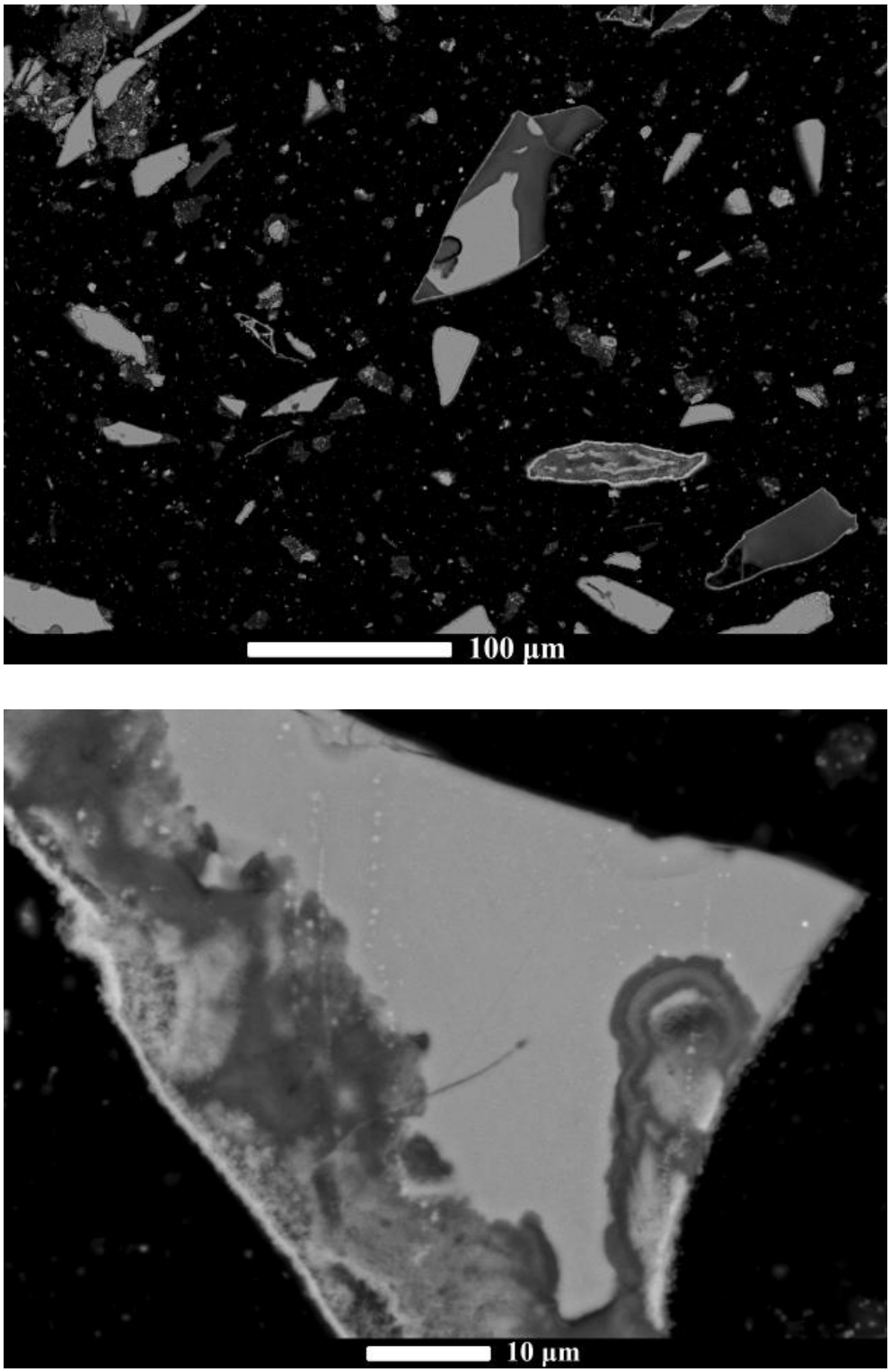

Fig. 6.4 SEM-BSE images residue after leaching for 2 hours

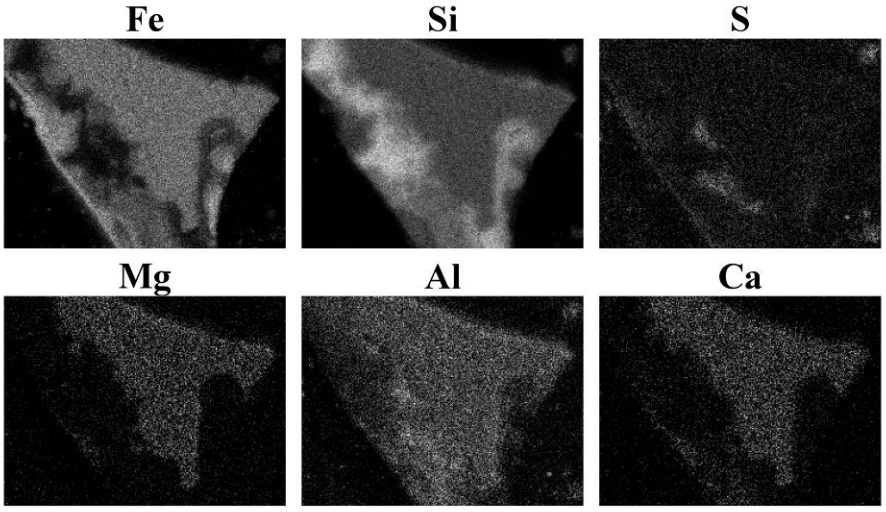

Fig. 6.5 Element maps of the particle from Fig. 6.4.

6.3 Low Temperature Acid Leaching

The additional dissolution of slag taking place at lower temperatures during cooling and filtration (Fig. 6.1 and 6.2) suggests that it is possible to overcome the issue of slag passivation with silica. Although the experiments with thermal cycling (60 to 250°C) did not lead to better extractions, it was attributed to the formation of the passive layer during the initial 5 minutes of leaching conducted at 250°C. To overcome the limitation, two room temperature experiments were conducted under anoxic conditions. According to Fig. 6.6, ~ 90% of Fe, Si and Co dissolved within 40 min. Dissolution of Ni and Cu, however, was hindered by the absence of an oxidant, limiting matte dissolution rate by the rate of H_2S removal from the solution.

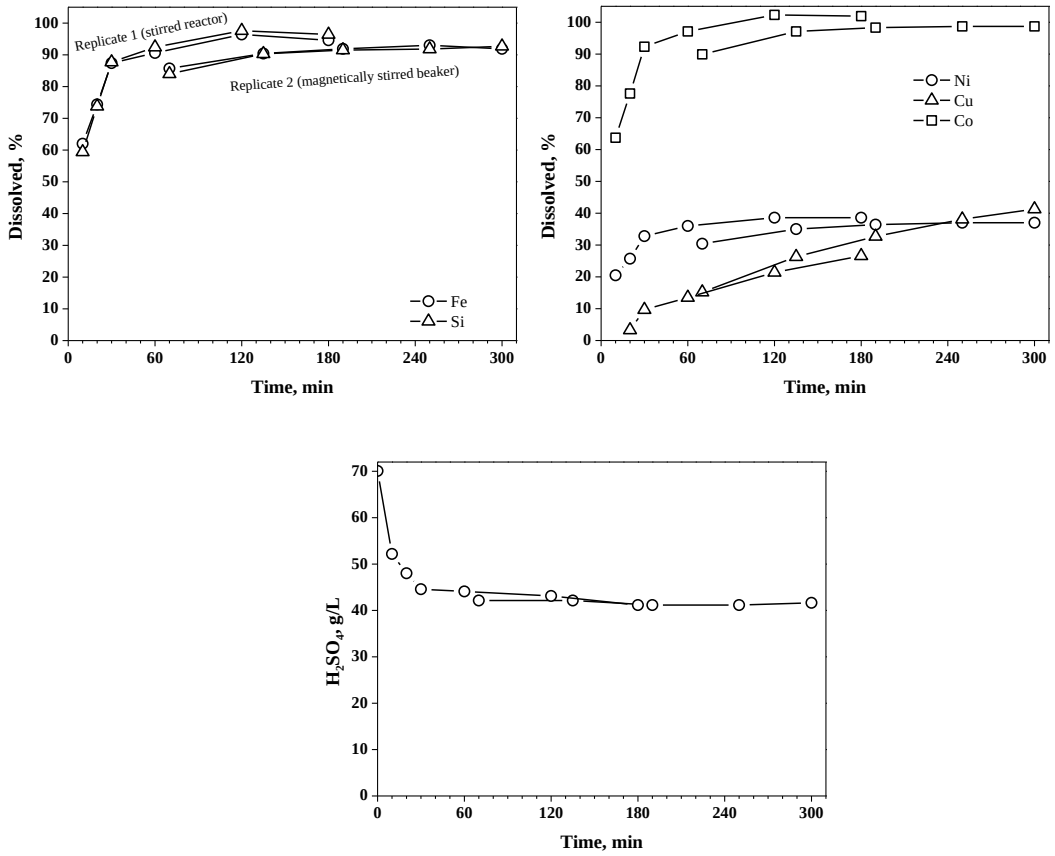

Fig. 6.6 Dissolution profiles. 23-29°C, 2% solids, 70 g/L initial H_2SO_4

6.4 Mechanism of Amorphous Slag Leaching

A schematic of slag structure is shown in Fig. 6.7a. The amorphous material contains networks of joined SiO_4 tetrahedra (similar to vitreous SiO_2 - Sitarz, 2011), and metal ions (Fe, Mg, Al, Ca, K, Na) which bridge the networks of SiO_2. Formation of the metal-depleted siliceous layer around unreacted particle cores (Fig. 6.3, 6.4) indicates that Fe, Mg, Ca and other metals dissolve preferentially from the slag material. This is consistent with the percolation model of glass dissolution, in which metal cations are exchanged with protons and leached out leaving a siliceous layer behind (Ledieu et al., 2004; Devreux et al.; Cailleteau, 2008), e.g. for a divalent metal:

$$\equiv Si{-}O{-}Me{-}O{-}Si\equiv + 2H^+ \rightarrow \equiv Si{-}OH + OH{-}Si\equiv + Me^{2+} \qquad (6.2)$$

(The triple dash represents the unbroken bonds in the glass.)

The most likely route for acid attack is indicated in Fig. 6.7b.

The formation of -OH groups (Eq. 6.2) reduces the number of bonds holding the networks of SiO_4 tetrahedra together, and aids in their dissolution via the hydrolytic breaking of the Si-O bonds (Baucke, 1994; Weissbart and Rimstidt, 2000):

$$\equiv Si{-}O{-}Si(OH)_3 + H_2O \rightarrow \equiv Si{-}OH + Si(OH)_{4(aq)} \quad (6.3)$$

Si and Fe (II) concentration profiles (Fig. 6b and c) indicate that the produced silicic acid and metal cations will make their way through the leached layer towards the surface of the slag material as per Fig. 6.7c.

While a portion of protonated tetrahedra dissolve per Eq. 3, it was shown by Casey et al. (1988, 1989 and 1993) that re-polymerization also takes place:

$$\equiv Si{-}OH + HO{-}Si\equiv \rightarrow \equiv Si{-}O{-}Si\equiv + H_2O \quad (6.4)$$

This process (illustrated by Fig. 6.7d) may cause pore closing and prevents further dissolution of the slag material. Casey et al. (1988) pointed that Al^{3+} is able to assist re-polymerization by adding crosslinks. This can explain the presence of hydronium alunite within the leached layer: aluminium ions re-embedded into amorphous silicate provide centres of nucleation for more ordered structures of hydronium alunite. The hypothetical re-polymerization of protonated tetrahedra can be further aggravated by precipitation of silica when dissolved silicic acid (Eq. 6.3) moves towards the edge of the particle and enters the high acidity zone. Since this precipitation would occur within the pores, it is difficult to determine whether it solid re-polymerization or in-situ precipitation that hinders dissolution.

The amenability of amorphous slag to low temperature leaching is likely to be related to a decrease in the rate of re-polymerization (Eq. 6.4) and increased stability of supersaturated solutions of silicic acid. It was observed that it took several weeks for filtrates with over 4 g/L of Si content to turn into gels (the filtrates were stored in plastic containers at room temperature).

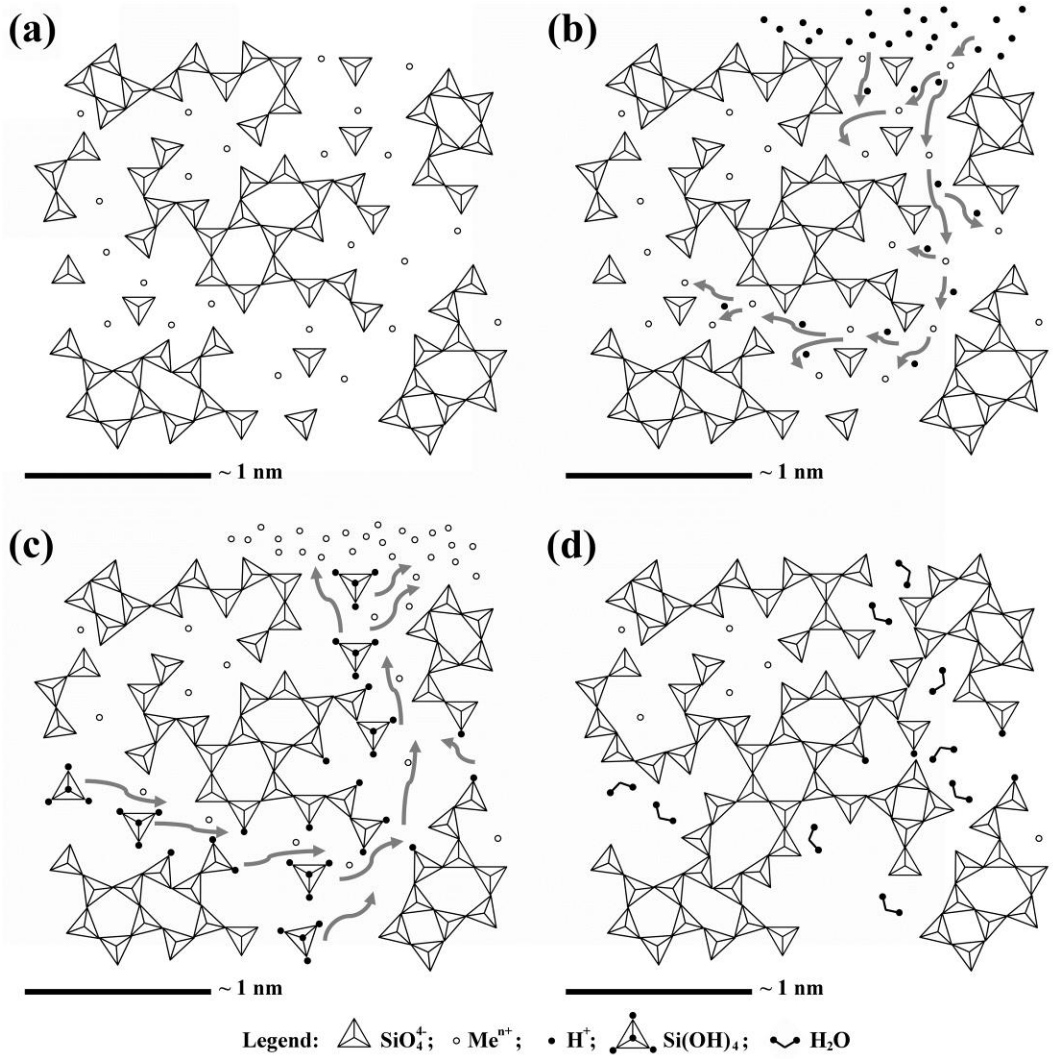

Fig. 6.7 Conceptual schematics of the slag dissolution mechanism:
a) Original material; b) Paths of acid attack; c) Removal of silicic acid; d) Re-polymerization of silica

The ability of crystalline $FeO\text{-}SiO_2$ slags to dissolve fast and completely stems from good spatial separation of silica and fayalite (Fe_2SiO_4) during solidification. Readily accessible zones of crystalline fayalite, having an ordered structure shown in Fig. 6.8, are able to dissolve congruently due to the fact that silica tetrahedra are separated by Fe (II) cations, and the dissolution of the latter completely breaks down the silicate network.

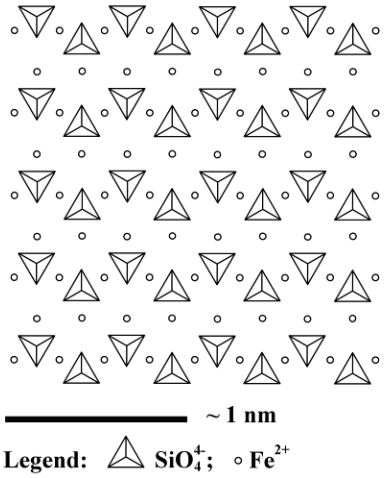

Fig. 6.8 Structure of fayalite

6.5 Summary

Amorphous FeO-SiO_2 slags are not amenable to high pressure leaching due to the formation of a passive layer of amorphous silica upon reacting with acid. The formation of silica occurs because of the incongruent dissolution of the metal components (Fe, Mg, Ca, Al, Na, K). The zones where the front of dissolution advanced deep towards the core likely contained crystalline components. The maximum extractions of Ni, Co and Cu obtained after 1.5-2 hours of leaching 250°C, 20% solids, ~70 g/L initial H_2SO_4, ~90 psi (6.2 bar) O_2 were in the 45-60% range.

The dissolution mechanism corresponds to the percolation model of glass corrosion in which acid attack occurs along the continuous channels of metal cations. The metal cations connecting small networks of SiO_4 tetrahedra are substituted with protons reducing integrity of the slag material. Hydrolysis of the Si-O bonds leading to silica dissolution is thought to compete with re-polymerization silica and precipitation of dissolved silicic acid along the path of the acid attack, thus preventing the complete dissolution. Effective dissolution of slag at low temperatures is explained by the increased stability of supersaturated solutions of silicic acid as well as lower rates of re-polymerization of silicates.

References

Baghalha, M., Papangelakis, V.G., Curlook, W., 2007. Factors affecting the leachability of Ni/Co/Cu slags at high temperature. Hydrometallurgy 85, 42-52.

Basegio, T., Beck Leão, A.P., Bernardesa, A.M., Bergmanna, C.P., 2009. Vitrification: An alternative to minimize environmental impact caused by leather industry wastes. Journal of Hazardous Materials 165, 604-611.

Baucke, F.G.K., 1994. Corrosion of glasses and its significance for glass coating. Electrochimica Acta 39, 1223-1228.

Cailleteau, C., Weigel, C., Ledieu, A., Barboux, Ph., Devreux, F., 2008. On the effect of glass composition in the dissolution of glasses by water. Journal of Non-Crystalline Solids, 354, 117-123.

Casey, W.H., Westrich, H.R., Arnold, G.W., 1988. Surface chemistry of labradorite feldspar reacted with aqueous solutions at pH = 2, 3, and 12. Geochimica et Cosmochimica Acta 52, 2795-2807.

Casey, W.H., Westrich, H.R., Arnold, G.W., Banfield, J.F., 1989. The surface chemistry of dissolving labradorite feldspar. Geochimica et Cosmochimica Acta, 53, 821-832

Casey, W.H., Westrich, H.R., Banfield, J.F, Ferruzzi, G., Arnold, G.W., 1993. Leaching and reconstruction at the surfaces of dissolving chain-silicate minerals. Nature 366, 253-255.

Devreu, F., Ledieu, A., Barboux, P., Minet, Y., 2004. Leaching of borosilicate glasses. II. Model and Monte-Carlo simulation. Journal of Non-Crystalline Solids 343, 13-25.

He X, 2009. Integration of physical, chemical, mechanical, and biopharmaceutical properties in solid oral dosage form development, in: Y. Qiu, Y. Chen, G.G.Z. Zhang, L. Liu, W.R. Porter (Eds.), Developing solid oral dosage forms: pharmaceutical theory and practice. Elsevier Inc., pp. 407-441.

Hench, L.L., Clark, D.E., 1978. Physical chemistry of glass surfaces. Journal of Non-Crystalline Solids, 28, 83-105.

Kuo, Y.-M., Wang, J.-W., Chao, H.-R., Wang, Ch.-T., Chang-Chien, G.-P., 2008. Effect of cooling rate and basicity during vitrification of fly ash, Part 2. On the chemical stability and acid resistance of slags. Journal of Hazardous Materials, 152, 554-562.

Ledieu, A., Devreu, F., Barboux, P., Sicard, L., Spalla, O, 2004. Leaching of borosilicate glasses. I. Experiments. Journal of Non-Crystalline Solids 343, 3-12.

Li, Y., Papangelakis, V.G., Perederiy, I., 2009. High pressure oxidative acid leaching of nickel smelter slag: Characterization of feed and residue. Hydrometallurgy 97, 185-193.

Pandit, N.K., 2007. Introduction to the pharmaceutical sciences. Lippincott Williams & Wilkins. p.31.

Park, Y.J., Heo, J, 2002. Vitrification of fly ash from municipal solid waste incinerator. Journal of Hazardous Materials B91, 83–93

Perederiy, I., Papangelakis, V.G. High pressure oxidative leaching of amorphous FeO-SiO2 slag: leaching mechanism (in preparation)

Pierce, E.M., Rodriguez, E.A., Calligan, L.J., Shaw, W.J., McGrail, B.P., 2008. An experimental study of the dissolution rates of simulated aluminoborosilicate waste glasses as a function of pH and temperature under dilute conditions. Applied Geochemistry, 23, 2559-2573.

Ptáček, P., Nosková, M., Brandštetr, J., Šoukal, F., Opravil, T., 2011. Mechanism and kinetics of wollastonite fibre dissolution in the aqueous solution of acetic acid. Powder Technology, 206, 338-344.

Sitarz, M., 2011. The structure of simple silicate glasses in the light of Middle Infrared spectroscopy studies. Journal of Non-Crystalline Solids, 357, 1603-1608.

Terry, B., 1983. The acid decomposition of silicate minerals: part I. Reactivities and modes of dissolution of silicates. Hydrometallurgy, 10, 135-150

Weissbart, E.J., Rimstidt, J.D., 2000. Wollastonite: Incongruent dissolution and leached layer formation. Geochimica et Cosmochimica Acta, 64, 4007-4016.

Yalmali, V.S., Deshingkar, D.S., Wattal, P.K., Bharadwaj, S.R., 2007. Preparation and characterization of vitrified glass matrix for high level waste from MOX fuel processing. Journal of Non-Crystalline Solids, 353, 4647-4653.

CHAPTER 7 CONCLUSIONS

Characterization of crystalline slags revealed the presence of fayalite (Fe_2SiO_4) as the dominant mineral phase. Magnetite (Fe_3O_4) was identified as the second major crystalline constituent in the slag. Other mineral phases found in the slag include matte ($MeS_{n<1}$) and silica (SiO_2).

Natural cooling of slag melt promotes the segregation and growth of magnetite zones, which are often surrounded by silica. Granulation can lead to poorly segregated crystalline structures or homogeneous amorphous solid solutions of FeO, SiO_2 and other metal oxides with minor inclusions of fine matte and magnetite.

Nickel and copper were encountered as both sulphides (in matte inclusions) and dissolved oxides. Cobalt could not be identified to overlapping of its Kα lines with those of Fe; however, pyrometallurgical studies indicate that cobalt is present almost exclusively in the oxide form. In the naturally cooled flash furnace slag, nickel and copper were encountered in matte with the same probability, whereas in the naturally cooled converter slag, copper was encountered in matte more often than nickel.

Considering the fact that portions of nickel, copper and especially cobalt are dissolved in the oxide and silicate mineral phases, and that matte inclusions are often only a couple of micrometers in diameter, flotation cannot be effective for the removal of base metals from slags. As a result, the base metals need to be liberated chemically.

High pressure oxidative acid leaching (HPOXAL) was successfully applied to crystalline flash furnace and converter slags. Extractions of Ni, Co and Cu exceeded 90% within 15-20 min and arrived at 95-97% after 45 min at 250°C, 90 psi (6.2 bar) O_2 partial pressure and 70 g/L initial H_2SO_4.

Fayalite was identified as the fastest dissolving component. Leaching performance is best with fayalite-dominated slags. Since fayalite dissolution is an acid-driven reaction, high acidities favour the kinetics of dissolution. High acidity, however, causes elevated levels of iron (III). An initial acidity of ~70 g/L was deemed to provide a good balance between the rate of dissolution and the concentration of residual iron in the leach solution. Temperature is another factor affecting both the kinetics of dissolution and the

concentration of iron after leaching. Temperatures between 225 and 250°C were recommended.

HPOXAL operates with substoichiometric additions of sulphuric acid (10-20% of the stoichiometric requirement). This is made possible by acid regeneration due to iron oxidation and hydrolysis. Partial pressure of oxygen (and oxygen dispersion efficiency) plays a vital role in the regeneration of acid as well as oxidation of matte.

Magnetite was found to dissolve slower than fayalite, and was observed in the residue even when more than 80% of Ni and Co dissolved. A slow increase in the concentration of Ni and Co at the end of leaching is likely related to the slow dissolution of the remaining magnetite. Silica is found to be least affected by leaching. Although it is neither a major mineral phase nor a carrier of base metals, it can act as an efficient barrier for reagent transport to other minerals (primarily, magnetite).

The residues of leaching were identified as aggregates of crystalline hematite (Fe_2O_3) and amorphous silica. Their similarity to the residues of laterite HPAL suggests that they can be discarded safely.

The use of pyrrhotite tailings a substitute of sulphuric acid in slag leaching was investigated. Pyrrhotite tailings were selected for their content of Ni (~0.6%), reactivity and adverse environmental impact (acid mine drainage). The amount of stoichiometrically equivalent acid produced was found to be a linear function of tailings addition. Pyrrhotite oxidation and iron hydrolysis were completed within ~20 min for pyrrhotite tailing additions under 92 g/ kg H_2O at 250°C, 90 psi (6.2 bar) partial pressure of oxygen.

Oxidative co-leaching of pyrrhotite tailings with naturally cooled converter slag at 250°C, 90 psi (6.2 bar) O_2, 68 g/L equivalent H_2SO_4 (corresponding to an acid addition of ~20% of solid feed weight at 25% solids) was shown to have kinetics comparable to adding sulphuric acid with final extractions reaching 95-97% in 45 min. The detrimental effect of high temperature (250°C) combined with a low equivalent acidity (34 g/L) on the kinetics of Ni and Co dissolution was explained in terms of precipitation of divalent

metal sulphates ($FeSO_4$, $NiSO_4$, $CoSO_4$) caused by a shift in the sulphate-bisulphate equilibrium.

On-line acid monitoring using conductivity confirmed that acidity gradually builds up in the system in the first 7-13 min, with oxygen overpressure (and dispersion) determining the rate of acid generation and re-generation. A short disruption in the supply of oxygen resulted in a fast drop in the concentration of sulphuric acid, providing further evidence of fast rates of fayalite dissolution.

It was shown that granulated converter slag with intergrown crystalline mineral phases is also amenable to pressure leaching. Extraction of Ni, Co and Cu exceeded 90% in 10 min at 250°C, 68 g/L equivalent H_2SO_4, 90 psi (6.2 bar) O_2.

Amorphous FeO-SiO_2 slags were found not amenable to high pressure leaching due to the formation of a passive layer of amorphous silica upon reacting with acid. The formation of silica occurs because of the incongruent dissolution of the metal components (Fe, Mg, Ca, Al, Na, K). The extractions of Ni, Co and Cu obtained at 250°C were in the 45-60% range.

The dissolution mechanism was linked to the percolation model of glass corrosion in which acid attacks metal-oxygen bonds, removing connections between networks of silica and reducing the integrity of the slag material. However, solid re-polymerization of silica tetrahedra as well as in situ precipitation of dehydrated silicic acid along the path of the acid attack was hypothesized to cause pore closure at high temperature, creating a protective layer of silica. Effective dissolution of slag at low temperatures is explained by slower rates of re-polymerization as well as increased stability of supersaturated solutions of silicic acid.

CHAPTER 8 RECOMMENDATIONS FOR FUTURE WORK

The current study addresses the effect of process parameters in a limited range. Kinetics of leaching at temperatures in excess of 250° and partial pressures above 90 psi (6.2 bar) should be investigated. In the current work it was not possible due to the limitations of the batch experimental setup in coping with heat evolution.

The profiles of Fe(II) and Fe(III) were often found inconsistent between replicate experiments despite good reproducibility of the kinetics of base metal dissolution. This was linked to inconsistent dispersion of oxygen. The use of a dip tube provided good dispersion of oxygen during feeding (when the current pressure is below the set point). However, since the pressure controller operated in cycles (due to temperature fluctuations causing fluctuations in the determination of the pressure), dispersion of oxygen suffered during the times when the current pressure was above the set point. This issue can be addressed by using a gas entrainment impeller which would ensure continuous even dispersion (being a function of stirring speed with other parameters fixed).

The morphology of residues was linked to the initial conditions of leaching, such as oxygen pressure and the rate of acid injections. Acid injection by propelling with oxygen under pressure confused the temperature controller due to the heat of mixing. Fast changes in the temperature prevented efficient adjustment of the pressure setpoint and caused fluctuations in the partial pressure. As a result, filtration times could not be reproduced consistently and were not investigated in this study. In the future, acid injection can be performed with pressure syringe enabling better control of the initial conditions of leaching. In addition, the effect of seeding needs to be investigated.

The mechanism of amorphous slag leaching has been proposed. However, additional work (such as characterization with high-resolution TEM) needs to been done to identify the dominant process determining pore closure in the leached layer and confirm the effect of structural anisotropy on direction and thickness of leached layer formation.

Finally, a search for conditions enabling the treatment of amorphous slags should continue. Room temperature experiments suggest that temperature plays an important

role in the control of slag passivation. Pressure leaching of amorphous slags needs to be investigated at medium temperatures (140-180°C).

Appendix A. Compositions of various converter slag samples from the Copper Cliff Smelter

Table A.1 Ni content (%) in various converter slags

Blow #				
2nd	**3rd**	**4th**	**5th**	**Last**
1.45	1.29	1.47	3.49	3.97
0.924	0.98	1.18		
	1.55			

Table A.2 Co content (%) in various converter slags

Blow #				
2nd	**3rd**	**4th**	**5th**	**Last**
0.97	1.10	1.12	1.51	2.36
0.65	0.69	0.87		
	1.08			

Table A.3 Cu content (%) in various converter slags

Blow #				
2nd	**3rd**	**4th**	**5th**	**Last**
0.70	0.60	0.65	1.56	1.4
0.55	0.55	0.54		
	0.64			

Table A.4 Mass ratio of magnetite to fayalite in various converter slags

Blow #				
2nd	**3rd**	**4th**	**5th**	**Last**
0.32	0.22	0.22	0.19	0.19
0.26	0.26	0.19		
	0.20			

Appendix B. Composition of various size fractions of flash furnace slag

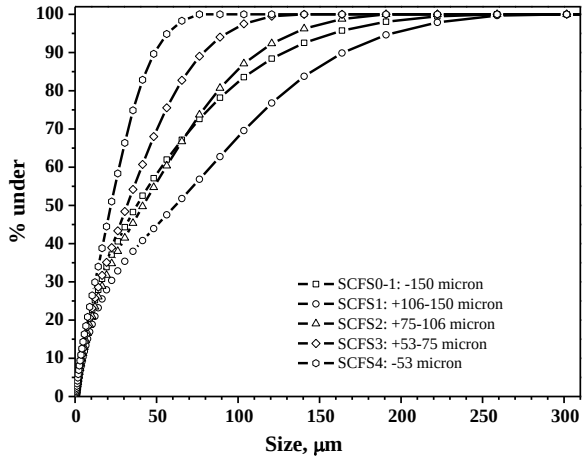

Fig. B.1 Particle size analysis of flash smelter slag samples

Table B.1 Chemical composition of flash smelter slag samples, %wt.

Sample	Ni	Co	Cu	Zn	Al	Si	S	Mg	Ca	Fe(II)	Fe(T)
#0	1.018	0.244	1.070	0.141	1.65	17.7	1.54	0.80	0.79	34.7	39.8
#1	0.928	0.234	0.985	0.140	1.64	17.5	1.43	0.79	0.70	35.1	39.8
#2	1.035	0.244	1.060	0.140	1.64	17.9	1.56	0.80	0.70	36.0	41.0
#3	1.085	0.248	1.175	0.140	1.69	18.2	1.64	0.81	0.81	36.1	41.3
#4	1.185	0.244	1.345	0.140	1.66	17.6	1.78	0.79	0.78	35.8	40.4

Appendix C. Additional SEM images, EDX spectra and elemental maps of flash furnace slag

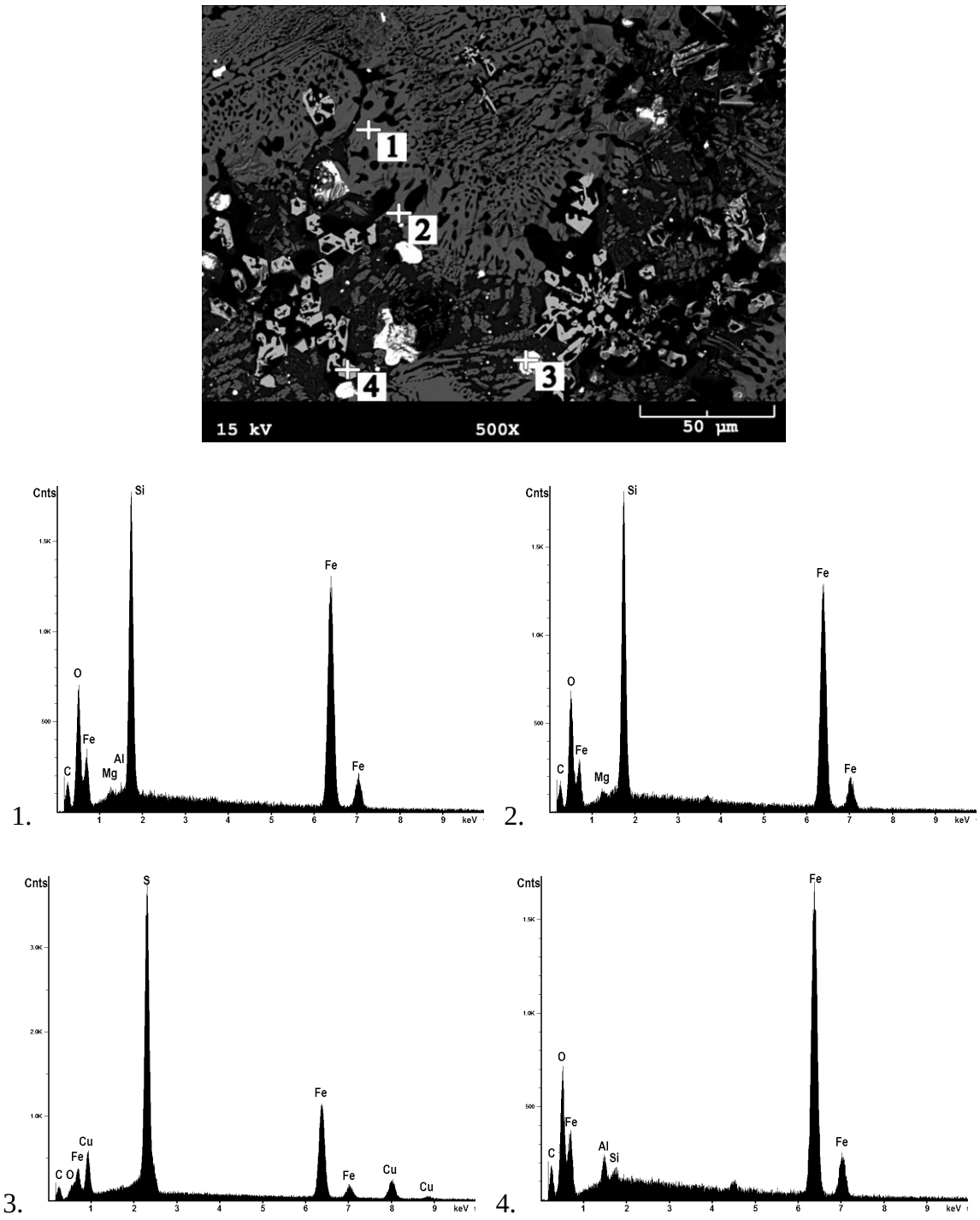

Fig. C.1 SEM-BSE and EDX images of flash furnace slag before grinding (from Li et al., 2008).

1, 2 - fayaltie, 3 – matte, 4 – magnetite.

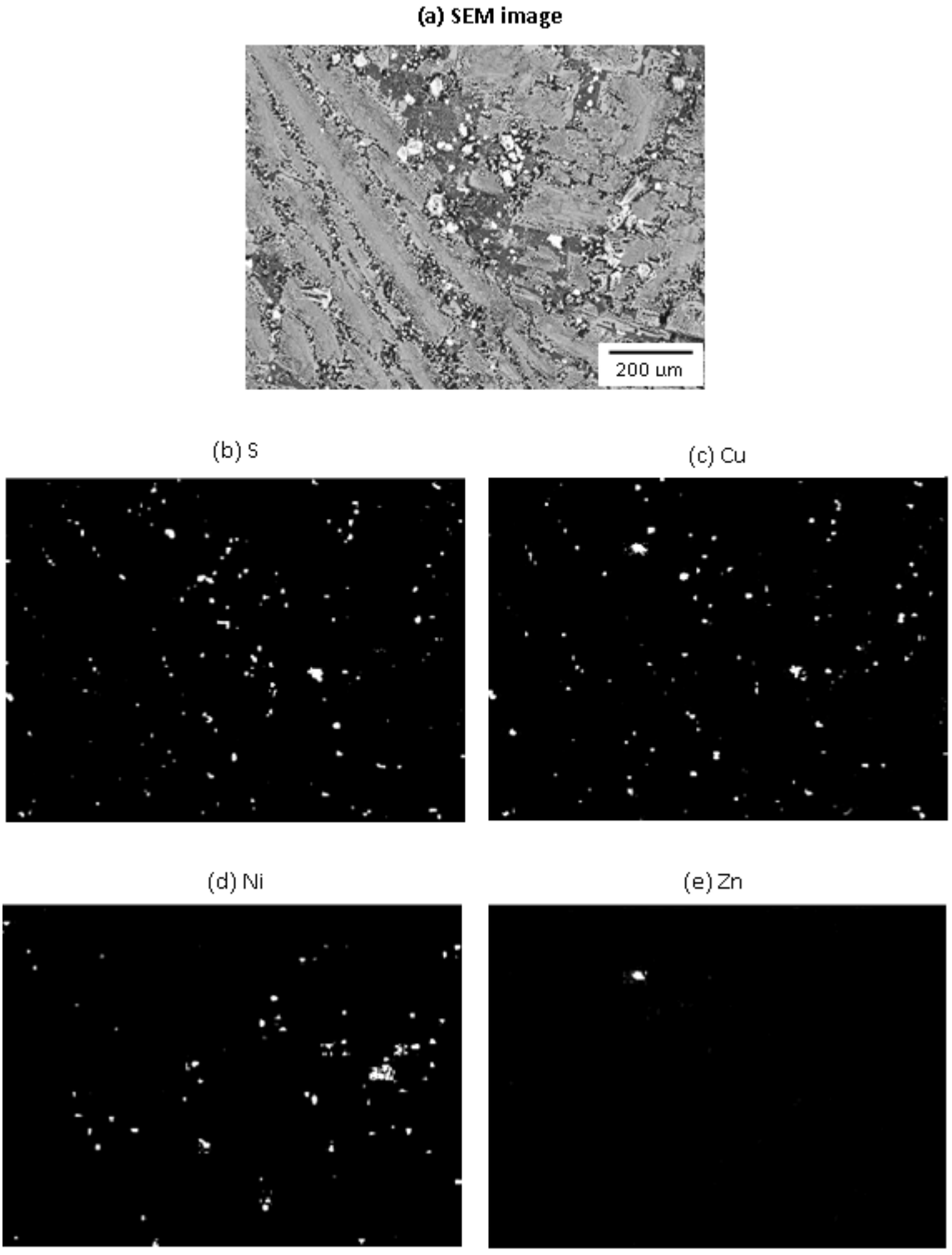

Fig. C.2 SEM-BSE image and elemental EDX maps of flash furnace slag before grinding (from Li et al., 2008)

Appendix D. Additional SEM images, EDX spectra and elemental maps of converter slag

Naturally cooled converter slag

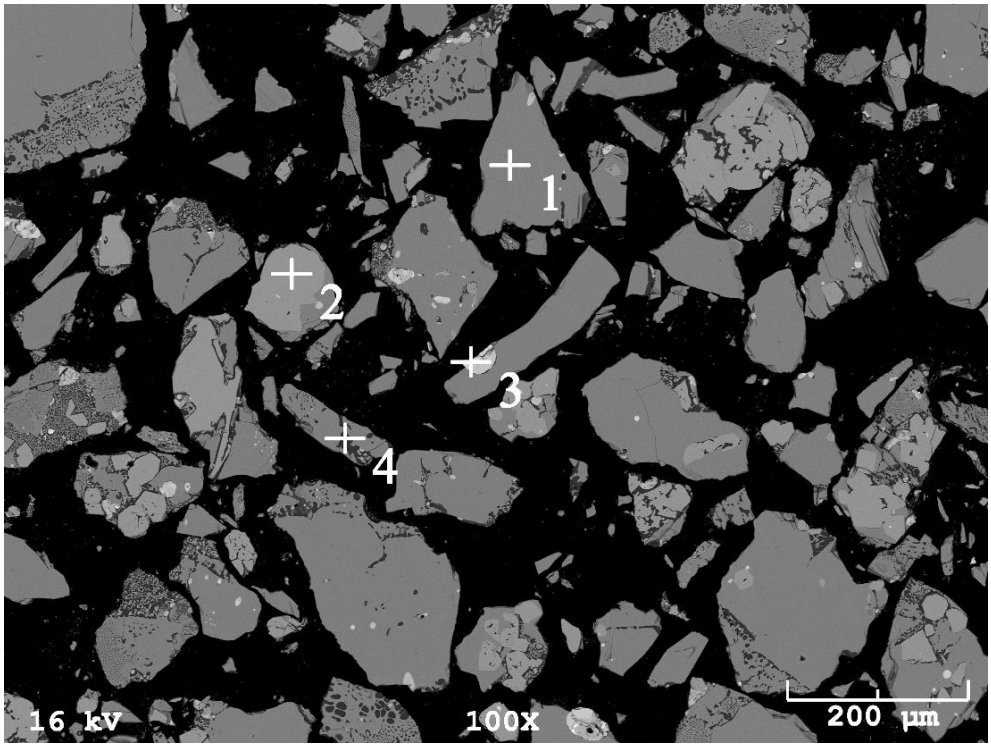

Fig. D.1 SEM-BSE cross-section image of converter slag sample #1

1 – fayalite, 2 – magnetite, 3 – matte, 4- silica.

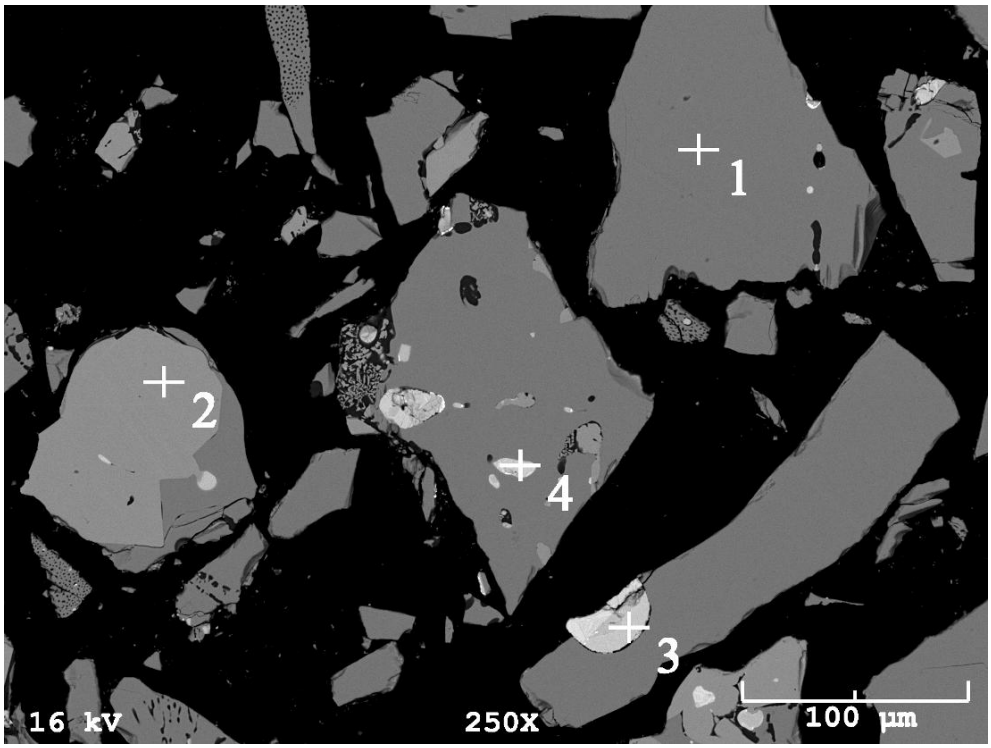

Fig. D.2 SEM-BSE cross-section image of converter slag sample #1

1 – fayalite, 2 – magnetite, 3, 4 – matte.

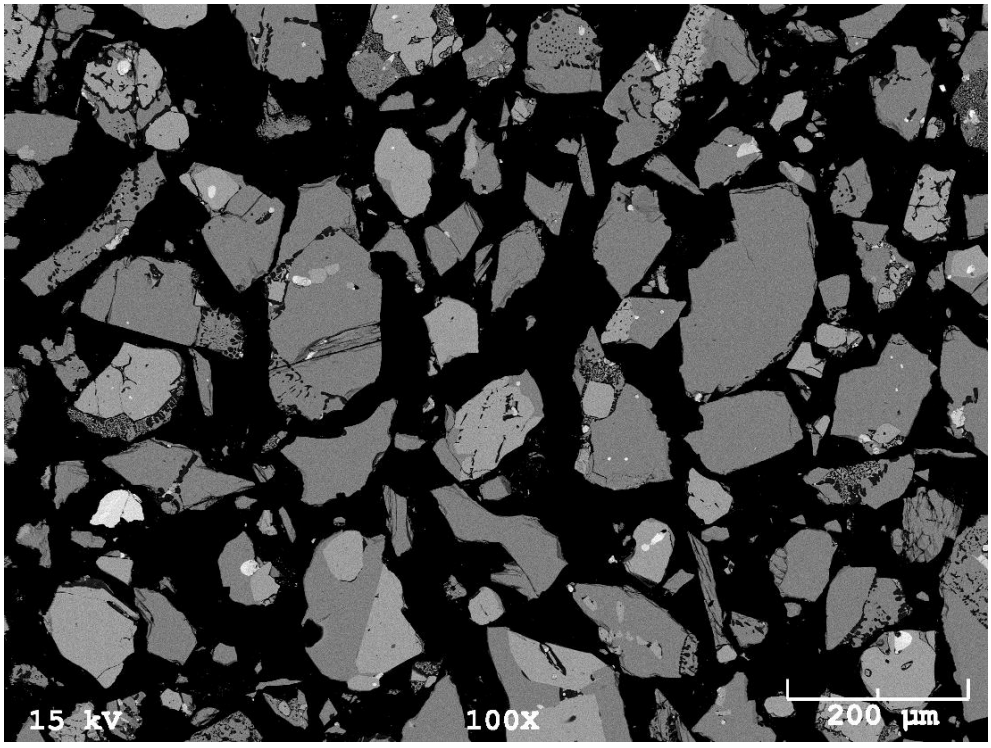

Fig. D.3 SEM-BSE cross-section image of converter slag sample #1

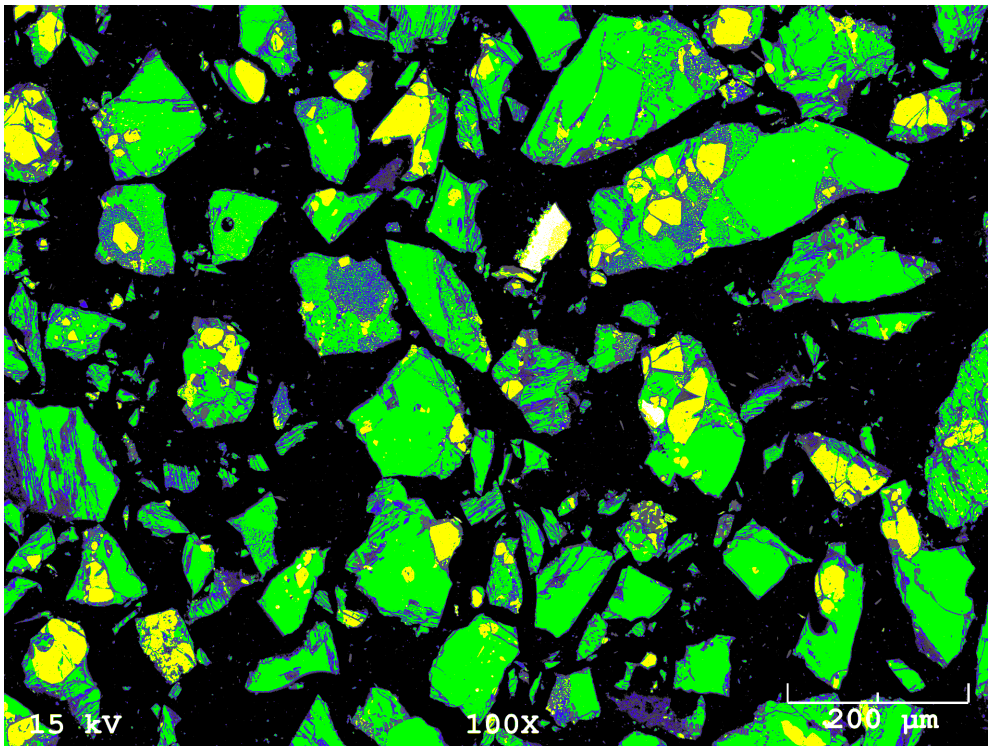

Fig. D.4 Colour-coded SEM-BSE cross-section image of converter slag sample #2
Green – fayalite, yellow – magnetite, blue – silica, white – matte.

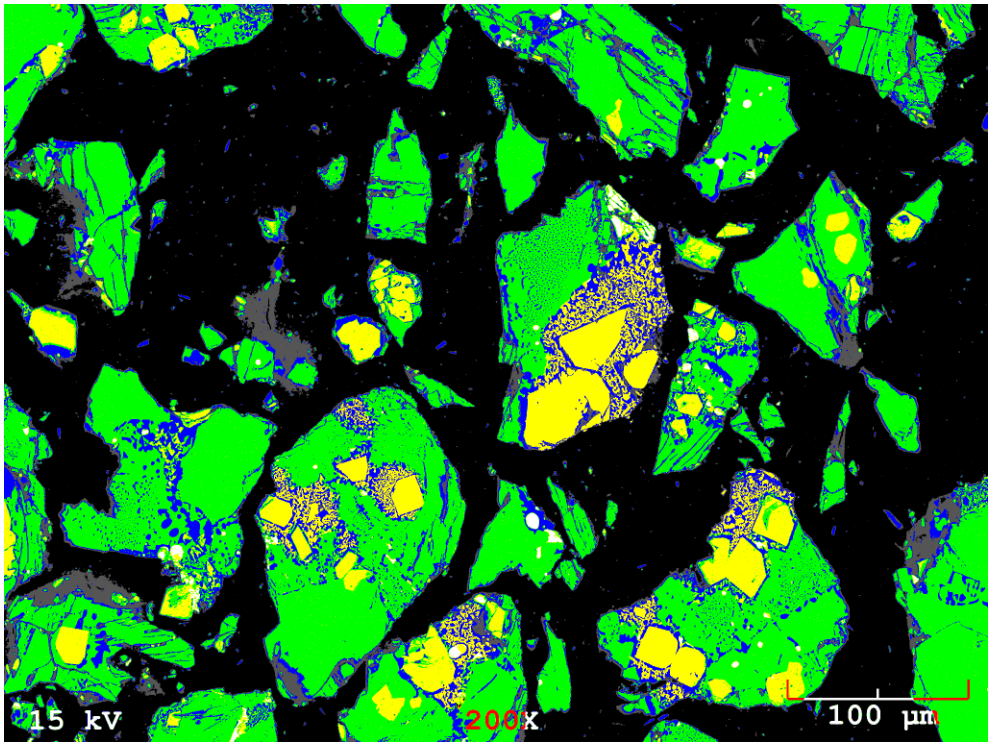

Fig. D.5 Colour-coded SEM-BSE cross-section image of converter slag sample #2
Green – fayalite, yellow – magnetite, blue – silica, white – matte.

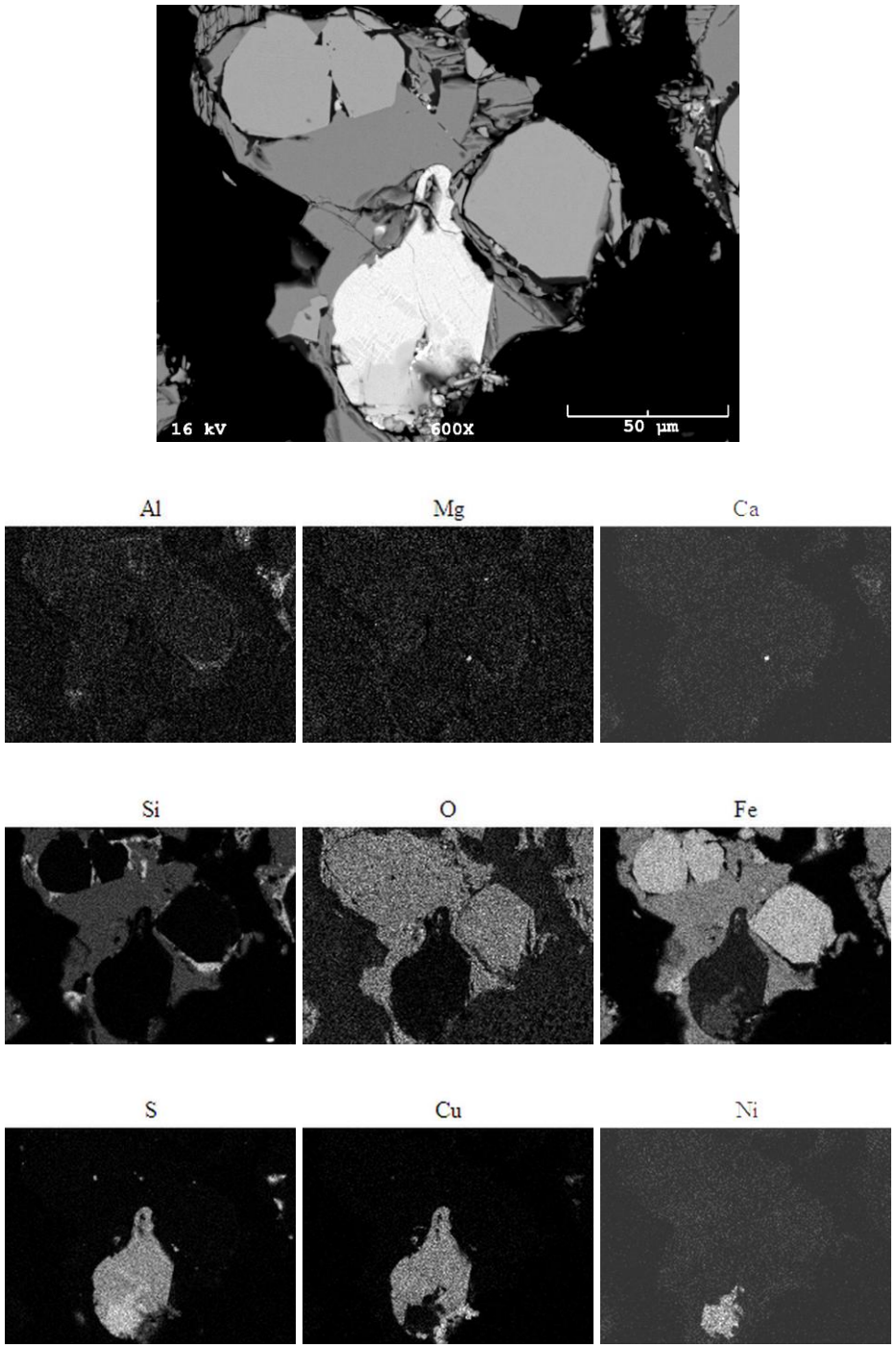

Fig. D.6 SEM-BSE cross-section image and elemental maps of converter slag sample #2

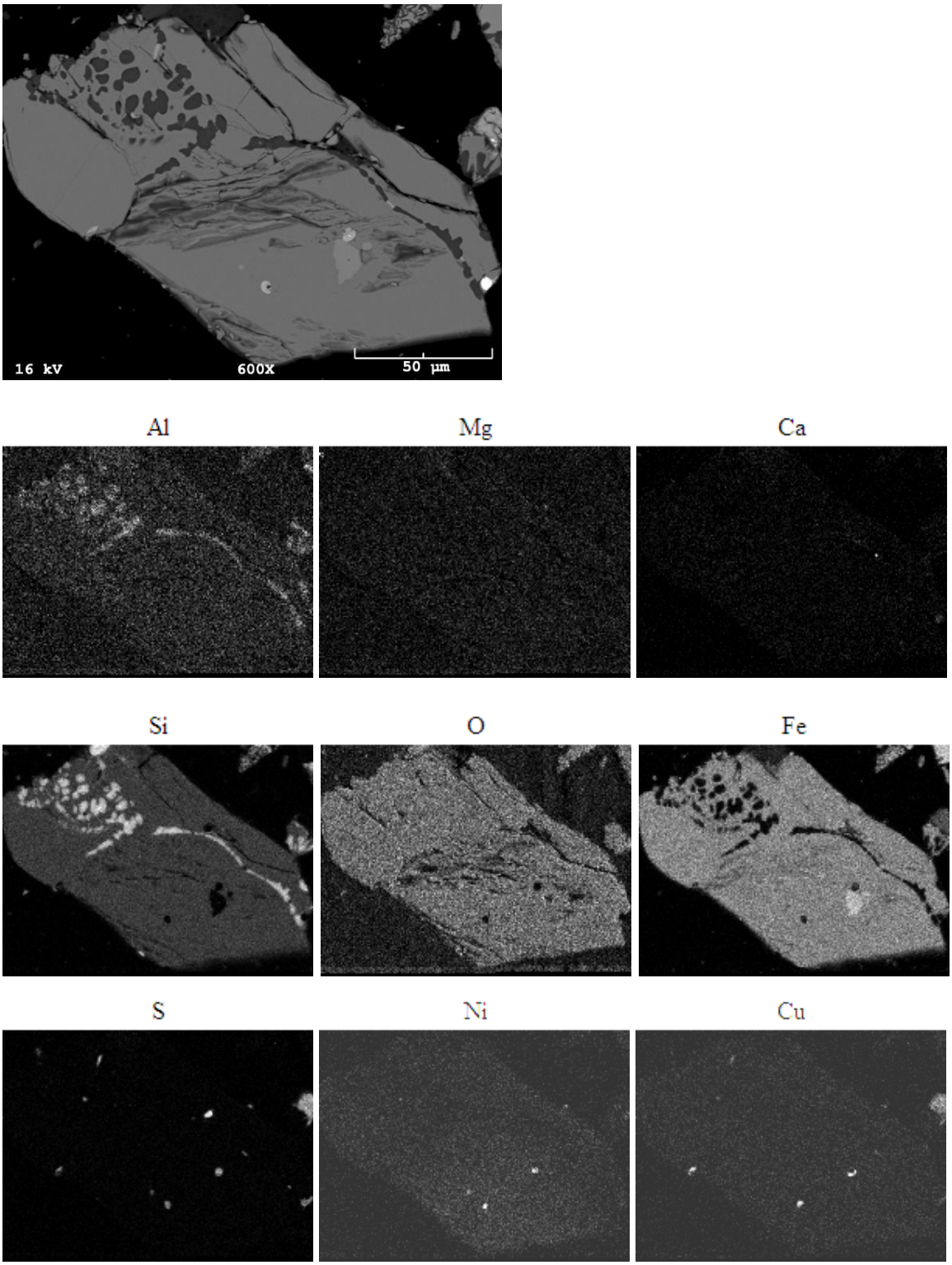

Fig. D.7 SEM-BSE cross-section image and elemental maps of converter slag sample #2

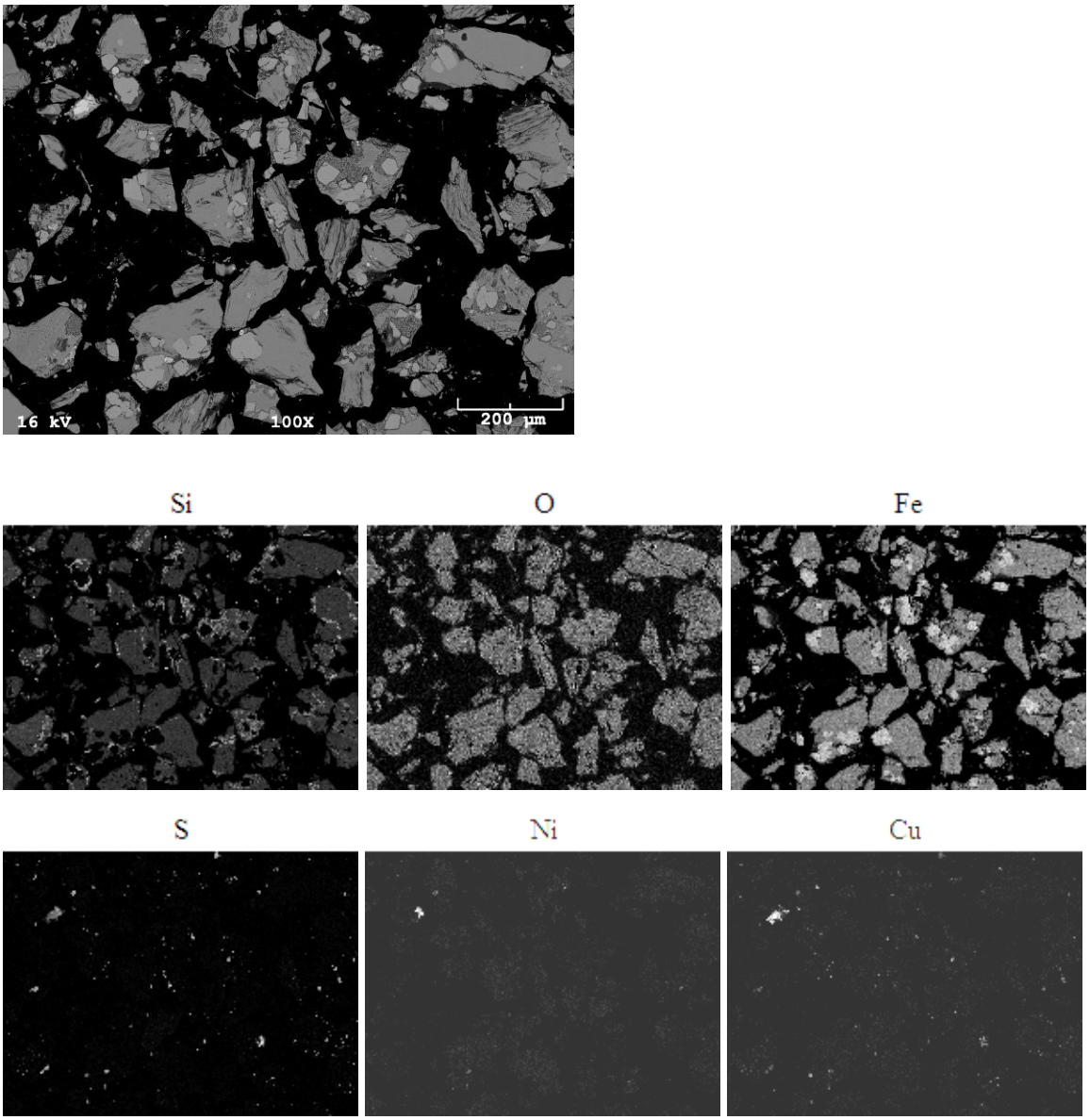

Fig. D.8 SEM-BSE cross-section image and elemental maps of converter slag sample #2

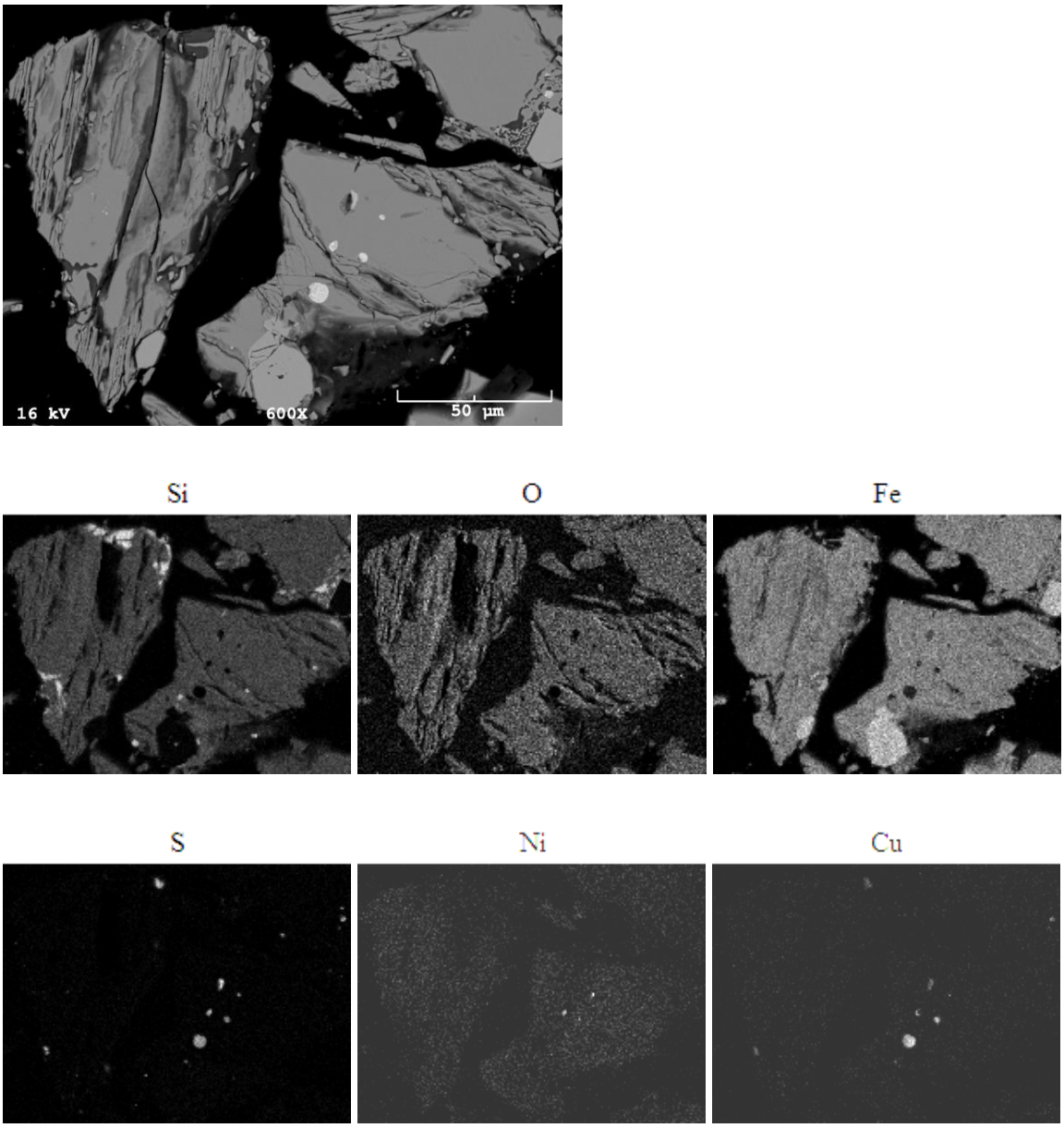

Fig. D.9 SEM-BSE cross-section image and elemental maps of converter slag sample #2

Granulated converter slag

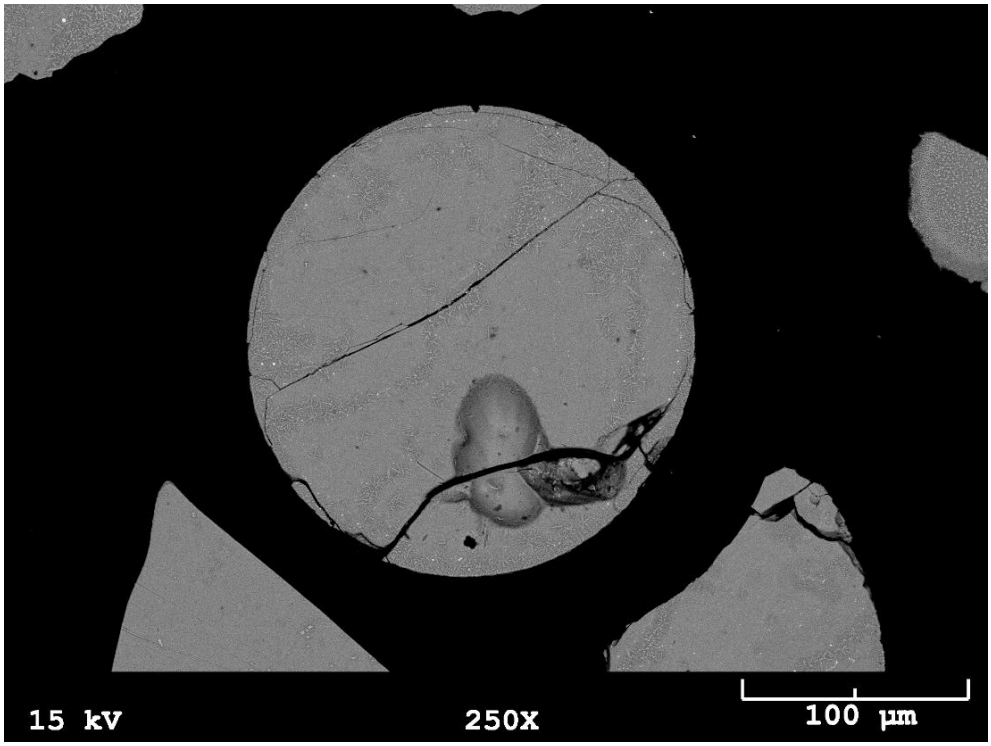

Fig. D.10 SEM-BSE cross-section image of granulated converter slag (before grinding).

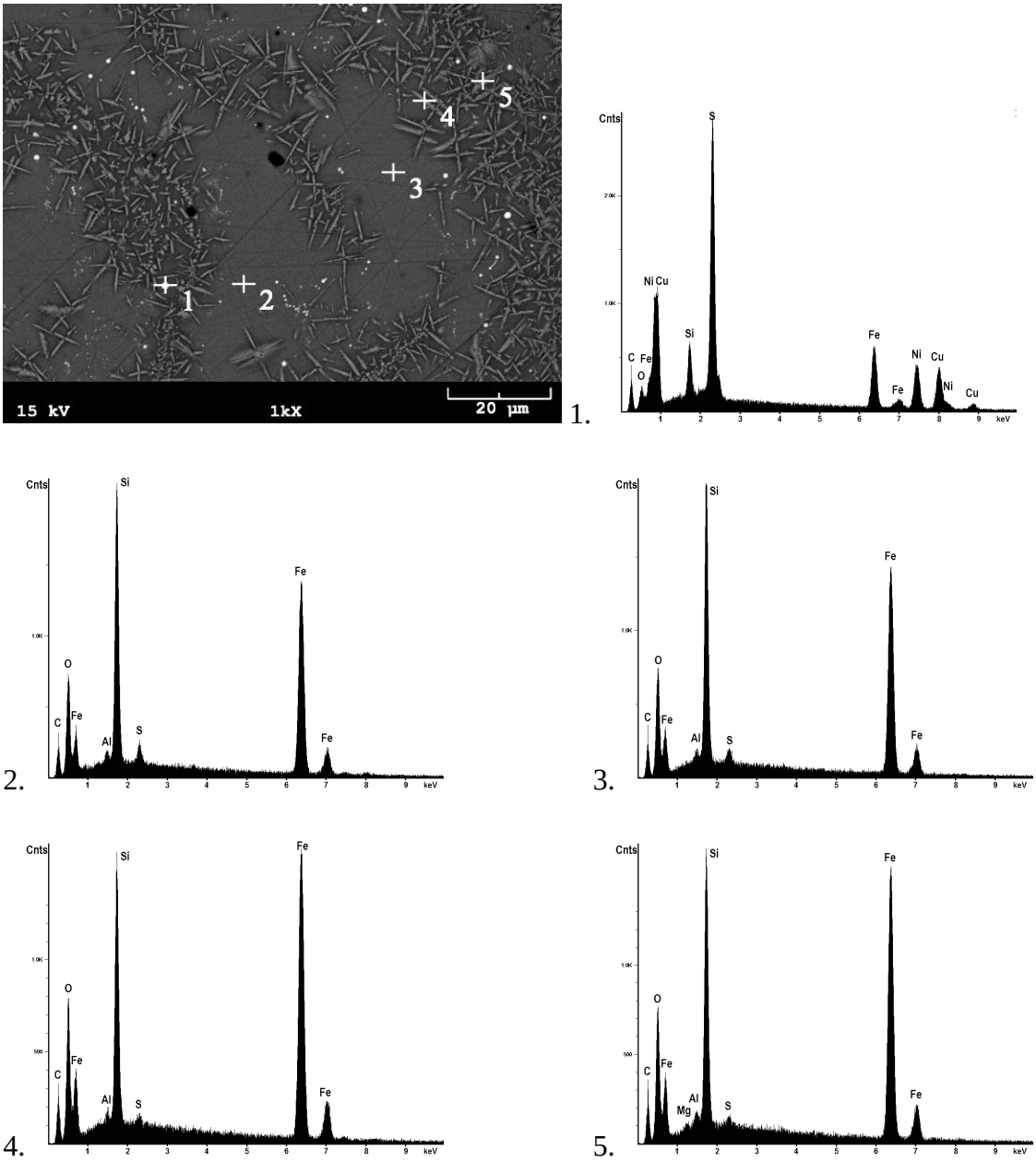

Fig. D.11 SEM-BSE cross-section image and EDX spectra of granulated converter slag (before grinding).

Appendix E. Additional SEM images and EDX spectrum of granulated electric furnace slag

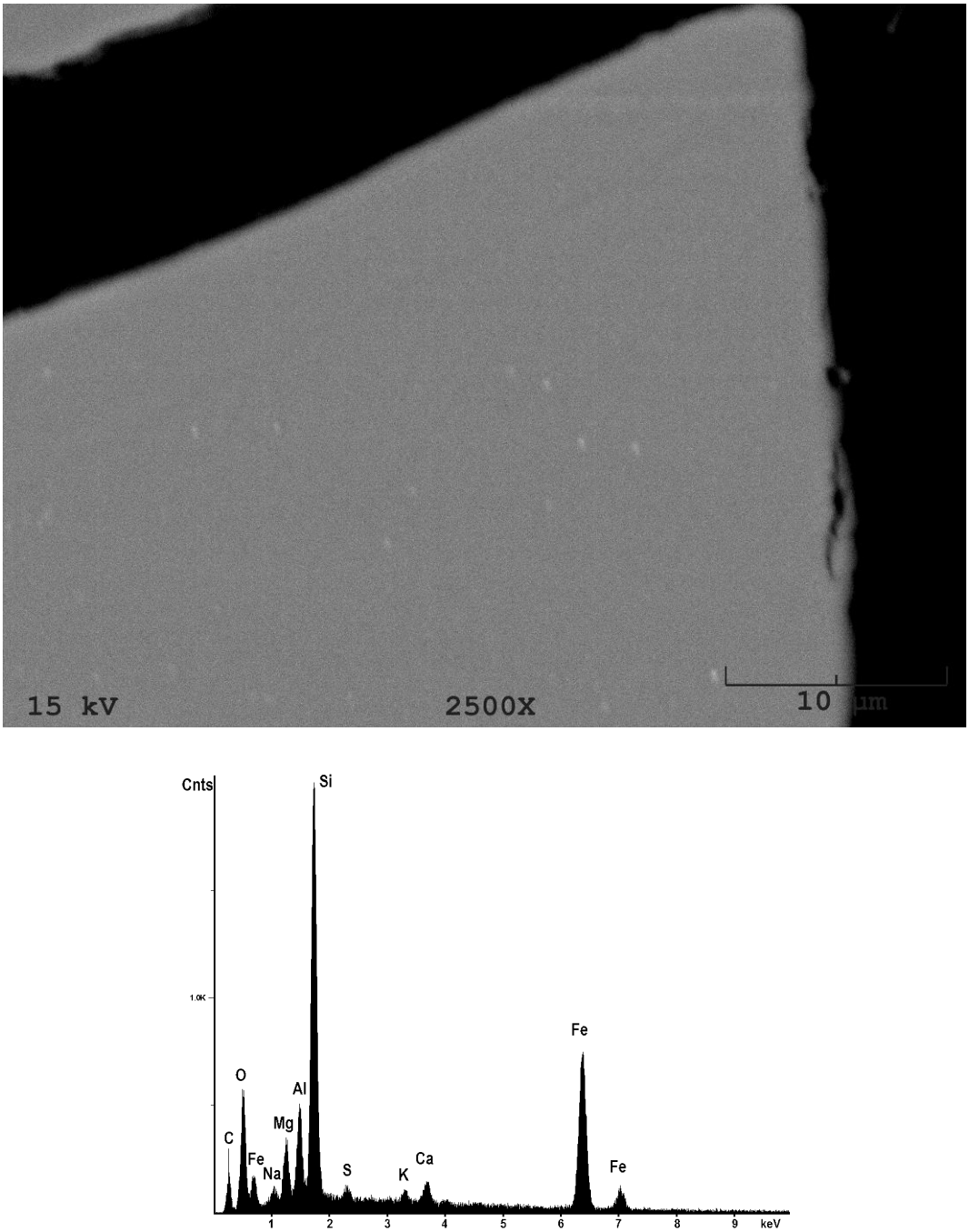

Fig. E.1 SEM-BSE cross-section image and EDX spectrum of electric furnace slag sample

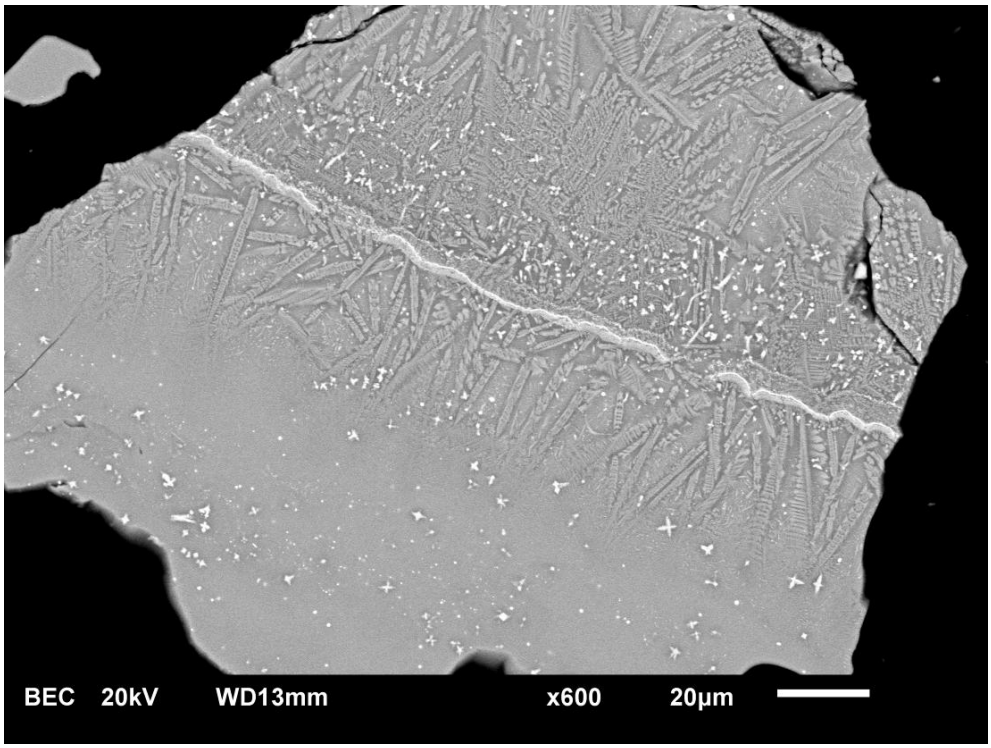

Fig. E.2 SEM-BSE cross-section image of electric furnace slag sample.

Partially crystalline particle. Bright spots – magnetite, the mineral phases differ in the content of Al and Mg.

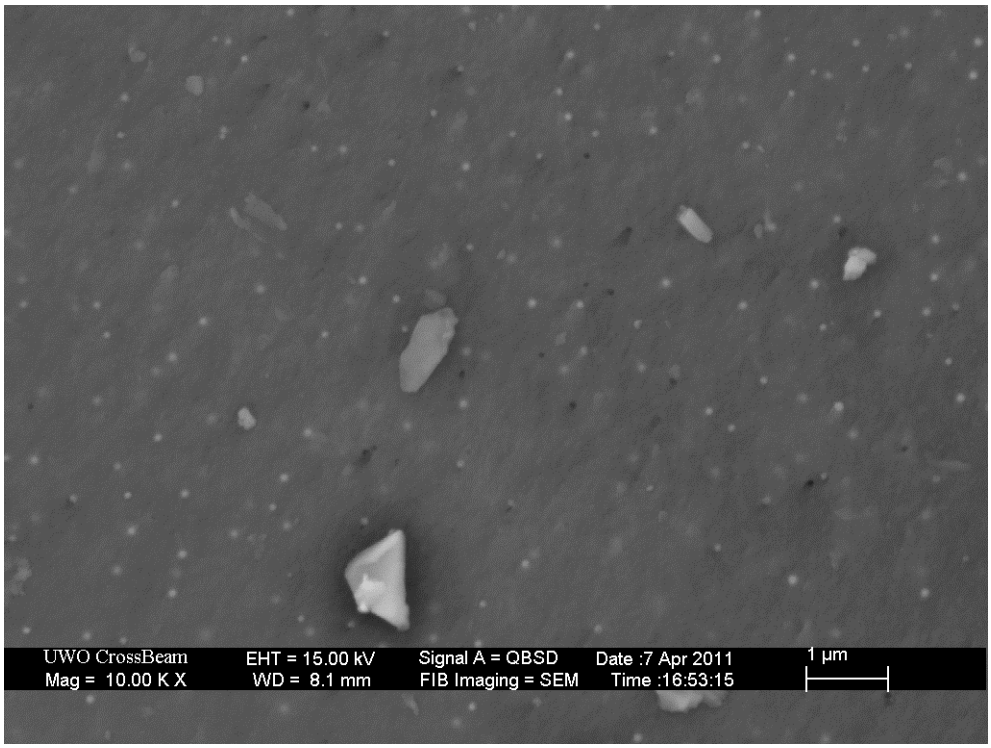

Fig. E.3 SEM-BSE cross-section image of electric furnace slag sample.

Bright spots - magnetite.

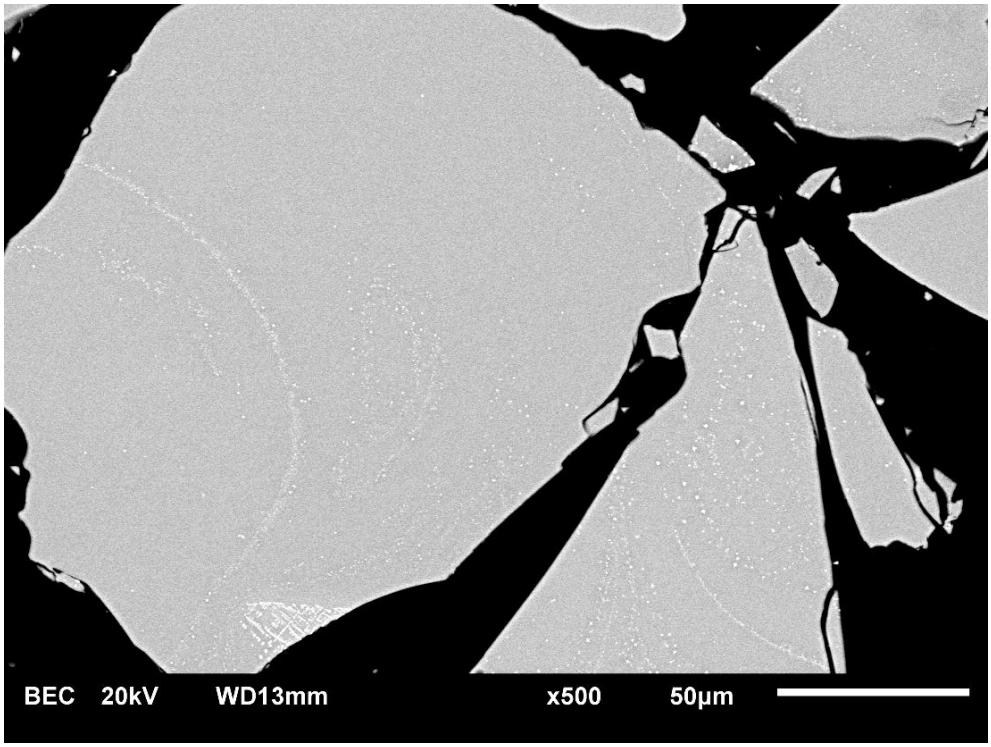

Fig. E.4 SEM-BSE cross-section image of electric furnace slag sample.

Bright spots - magnetite.

Appendix F. Metal sulphate precipitation

The reduction in soluble sulphur levels was observed in some slag HPOXAL experiments at 250°C where interruption in oxygen dispersion impeded acid regeneration. The drop in soluble sulphur was attributed to metal sulphate precipitation. To confirm the assumption, an experiment was run, in which sulphuric acid was added deliberately prior to heating up the autoclave. As can be seen from Fig. F1, by the time the autoclave is heated up to 250°C, both metals and sulphur leave the solution (as precipitated metal sulphates). The subsequent introduction of oxygen, however, reverses sulphate precipitation as sulphuric acid is regenerated.

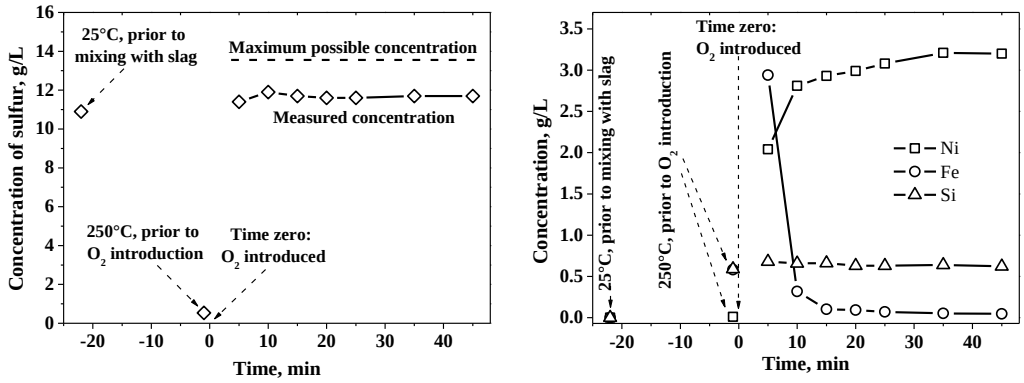

Fig. F.1 Leaching experiment with pre-acidification.

Conv. slag #2, 25% solids in slurry, 250°C, 60 psi (4.1 bar) O_2, ~35 g/L H_2SO_4

Precipitation of metal sulphates is suspected to take place in the co-leaching experiments with the pyrrhotite tailings at 250°C and 34 g/L equivalent acidity. According to Table F1, the concentration of ferrous iron increased from under 100 ppm at temperature to more than 1 g/L after cooling and filtration. The presence of Fe(II) is indicative of incomplete oxidation due to precipitation of ferrous sulphate. The increase in the concentration of Fe(II) after cooling and filtration can be explained by hematite silica precipitating along with ferrous sulphate and encapsulating it, thus preventing re-dissolution until cooling, when particles become partially disintegrated due to rapid pressure changes. The slower kinetics of leaching at 250°C (vs. 225°C) at 34 g/L

equivalent acidity (Fig. 5.5) can be attributed to the precipitation of nickel and cobalt sulphates along with ferrous sulphate. This assumption is supported by the fact that there is a noticeable increase in Ni and Co extraction after cooling and filtration in the experiment run at 250°, while in the experiment run at 225°C, the extractions of Ni and Co did not change significantly after cooling.

Table F.1 Concentration of Fe(II) before and after cooling and filtration

T, °C	Acidity, g/L	Acid source	Fe(II) before cooling, g/L	Fe(II) after cooling, g/L
250	68	H_2SO_4	0.09-0.18	0.12-0.23
250	68	*Tailings*	0.06	0.11
250	34	H_2SO_4	0.04	**1.12**
250	34	*Tailings*	0.01-0.03	**1.09-1.82**
225	68	*Tailings*	0.16	0.22-0.27
225	34	*Tailings*	0.06-0.15	0.16-0.34

Appendix G. Additional SEM images and EDX spectra of residues of amorphous slag leaching

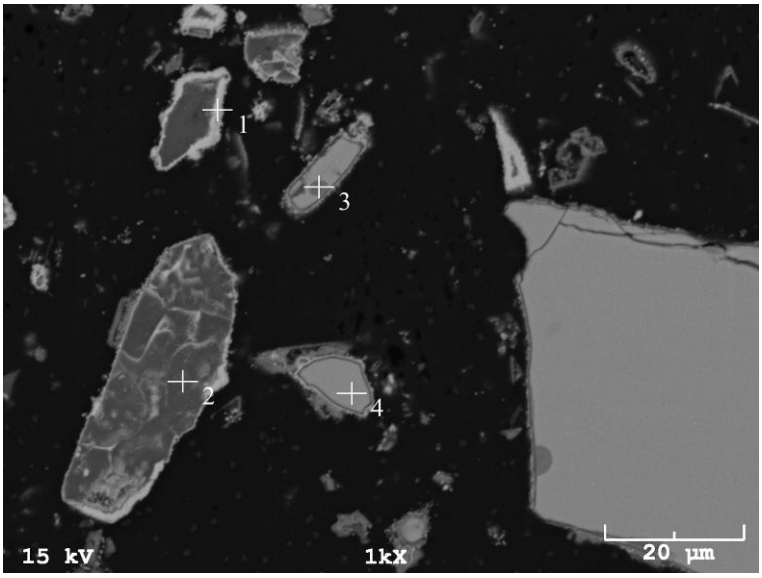

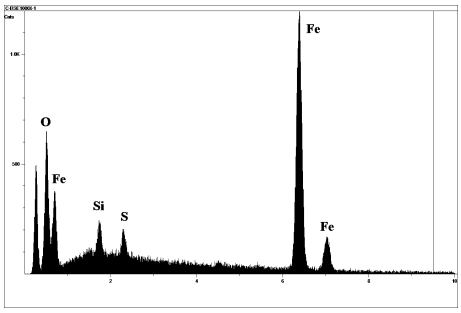

1.

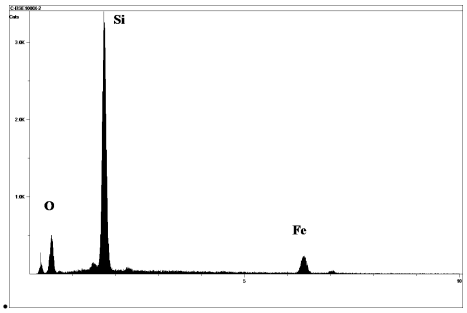

2.

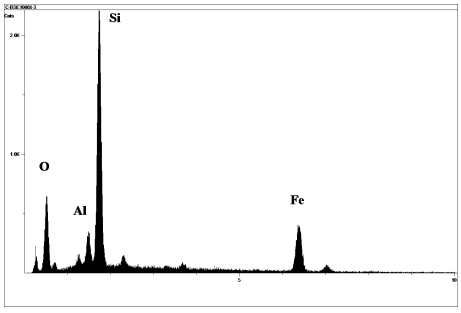

3.

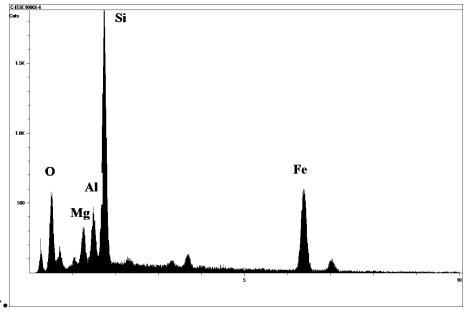

4.

Fig. G.1 SEM-BSE cross-section image and EDX spectra of the residue of the 45 min experiment (250°C)

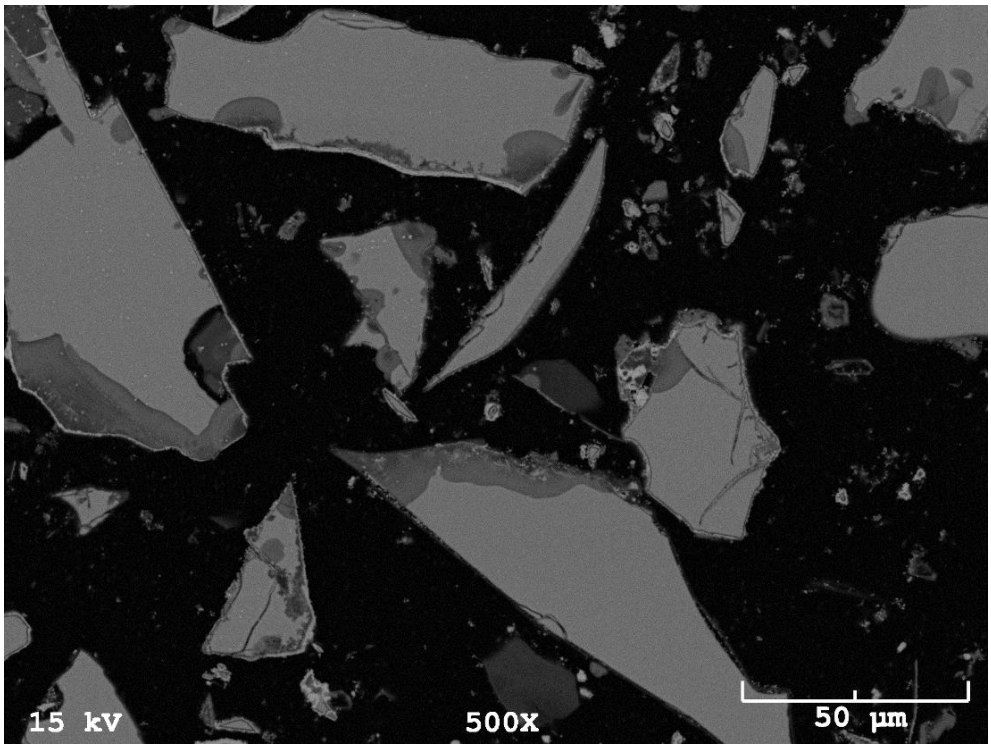

Fig. G.2 SEM-BSE cross-section image of residue of the 45 min experiment (250°C)

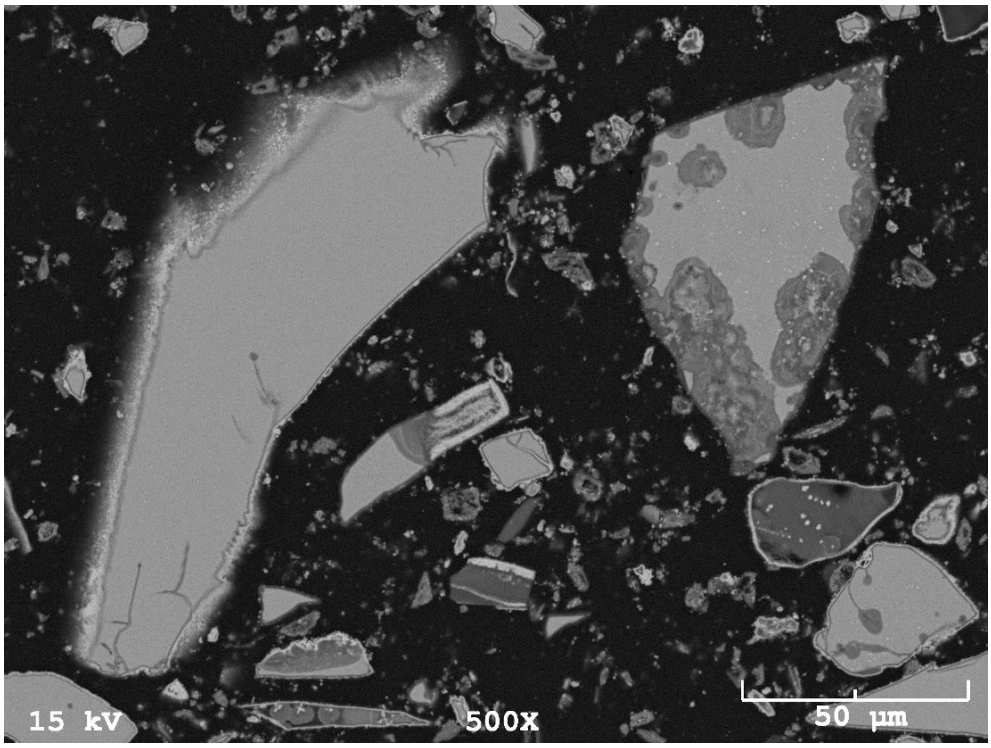

Fig. G.3 SEM-BSE cross-section image of residue of the 90 min experiment (170-250°C)